UNIVERSITY OF CINCINNATI

Date: October 29, 2004

I, Ricardo Torres-Jardon,

hereby submit this work as part of the requirements for the degree of:

Doctor of Philosophy

in:

Environmental Engineering

It is entitled:

Comparative Assessment of the Sensitivity of
Ozone to Nitrogen Oxides and Volatile Organic Compounds in
Two Dissimilar Metropolitan Areas of North America
Cincinnati, OH (U.S.A.) and Mexico City, DF (Mexico)

This work and its defense approved by:

Chair: Dr. Timothy C. Keener

Dr. Soon-Jain Khang

Dr. Mingming Lu

Dr. George Sorial

Mr. George J. Schewe

Comparative Assessment of the Sensitivity of Ozone to Nitrogen Oxides and Volatile Organic Compounds in Two Dissimilar Metropolitan Areas of North America: Cincinnati, OH (U.S.A.) and Mexico City, DF (Mexico)

A dissertation submitted to the

Division of Research and Advanced Studies
of University of Cincinnati

In partial fulfillment of the
requirements for the degree of

DOCTORATE OF PHILOSOPHY (Ph.D.)

in the Department of Environmental Engineering
of the College of Engineering

2004

by

Ricardo Torres Jardón

B.S. (Chem. Eng.), Universidad Nacional Autónoma de México, 1989
M.S. (Environ. Eng.), Universidad Nacional Autónoma de México, 1997

Committee Chair: Professor Timothy C. Keener, Ph.D., PE, QEP

ABSTRACT

Because of the complexity of urban ozone (O_3) formation, photochemical modeling and ambient data analysis are now needed to provide feedback regarding the effectiveness of O_3 control strategies. However, procedures for diagnosing the O_3 sensitivity to nitrogen oxides (NO_x) or volatile organic compounds (VOC) based on ambient data analysis still require further development and testing. This dissertation presents the results of an experimental investigation into the usefulness of using a combination of observational-driven techniques to determine the O_3-NO_x-VOC sensitivity in urban areas. Afternoon O_3/NO_y, O_3/NO_z and NO_y (where NO_y represents the total oxidized nitrogen species and NO_z represents the reaction products of NO_x) photochemical indicators were measured in two dissimilar cities: Cincinnati, Ohio (U.S.A.) and Mexico City, Federal District (Mexico). The evaluation the photochemical indicator analysis diagnosed VOC-sensitive conditions in both cities. The prevalence of these conditions, were confirmed with a complementary statistical analysis of the differences in average weekend/weekday O_3 peak and morning NO emissions (WE/WD effect). The comparative assessment of the factors determining the O_3-NO_x-VOC sensitivity in Cincinnati and Mexico City revealed strong differences on population, urban characteristics, topography, precursors emissions densities, and magnitude of VOC emissions, but an apparent similarity in NO_x emissions between these two urban areas. However, measured maximum O_3 were high in Mexico City as compared to Cincinnati. This phenomenon could be explained as the result of the higher VOC emissions and stronger VOC reactivity in Mexico City than in Cincinnati. A comparative assessment between the photochemical indicators method and the VOC/NO_x emission ratio to diagnose O_3-NO_x-VOC sensitivity demonstrated the consistency of the first approach to perform this identification under severe conditions of O_3 formation. The O_3 air quality management implications were, due to the predominating VOC-sensitive conditions, that additional reductions in NO_x emissions, stipulated by previous model-based O_3 control strategies now in progress in both areas, should be avoided or at least thoroughly reviewed. Otherwise, O_3 levels might increase. This research demonstrates that the combination of the photochemical indicators method with the analyses of the WE/WD effect can be a useful tool in the development and evaluation of O_3 air quality management strategies.

ACNOWLEDGEMENTS

First and foremost, I would like to express my gratitude to my committee chair and advisor Dr. Tim C. Keener for his guidance, support, and trust throughout my Ph.D. study. In addition, I want to express my acknowledgement to Dr. Mingming Lu, Dr. George Sorial, Dr. Soon-Jain Khang and Mr. George J. Schewe for serving in my dissertation committee. Although did not serve as member of my committee, I would like to thank Dr. Luis Gerardo Ruíz-Suárez for his advice and support as my external national advisor at the National Autonomous University of Mexico (UNAM).

I would like to acknowledge the Hamilton County Department of Environmental Services for the use of their instruments and facilities at the Taft Monitoring Station in Cincinnati, Ohio. In particular, I want to thank Mr. Harry St. Clair and the personnel at Taft for his support throughout the development of the monitoring campaign in Cincinnati. I also like to acknowledge Mr. Dennis Fitz from the CERT-University of California at Riverside, CA, and Larry Garrison from the Kentucky Division of Air Quality, Frankfurt, KY, for the loaning of part of the instrumentation used for my research.

I would also like to acknowledge to the Red Automática de Monitoreo Atmosférico from the Gobierno de la Ciudad de México for the use of their monitoring station at Santa Ursula in Mexico City, Federal Distric. I truly appreciate the assistance from Mr. Armando Retana and his technician personnel for the equipment and supplies used during the monitoring campaign in Mexico City. Additional thanks go to the personnel at the FQA Group at the Center for Atmospheric Sciences, UNAM for their help and friendship during my research sojourns in Mexico City. Special thanks go to Dr. Aron Jazcilevich and Dr. Agustín García for their assistance in the modeling simulations. Dr. Victor Magaña at the Center for Atmospheric Sciences is acknowledged for the meteorological database.

This work is dedicated to my wife Laura Margarita and my child Raúl, because having you in mind I could finish this mission. We had difficult times and we could to make it together. Thank you very much. I hope one day I can reward you for all the time I was far from you. I cannot find words also to express my thanks to my parents Fausta and Alfonso, my brother Raúl Guillermo, and my family-in-law for their continuous prayers and cheers along all of this time. My acknowledgement is extended to my friends at UC: Phirun, Kessinee, Prabhat, Prabhat, Ganesh, Alberto, Adriana and Pablo. I thoroughly enjoyed their friendship.

I would like to thank the Scholarship Subcommittee from the Center for Atmospheric Sciences, UNAM, and the Dirección General de Asuntos del Personal Académico (DGAPA), UNAM, for the scholarship provided to my PhD study. Last, but not least, I would like to express my gratitude to the Dirección General de Relaciones Internacionales, Public Education Secretariat of Mexico (SEP) for the complementary fellowship they granted me.

TABLE OF CONTENTS

LIST OF TABLES

LIST OF FIGURES

GLOSSARY OF ACRONYMS AND SYMBOLS

APC-CAS	Atmospheric Physical Chemistry-Center for Atmospheric Sciences
BUWAL	Bundesamt für Umwelt, Wald und Landschaft (Federal Office for Environment, Forest and Landscape)
CIT	California/Carnegie Institute of Technology
CO	Carbon monoxide
EKMA	Empirical Kinetical Modeling Approach
EPA	Environmental Protection Agency
GC	Greater Cincinnati
h	Planck's constant (6.6256×10^{-34} J·s)
H_0, H_1	Terms to describe the statistical null hypothesis and the statistical alternative hypothesis, respectively
H_2O_2	Hydrogen peroxyde
HCDOES	Hamilton County Environmental Services
HNO_3	Nitric acid
HO_2	Hydroperoxyl radical
HONO	Nitrous acid
HO_x	Hydrogen-containing free organic radicals
IMP	Instituto Mexicano del Petróleo
ININ	Instituto Nacional de Investigaciones Nucleares
LST	Local Standard Time
M	A third molecule in a chemical reaction, usually oxygen or nitrogen
MCCM	Multiscale Climatic and Chemistry Model
MCMA	Mexico City Metropolitan Area
MoO	Molybdenum oxide
MTBE	Methyl-*t*-butyl ether
N	Number of samples
NARSTO	North American Research Strategy for Tropospheric Ozone
NBS	National Bureau Standards
NCDC	National Climatic Data Center
NH_3	Ammonia
NIST	National Institute of Standards and Technology

NMHC	Non-methane Hydrocarbons
NO	Nitrogen oxide
NO*	NO_y compounds reduced to NO in a thermal catalytic converter
NO_2	Nitrogen dioxide
NO_2*	Estimated nitrogen dioxide concentration from empirical numerical approaches
NO_3^-	Particulate nitrate
NO_x	Nitrogen oxides ($NO_x = NO + NO_2$)
NO_x*	NO_x measurement performed with a chemiluminescent analyzer
NO_x-sensitive	A term to define the condition in which lowering NO_x emissions most effectively reduces peak ozone.
NO_y	Total reactive nitrogen ($NO_y = NO_x + NO_z$), also, total oxidized nitrogen species
NO_y*	NO_x analyzer adapted to measure NO_y
NO_z	NO_x reaction products ($NO_y - NO_x$), also the sum of: PAN + HNO_3 + NO_3^- + others
NO_z*	Estimated NO_z concentration from empirical numerical approaches
O_3	Ozone
OBMs	Observational-Based Models
OH	Hydroxyl radical
p	Level of significance to express the probability of making a given percent of a Type I error (degree of confidence “alpha”); this error occurs when one reject a hypothesis when it should be accepted.
PAN	Peroxyacetyl nitrate
P_i	Production rate of formation of any “*i*” compound
PIM	Photochemical Indicators Method
ppb	Parts per billion, or parts per 10^9, by volume
ppm	Parts per million, or parts per 10^6, by volume
ppmC	Parts per million of one organic carbon compound or hydrocarbon compound x number of carbon atoms per molecule
RAMA	Red Automática de Monitoreo Atmosférico (Automated Air Monitoring Network)
RCHO	Carbonyl
RH	Generic hydrocarbon
RO	Alcoxy radical
RO_2	Alkyl peroxy radical
RO_2NO_2	Generic organic peroxy nitrates
$RONO_2$	Generic organic nitrates

ROOH	Generic higher peroxides
S.D.	Standard Deviation
S_H	Summed source of odd hydrogen radicals
SUMS	Santa Ursula Monitoring Station
URG	University Research Glassware (trade mark)
VOC	Volatile organic compounds
VOC/NO_x	Ratio of emissions of volatile organic compounds to nitrogen oxides
VOC-sensitive	A term to define the condition in which lowering VOC emissions most effectively reduces peak ozone.
WD	Weekday (Monday, Tuesday, Wednesday, Thursday, or Friday)
WE	Weekend day (Sunday or Saturday)
WE/WD effect	Term that refers to the change on peak ozone due to the change on precursors emissions in weekends as compared with the weekdays
3-D model	Three-dimensional photochemical air quality simulation model
ν	Frequency associated with a particular photon (s^{-1})
λ	Wavelength (nm)
μ	Population mean; also, micro or 1×10^{-6}
μg	micrograms, 1×10^{-6} g

Chapter 1
INTRODUCTION

1.1 Background and Motivation

The design of effective control strategies for tropospheric ozone (O_3), whose harmful effects on human health, forest ecosystems, agricultural crops, and materials are well known, still represents a complex scientific, technological, and social issue, in both developed and developing countries (Kley et al., 1999; Molina and Molina, 2004). O_3 is a secondary pollutant formed in the ambient air as a result of a complex, nonlinear function of: (1) the relative proportion of the emissions of its precursors, primary emissions of nitrogen oxides (NO_x = NO + NO_2, where NO is nitrogen oxide and NO_2 is nitrogen dioxide) and volatile organic compounds (VOCs) from anthropogenic and natural sources; (2) the reactivity of the VOC; (3) the advective transport of these emissions and their reaction products; (4) the temperature, humidity, and solar radiation; and (5) the complex set of sunlight initiated chemical reactions occurring in the troposphere concurrent with the transport and dispersion of the emissions (US EPA, 1996). These processes lead to the formation of O_3 and other photochemical oxidants, such as peroxyacetyl nitrate (PAN), nitric acid (HNO_3), and aerosol nitrates (NO_3^-). The overall reaction of this system can be written as:

$$\text{VOC} + NO_x + h\nu \rightarrow O_3 + \text{PAN} + HNO_3 + \ldots\ldots + \text{aerosols} + \text{etc.}, \qquad (1)$$

The complex dependence of tropospheric ozone formation on the availability of its precursors NO_x and VOC gives origin to the so-called O_3-NO_x-VOC sensitivity term. Under NO_x-sensitive conditions (high VOC/NO_x ratios), ambient O_3 can be effectively reduced by reductions on NO_x emissions and is, practically, not sensitive to VOC changes. Under VOC-sensitive conditions, reductions on anthropogenic VOC emissions (low VOC/NO_x ratios) will be effective to reduce O_3 but can also increase peak ozone concentrations if NO_x emissions are decreased (Finlayson-Pitts and Pitts, Jr., 2000). 3-D photochemical models are useful to predict the features of this complex O_3-NO_x-VOC chemistry, but the accuracy of the

predictions that determine whether O_3 formation during specific circumstances is associated with NO_x-sensitive chemistry or VOC-sensitive conditions is still limited and unknown (Blanchard and Stoeckenius, 2001; Chameides et al., 2000). Because similar quantities of O_3 can be predicted in VOC-sensitive and NO_x-sensitive environments and because of the possibility of compensating errors in photochemical models, one photochemical model can acceptably predict diurnal O_3 but incorrectly predict the sensitivity of O_3 to changes in NO_x and VOC emissions (Sillman, 1995; Toneesen and Dennis, 2000). Moreover, there is also no direct way to test whether the NO_x-VOC predictions are accurate—a central concern when designing O_3 control strategies.

Despite the considerable analytical power that photochemical models offer to the policy maker to define an O_3 air quality strategy, a key limitation of these models is that they are driven by highly uncertain emission inventories (Sillman, 1999; Chameides, et al. 2000). Major inaccuracies in simulation results have been associated with discrepancies in current NO_x and VOC emission inventories (expressed as the ratio VOC/NO_x).

The failure of models to accurately predict the response of O_3 to reductions in NO_x and VOC emissions has resulted in considerable skepticism about the use of these models as basis for environmental policy (Chameides et al., 2000; Finlayson-Pitts and Pitts, Jr., 2000). However, the design of control strategies still relies on the predictions of photochemical models. For example, with recent court approval of the new U.S. Environmental Protection Agency (EPA) 8-hr Ozone Standard, state and local agencies must improve emissions inventories, develop or strengthen control strategies, and demonstrate, with photochemical modeling, that the proposed strategies will be sufficient to attain and maintain the standard (Wierman, 2003).

In recognition of the above limitation, the North American Research Strategy for Tropospheric Ozone group (NARSTO) has pointed out the necessity of improving the present emission-based O_3 air quality management process. To achieve this, they have recommended using all available information to determine whether a control strategy is expected to achieve a specific standard or whether a current model-based O_3 control strategy is appropriately functioning (Chameides et al., 2000).

The cases of Cincinnati, OH (U.S.A.) and Mexico City, DF (Mexico) provide a neat illustration of the complexity of this situation. Cincinnati, typical of medium sized U.S. metropolitan areas, is in compliance with the EPA's 1-hr O_3 standard but has the potential to be noncompliance with the new, more restrictive 8-hr O_3 standard. The O_3 control strategies imposed in this region were the result of recommendations from a multi-state photochemical modeling effort undertaken in order to control ozone regional transport over the East and Midwest of the U.S. These strategies have focused mainly on the reduction of NO_x emissions, as if the whole region (East and Midwest) were under a NO_x-sensitive environment (Guinnup and Collom, 1997; The Ohio Environmental Council, 2002; US EPA, 2004).

The Mexico City Metropolitan Area (MCMA) is an example of an urban metro-complex in a developing country that still has yet to find the appropriate control strategy to reduce the observed daily O_3 levels. Past and present O_3 control strategies have been the result of recommendations from preliminary photochemical modeling efforts and linear programming analysis combined with political and economical assessments (Streit and Guzman, 1996; Molina and Molina, 2002; McKinley et al.., 2003). Although the non-systematic combination of both NO_x and VOC controls has been common issue in the several control plans enforced in the past 15 years, the general recommendation to policymakers has been to control NO_x-emissions, as if it was a case of NO_x-sensitive conditions (Molina and Molina, 2002).

Two central questions arise from these examples. How can the effectiveness of ongoing O_3 control strategies be scientifically demonstrated? If determined to be ineffective, what basis is there for recommending changes to a given control strategy? One possible way of answering these questions is an objective analysis of the O_3-NO_x-VOC sensitivity based on ambient air-quality measurements.

In recognition of the limitations of photochemical models, scientists have developed a new category of analytical tools. These tools are the so-called "observation-based methods" (OBMs). These methods use ambient air-quality observations to infer important relationships between O_3, its precursor compounds, and/or the sources of these precursor compounds. These tools differ significantly from emission based methods (i.e., photochemical models) that use emission inventories to simulate photochemical scenarios (Blanchard et al., 1999; Sillman, 1999; Chameides et al., 2000). OBMs offer

several general advantages over photochemical models for assessing the sensitivity of O_3 to VOC and NO_x in a given air mass. Because OBMs rely on ambient measurements (real-world conditions) and do not depend on the accuracy of emission inventories, they provide a way to evaluate the consistency of typical model predictions and thus reduce the level of uncertainty associated with these predictions. In turn, this improves the characterization of O_3 precursor relationships. Sillman (2002) has suggested that the combination of OBMs with photochemical models can provide an excellent link between photochemical models and ambient measurements that is often missing in typical modeling analysis.

However, OBMs have some operational drawbacks, as they depend on measurements of relevant constituents (Chameides et al., 2000). If the data are inaccurate or incomplete, there is the potential for uncertain or erroneous results. There is also the potential for misinterpretation if the OBM is not tested for uncertain assumptions. Because OBMs are diagnostic approaches, they do not predict the future state of the atmosphere (e.g., the peak O_3 concentration resulting from a given reduction in pollutant emissions).

OBMs include receptor models, regression techniques, ambient ratios, indicator species, and semi-empirical based OBMs. From among the various indicator species techniques, the photochemical indicators method (PIM) has emerged as the most practical for evaluating the O_3-NO_x-VOC sensitivity. It does so directly from an analysis of correlations and ratios between measured secondary photochemical products such as O_3, total reactive nitrogen (NO_y), and other key secondary species (Sillman et al., 1997; Sillman, 1999; Sillman and He, 2002). This method has also been used to evaluate the consistency of photochemical models currently used to set up O_3 control policies.

However, the acceptance of the PIM is not universal. The NARSTO group has cited the need of further confirmation and development of these complementary tools, from both a policy and a scientific/technical standpoint, before such iterative scheme process could be fully implemented (Chameides et al., 2000). To achieve a wider acceptance, two important disadvantages of OBMs must be tackled. First, their sources of errors must be clarified, and, second, there needs to be more documented experiences to develop appropriate standard procedures.

The present applied research has three motivations. The first is to investigate the expediency of combining the photochemical indicators approach with other data analysis techniques for assessing current O_3-NO_x-VOC sensitivity, instead of using a single insolated OBM. The second is to demonstrate the usefulness of the photochemical indicators to explain confusing NO_x-VOC sensitive situations predicted by other modeling and measurement methods. The third is to provide research grade evidence of the convenience of observational-measurement analyses to support O_3 air quality management policies.

1.2 Overview of Ozone-NO_x-VOC Sensitivity

Ozone production occurs via the free-radical-initiated oxidation of VOC or CO in the presence of NO_x and sunlight (Chameides et al., 1992). The solar radiation dissociates stable molecules present in the atmosphere (i.e., carbonyls or aldehydes and hydrogen peroxide) to form hydrogen-containing free radicals (HO_x), which, in the presence of NO_x, catalyze the oxidation of VOCs to form, ultimately, carbon dioxide and water vapor. Partially oxidized organic species such as aldehydes, ketones, and carbon monoxide are produced as intermediate oxidation products, with O_3 formed as a by-product. The typical chemical mechanism for the oxidation of a generic hydrocarbon (RH) is represented by Reactions (2) through (6):

$$RH + OH \rightarrow R + H_2O \quad (2)$$

$$R + O_2 + M \rightarrow RO_2 + M \quad (3)$$

$$RO_2 + NO \rightarrow RO + NO_2 \quad (4)$$

$$RO + O_2 \rightarrow HO_2 + RCHO \quad (5)$$

$$HO_2 + NO \rightarrow OH + NO_2 \quad (6)$$

In this set, R is a hydrocarbon alkyl radical chain (for example, $CH_3CH_2CH_2$-H will stand for RH = propane), and M is a third molecule (N_2 or O_2). RO represents an alcoxy radical, and RO_2 an alkyl peroxy radical. RCHO represents a carbonyl. Alkyl peroxy radicals reactions (R4) with NO reduce the concentration of NO and increase the concentration of NO_2. Reaction (6) regenerates hydroxy (OH)

radicals and also produces NO_2. This mechanism can be interpreted as a catalytic cycle, where radicals (OH, R, RO_2, RO, and HO_2) act to propagate a chain of additional radicals. Reactions (4) to (6) play a key role in O_3 formation by oxidizing NO to NO_2. Subsequently, photodissociation of NO_2 by sunlight generates O_3 by Reactions (7) and (8):

$$2x[NO_2 + h\nu\ (\lambda<420\ nm) \rightarrow NO + O] \quad (7)$$

$$2x[O + O_2 + M \rightarrow O_3 + M] \quad (8)$$

$$\text{NET:} \qquad RH + 4O_2 + 2h\nu \rightarrow RCHO + 2H_2O + 2O_3$$

As shown in the net oxidation set of reactions, one molecule of RH (i.e., one cycle) is accompanied by the generation of two molecules of ozone. The carbonyl compound produced in the sequence (RCHO in reaction (5) and net reaction) is, in general, subject to further oxidation that can lead to the production of additional O_3. In this sequence, VOCs are consumed, while both OH/HO_2 and NO_x act as catalysts. Termination occurs when the catalysts are removed, often by one of the two paths:

$$OH + NO_2 + M \rightarrow HNO_3 + M \quad (9)$$

$$HO_2 + HO_2 + M \rightarrow H_2O_2 + O_2 + M \quad (10)$$

The predisposition for O_3 formation in the air is essentially proportional to the number of free-radical propagated cycles that can occur before radical removal (Jenkin and Clemitshaw, 2000). This is usually referred to as the chain for O_3 formation. Therefore, when considering the influence of changing the concentration of NO_x or VOC on the production of O_3, the effect of such a change on the chain-length is very important. This length is determined by the rate of the chain terminating reactions as compared to the competing chain propagating reactions. Oxidation mechanisms for olefins, which react with O_3 as well as OH radicals, aldehydes, which photodissociate into free radicals and react with OH, and aromatics are more complex but have similar chain initiation, carrying, and termination steps. The most important features of an O_3 abatement strategy are illustrated in Figure 1.1.

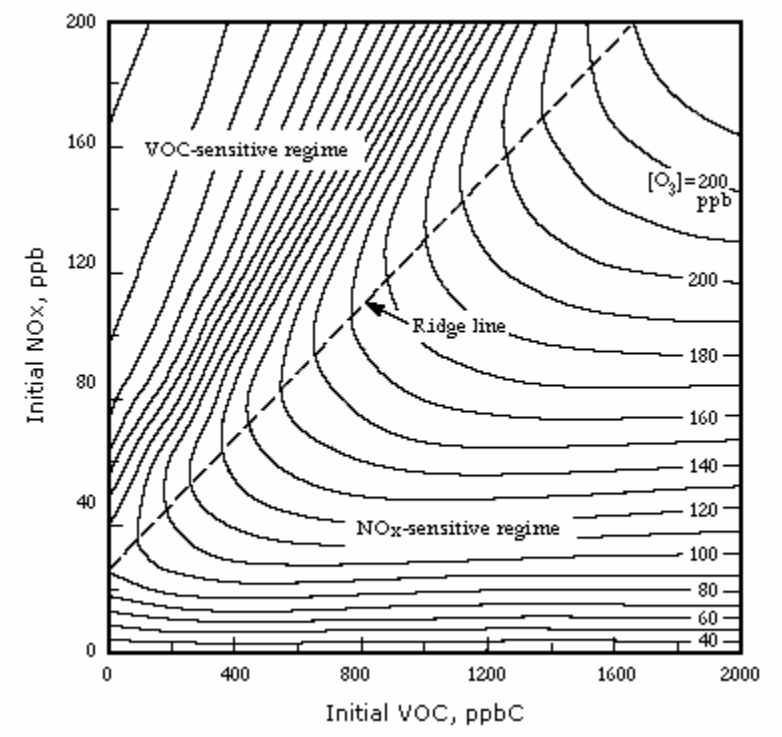

Figure 1.1. Typical peak ozone isopleths diagram. Peak O_3 concentrations in parts per billion (by volume) as a function of various initial VOC and NO_x concentrations. Ozone isopleth based on simulation of chemistry along air trajectories in Atlanta. (Adapted from Jefferies and Crouse, 1990).

Figure 1.1 shows the typical model-calculated isopleths of peak O_3 concentrations. Such isopleths have been commonly generated using computer models, such as the Empirical Kinetic Modeling Approach (EKMA), where the results of the model are tested against smog chamber data (Finlayson-Pitts and Pitts, Jr., 2000). Although EKMA plots have been replaced by sophisticated 3-D photochemical models, they still give valuable information about the expected peak O_3 levels as a function of initial VOC and NO_x concentrations or as a function of the amounts of VOC or NO_x that are added to the system as volumetric emissions. The diagonal line that extends from the lower left to the upper right corner of the graph has a slope corresponding to a VOC/NO_x ratio of about 8:1. The OH radical chain length, equal to the number of times a newly formed OH radical is regenerated through radical chain propagation before it is destroyed, reaches a maximum at this VOC/NO_x ratio. Thus, the ridgeline corresponds to the VOC/NO_x ratio, at which O_3 is most efficiently formed.

At low VOC/NO_x ratios to the left of the ridgeline, a decrease in the concentration of RH, would decrease the chain length and hence the rate of O_3 formation. The rate of formation of HNO_3 surpasses the rate of formation of H_2O_2 and O_3 production is ***VOC-sensitive*** (i.e., lowering VOC emissions most effectively reduces peak O_3). The OH radicals that propagate VOC oxidation and NO-to-NO_2 conversion are scavenged by the relatively high concentrations of NO_x. However, a decrease in the concentration of NO_2, which might result from NO_x emission reductions, would increase the chain length, as more of the OH pool is available to react with the VOCs (Jenkin and Clemitshaw, 2000). The reduction of NO_x lowers the rate at which OH and NO_2 are removed by formation of HNO_3 and leads to an increase in maximum O_3. This situation is frequently named "NO_x-disbenefit" and occurs only in the VOC-sensitive region.

For high VOC/NO_x ratios to the right of the ridgeline, lowering NO_x concentrations with a constant VOC concentration, results in an effective reduction on peak O_3 concentrations. However, decreasing VOCs alone at constant NO_x results only in a slowly decreasing O_3 peak levels. At these high VOC/NO_x ratios, O_3 formation is said to be ***NO_x-sensitive*** (i.e., lowering NO_x emissions most effectively reduces peak O_3). In this region of the isopleths on Figure 1.1, the source of OH radicals is greater than the source of NO_x. The chain propagating reactions (4) and (6) involve NO_x, and, consequently, any reduction in NO_x decreases the O_3 formation chain length. The rate of formation of H_2O_2 is greater than the rate of formation of HNO_3. Since RH is not itself directly involved in these competitions, the O_3 formation chain length is insensitive to changes in the concentrations of RH, which might result from VOC control.

It is important to point out that variation in the concentration of some reactive VOCs has an effect on O_3 formation under NO_x-sensitive conditions, because the degradation of some VOCs can lead to a significant removal of NO_x as organic nitrates and peroxy nitrates (PANs) as it is shown with general reactions (11) and (12) (Jenkin and Clemitshaw, 2000).

Reaction (12) is important in the photochemical formation process because can act as a temporal reservoir of NO_2 and as a sink of RO_2 radicals.

$$RO_2 + NO + M \rightarrow RONO_2 + M \quad (11)$$

$$RO_2 + NO_2 + M \rightleftarrows RO_2NO_2 + M \quad (12)$$

Finally, between the NO_x- and VOC-sensitive regions (the ridgeline zone) lies a transition region in which O_3 is equally sensitive to VOC and NO_x, but, compared to its sensitivity to VOC on the left side of the ridgeline and its sensitivity to NO_x on the right, it is relatively insensitive to both.

1.3 Observation-Based Methods for Evaluating O_3-NO_x-VOC Sensitivity

As previously discussed, OBM refers to a number of techniques that can be used to translate field observations into information on O_3 production. These techniques qualitatively assess the effectiveness of reductions of emissions of VOCs versus NO_x. OBMs offer several advantages as an analytical tool for evaluating the consistency of O_3 regulatory policies (Sillman, 2002). Examples of OBMs include: smog production (extent-of-reaction) algorithms (Chang and Suzio, 1995, Chang et al., 1997; Blanchard et al., 1999; Blanchard 2000); observation-based models using NO_x and VOC concentrations, meteorological data, and the concept of incremental reactivity (Cardelino and Chameides, 1995); constrained steady state (Kleinman 2000; Kleinman et al.,2001; Tonnesen and Dennis, 2000); and the photochemical indicators method (Sillman 1995; Sillman et al., 1997; Sillman and He, 2002).

The typical measurements required by most OBMs are: O_3, total reactive nitrogen (NO_y), NO, CO, and speciated VOC. Some of these methods actually combine two different techniques, such as modeling with one observational analytical technique. A detailed analysis of the theoretical bases, advantages, and disadvantages of these OBMs is given in Kleinman (2000) and Sillman (2002).

OBMs are classified into two broad categories: “present time-frame methods,” based on measurements of present ambient species such as VOC, NO_x, and CO, and “past time-frame methods,” based on measurements of secondary photochemical products (Kleinman, 2000). The photochemical indicators method (PIM) makes use of measurements of secondary reaction products. These measurements are absolute values of selected species or species ratios that have been found as consistent indicators of the

NO_x-VOC sensitivity by analyzing 3-D photochemical simulations results under different conditions of NO_x and VOC hypothetical emissions reductions. An example of one photochemical indicator is the ratio of the peak O_3 concentration (representing the O_3 that has built up since the precursor emissions occurred) to that of another secondary species (such as NO_z, the amount of NO_x that has been oxidized to higher nitrogen oxides or the sum of HNO_3, PAN, NO_3^-, and others). The species ratios can then provide clues as to how an air mass upwind of a receptor location has evolved to its present state.

The species ratios O_3/NO_y, (where $NO_y = NO_x + NO_z$), O_3/NO_z, O_3/HNO_3, H_2O_2/HNO_3, and other equivalent species correlations or individual species (i.e., NO_y as a whole) show different values depending on whether O_3 was built up under a NO_x- or VOC-sensitive environment. This approach is based on 3-D modeling results obtained by Milford et al. (1994), Sillman (1995, 1999), and Sillman et al. (1997, 1998). These authors found that, in general, high values of these ratios (and low values of NO_y) were associated with NO_x-sensitive chemistry and low values of the same ratios (and high values of NO_y) were associated with VOC-sensitive chemistry.

The theoretical justification for the main indicator ratios is based on the assumption that the split between NO_x-sensitive and VOC-sensitive regimes is driven by the chemistry of odd hydrogen radicals (OH, HO_2, and RO_2) (Sillman et al., 1990; Sillman, 1995). This split has been attributed to the relative strengths of odd hydrogen radical sources (S_H) and the production rates of its major sinks (peroxides, nitric acid and PAN): $S_H = 2P_{perox} + P_{HNO3} + P_{PANs}$. VOC-sensitive chemistry would occur whenever P_{HNO3} (and in a lower extent P_{PANs}) exceeds $2P_{perox}$. Under this condition, the production rate of O_3 is assumed to be proportional to the rate of the VOC + OH reactions (reaction 2), and its rate increases with increasing VOC and decreases with increasing NO_x. By contrast, NO_x-sensitive conditions would occur when the peroxide-forming Reactions (10a) and (13) are the dominant radical sinks:

$$HO_2 + HO_2 \rightarrow H_2O_2 + O_2 \qquad (10a)$$

$$HO_2 + RO_2 \rightarrow ROOH + O_2 \qquad (13)$$

Under this condition, the production rate of O_3 is assumed to be approximately equal to the rate of Reactions (4) and (6) (RO_2 + NO, HO_2 + NO). This rate increases with increasing NO_x but has little direct dependence on VOC.

In this way, the ratio O_3/NO_z and the correlation between O_3 and NO_z could be interpreted as the rate of production of O_3 to the rate of production of production of NO_x reaction products. This ratio has been interpreted as the "ozone production efficiency per NO_x" factor (OPE) in the analysis of rural events (Trainer et al., 1993). The ratio O_3/NO_y and the correlation between O_3 and NO_y have several interpretations. They reflect two separate processes, both of which are related to O_3-NO_x-VOC sensitivity. They reflect the process of photochemical production of O_3 (represented by the ratio O_3/NO_z) and the process of NO titration from fresh NO_x emissions (represented by the NO_x fraction in the total NO_y). Afternoon high O_3 and low NO_y would reflect relatively large radical sources and smaller radical sinks such as the NO_2 + OH reaction. This ratio is assumed also to indirectly account for photochemical aging. The ratio O_3/NO_y can be viewed as the ratio O_3/NO_z multiplied by an aging term (NO_z/NO_y) (Sillman and He, 2002). In photochemically young air masses the ratio NO_z/NO_y is close to 0. In photochemically old air masses a large fraction of NO_x has been processed to NO_z and under these conditions the NO_z/NO_y ratio is close to 1. On the other hand, Milford et al. (1994) and Sillman (1995) have shown that NO_y is a good empirical indicator of high precursor concentrations because acts as a measure of NO_x emissions through the period of photochemical activity and also reflects the impact of stagnant meteorology on NO_x-VOC sensitivity and on the photochemical production of O_3.

A number of reference values have been suggested for delineating the transition from VOC to NO_x sensitivity. These values are obtained from 3-D photochemical models in which the input NO_x and VOC emissions were varied systematically to predict an O_3 reduction in response to reduced NO_x and anthropogenic VOC. Table 1.1 shows some of the suggested transition values for different O_3 polluted conditions in the U.S.

The PIM allows one to identify NO_x- and VOC-sensitive conditions between different locations or for different smog events (Sillman, 2002). Comparisons of 3-D model predictions and measured values

have demonstrated that the photochemical model can accurately infer the appropriate VOC- or NO_x-sensitive chemistry. Alternatively, when 3-D model predicted correlations between O_3 and NO_y and similar indicator species are compared with measured values, the resulting scatterplot patterns can be interpreted as evidence of bias in the photochemical model to interpret the right VOC-sensitive or NO_x-sensitive chemistry.

Table 1.1. Values of selected photochemical indicators and their NO_x-VOC sensitive transitional range.

Indicator	Transition range	Reference
NO_y	10 to 25 ppb[a]	Milford et al., 1994; Sillman, 1995
Ozone/NO_y	11 to 15 (when $[O_3] < 80$ ppb)[b] 6 to 8 (when 80 ppb $< [O_3] < 200$ ppb)[b]	Sillman and He, 2002
Ozone/NO_z	15 to 20 (when $[O_3] < 80$ ppb)[b] 8 to 10 (when 80 ppb $< [O_3] < 200$ ppb)[b]	Sillman and He, 2002
Ozone/Nitric Acid	20 to 25 (when $[O_3] < 80$ ppb)[b,c] 12 to 15 (when 80 ppb $< [O_3] < 200$ ppb)[b,c]	Sillman and He, 2002
Hydrogen Peroxide/Nitric Acid	0.2 to 0.3[b]	Sillman and He, 2002
Hydrogen Peroxide/NO_y	0.12 to 0.17[b]	Sillman and He, 2002
Hydrogen Peroxide/NO_z	0.20 to 0.25[b]	Sillman and He, 2002

[a] Ratios lower than the transition range generally correspond to NO_x-sensitive conditions.
[b] Ratios lower than the transition range generally correspond to VOC-sensitive conditions.
[c] Interpolated from Figure 3 in Sillman and He (2002).

In order to use the method in field applications, several requirement must be fulfilled: (1) photochemical indicators can only be collected, modeled, and/or used for the afternoon period (between 13:00 and 17:00 hr) during relatively sunny days and without rain; (2) measurements of indicator species must be performed in the peak or near-peak O_3 regions of a given airshed; and (3) NO_y measurements must have uncertainties of less than 20% (preferably less than 10%) and must include HNO_3 species (Sillman, 2002). If measurements of photochemical indicators are available for a given airshed, the method itself can work as a "rule of thumb" to identify the NO_x- and VOC-sensitive regions. However, a

thorough application of the method includes testing with a 3-D photochemical model, as well as the evaluation of measured species correlations patterns (i.e., O_3 versus NO_y or O_3 versus NO_z) in comparison with model results.

Locations of successful applications of the method include: the northeast corridor, Lake Michigan and Atlanta (Sillman, 1995); New York and Los Angeles (Sillman et al., 1997); Nashville (Sillman, et al., 1998); Switzerland (Staffelbach et al., 1997, Dommen et al., 1999); Milan, Italy (Martilli et al., 2002; Hammer et al., 2002); and Paris, France (Sillman et al., 2003). Some of these applications have included both measurements and model-measurement comparisons for the relevant species. Although several different photochemical mechanisms were used in these 3-D model simulations, the results were consistent with photochemical indicator theory.

However, evidence running contrary to this method has been reported. Model-based investigations of the San Joaquin Valley (Lu and Chang, 1998) and Los Angeles (Chock et al., 1999) both gave results different from those reported by Sillman. Blanchard and Stoeckenius (2001) also reported opposing results in a review of OBM applications. Results from Paris, France (Sillman et al., 2003) revealed situations where measurements resulted in poor accuracy. Sosa et al. (2000) obtained contradictory results in their study of Mexico City. However, there is evidence that most of the above disagreements were associated either with problems in the input emissions inventories and in the treatment of deposition mechanisms in the models or with erroneous measurements (Sillman, 2002). Consequently, more research is required to confirm the universality of the method, especially in situations where the PIM has failed to produce consistent results.

1.4 Scope of the Research

1.4.1 Approach and Methodology

The overall strategy envisioned in this applied research consisted of sequential stages including: field experiments; statistical, graphical, and conceptual evaluations; and assessments of the consistency of the results and of the PIM application with modeling experiments and published results. The idea behind

this strategy was to combine the assessment of the particular conditions linked to the O_3-NO_x-VOC sensitivity of two dissimilar environments with the investigation of factors that may affect, improve and demonstrate the consistency of the PIM.

The first stage focused on obtaining data on photochemical processes related species for each of the two study sites. These data included measurements of O_3, NO, and NO_y, in Cincinnati and Mexico City during the smog season of each region. Additional measurements of HNO_3 and H_2O_2 were made in Cincinnati only. Several methods recommended by the EPA were used for ozone and the nitrogen oxidized species. An experimental procedure published in peer-reviewed literature was used for the measurement of H_2O_2. Quality assurance and quality analytical procedures recommended by the EPA were followed during the monitoring and sampling campaigns.

The second stage consisted in the diagnosis of the O_3-NO_x-VOC sensitivity for Cincinnati and Mexico City using the PIM. Several statistical, graphical, and conceptual evaluations were performed on the observed data. In both cases, empirical correlations from peer-reviewed literature or from observed data were used to obtain either an indirect corroboration of a given assumption or to obtain a surrogate of species concentrations not measured during the field campaigns. A combination of graphical and numerical comparison procedures recommended by Sillman (2002) was used to evaluate the consistency of the results.

The central objective of the third stage was the corroboration of the diagnosis previously generated with the results of a statistical analysis of weekend/weekday differences in observed peak O_3 and morning NO concentrations. A corroboration of the diagnosis with the results of an evaluation of the duration of morning-to-afternoon O_3 accumulation and the rate of O_3 accumulation was also undertaken. The confirmation of the diagnosis for Mexico City was extended with the inclusion of a comparison of the measured photochemical indicators with the results of an O_3-NO_x-VOC sensitivity analysis previously performed for this area. An intercomparison between the results of the PIM diagnosis in Mexico City with two photochemical models previously used to study the local O_3 control strategies was also performed.

The last stage of the research consisted in a comprehensive assessment of the factors associated with the specific O_3-NO_x-VOC sensitivity in each city making use of the photochemical indicators results and several empirical O_3 formation concepts. This assessment included an evaluation of the photochemical indicators results with regard to the VOC/NO_x ratio in the identification of the NO_x-VOC sensitivity.

1.4.2 Research Goals

Since ozone control strategies require predictions that are difficult to test with present photochemical models, and because observation-based methods represent a practical option for evaluating predicted O_3 control management scenarios, this research investigated the consistency and usefulness of a combination of two OBMs for evaluating O_3-NO_x-VOC sensitivity in two dissimilar urban areas. In doing so, the goal was to make a scientific/technical contribution to the improvement of O_3 air quality management practices within the context of the NARSTO recommendations for North America.

The specific objectives of the research were as follows: (1) to explore the expediency of combining the PIM with the weekend-weekday effect analysis to improve the accuracy of O_3-NO_x-VOC sensitivity diagnosis; (2) to characterize the O_3-NO_x-VOC sensitivity of Cincinnati and Mexico City and evaluate the consistency of current O_3 control strategies in both urban areas; (3) to investigate the usefulness of the photochemical indicator approach to identify inconsistencies of the VOC/NO_x ratio to diagnose NO_x-VOC sensitivities; and (4) to generate data for the enrichment of the PIM database towards the development of standard procedures useful in a regulatory context.

1.5 References

Blanchard, C.L. (2000) Ozone process insights from field experiments-Part III: extent of reaction and ozone formation. Atmos. Environ. **34**, 2035-2043.

Blanchard, C.L., Lurmann, F.W., Roth, P.M., Jeffries, H.E., Korc, M. (1999) The use of ambient data to corroborate analyses of ozone control strategies. Atmos. Environ. **33**, 369-381.

Blanchard, C.L., Stoeckenius, T. (2001) Ozone response to precursor controls: comparison of data analysis methods with predictions of photochemical air quality simulation models. Atmos. Environ. **35**, 1203-1215.

Cardelino, C., Chameides, W.L. (1995) An observation-based model for analyzing ozone-precursor relationships in the urban atmosphere. J. Air & Waste Manage. Assoc. **45**, 161-180.

Chameides, W.L., Fehsenfeld, F., Rodgers, M.O., et al. (1992) Ozone precursor relationships in the ambient atmosphere. J. Gephys. Res. **97**, 6037-6055.

Chameides, W.L., Demerjian, K.L., Albritton, D., et al., (2000) An Assessment of Tropospheric Ozone Pollution: A North American Perspective; NARSTO. July. Available at: http://www.cgenv.com/Narsto/

Chang, T.Y., Suzio, M. (1995) Assessing ozone-precursor relationships based on smog production model and ambient data. J. Air & Waste Manage. Assoc. **45**, 20-28.

Chang, T.Y., Chock, D.P., Nance, B.I., Winkler, S.L. (1997) A photochemical extent parameter to aid ozone air quality management. Atmos. Environ. **31**, 2787-2794.

Chock, D.P., Chang, T.Y., Winkler, S.L., Mance, B.I. (1999) The impact of an 8h ozone air quality standard on ROG and NO_x controls in Southern California. Atmos. Environ. **33**, 2471-2486.

Dommen, J.A., Prevot, A.S.H., Hering, A.M., Staffelbach, T., Kok, G.L., Schillawsky, R.D. (1999) Photochemical production and the aging of an urban air mass. J. Geophys. Res. **104**, 5493-5506.

Finlayson-Pitts, B.J., Pitts, Jr., J.N. (2000) Chemistry of the Upper and Lower Atmosphere. Academic Press. San Diego, CA.

Guinnup, D., Collom, B. (1997) OTAG Air Quality Analysis Workgroup. Ozone Transport Assessment Group. Final Report. June. Available at: http://capita.wustl.edu/otag/

Hammer, M. -U., Vogel, B., Vogel, H. (2002) Findings on H_2O_2/HNO_3 as an indicator of ozone sensitivity in Baden-Württemberg, Berlin-Brandenburg, and the Po Valley based on numerical simulations. J. Geophys. Res. **107**, D18, doi:10.1029/2000JD000211.

Jenkin, M.E., Clemitshaw, K.C. (2000) Ozone and other secondary photochemical polltants: chemical processes governing their formation in the planetary boundary layer. Atmos. Environ. **34**, 2499-2527.

Jefferies, H.E., Crouse, K. (1990) Scientific and Technical Issues Related to the Application of Incremental Reactivity. Department of Environmental Sciences and Engineering, University of North Caroline. Chapel Hill, NC.

Kleinman, L.I. (2000) Ozone process insights from field experiments – Part II, observation – based analysis for ozone production. Atmos. Environ. **34**, 2023-2034.

Kleinman, L.H., Daum, P.H., Lee, Y-N., Nunnermacker, L.J., et al. (2001) Sensitivity of ozone production rate to ozone precursors. Geophys. Res. Lett. **288**, 2903-2906.

Kley, D., Kleinman, M., Sanderman, H., Krupa, S. (1999) Photochemical oxidants: state of the science. Environ. Pollut. **100**,19-42.

Lu -C-H., Chang, J.S. (1998) On the indicator-based approach to assess ozone sensitivities and emissions features. J. Geophys. Res. **103**, 3453-3462.

Martillini, A., Neffel, A., Favaro, G., Kirchner, F., Sillman, S., Clappier, A. (2002) Simulation of the ozone formation in the northern part of the Po Valley with the TVM-CTM. J. Geophys. Res. **107**, D22, doi: 10.1029/2001JD000534.

McKinley, G., Zuk, M., Hojer, M., et al. (2003) The Local Benfits of Global Air Pollution Control in Mexico City. Final Report of the Second Phase of the Integrated Environmental Strategies Program. Instituto Nacional de Ecología and Instituto Nacional de Salud Pública. México D.F., August.

Milford, J.B., Gao, D., Sillman, S., Blossey, P., and Russell, A.G. (1994) Total Reactive Nitrogen (NO_y) as an Indicator of the Sensitivity of Ozone to Reductions in Hydrocarbon and NO_x Emissions. J. Geophys. Res. **99**, 3533-3542.

Molina, L.T., Molina, M.J. Eds. (2002) Air Quality in the Mexico Megacity: An Integrated Assessment. Alliance for Global Sustainability Bookseries. Volume 2. Kluwer Academic Publishers. Dordrecht, The Netherlands.

Molina, J.M., Molina, L.T. (2004) Megacities and atmospheric pollution. Critical Review. J. Air & Waste Manage. Assoc. **54**, 644-680.

Sillman, S. (1995) The use of NO_y, H_2O_2, and HNO_3 as indicators for O_3-NO_x-VOC sensitivity in urban locations. J. Geophys. Res. **100**, 11497-11508.

Sillman, S. (1999) The relation between ozone, NO_x, and hydrocarbons in urban and polluted rural environments. Atmos. Environ. **33**, 1821-1845.

Sillman, S. (2002) Evaluation of Observation-Based Methods For Analyzing Ozone Production and Ozone-NO_x-VOC Sensitivity. Report to: National Exposure Research Laboratory. Office of Research and Development. U.S. EPA. Research Triangle Park, NC 27711.

Sillman, S., Logan, J.A., Wofsy, S.C. (1990) The Sensitivity of Ozone to Nitrogen Oxides and Hydrocarbons in Regional Ozone Episodes. J. Geophys. Res. **95**, 1837-1851.

Sillman, S., He, D., Cardelino, C., Imhoff, R.E. (1997) The use of photochemical indicators to evaluate ozone-NO_x-hydrocarbon sensitivity: case studies from Atlanta, New York and Los Angeles. J. Air & Waste Manage. Assoc. **47**, 1030-1040.

Sillman, S., He, D., Pippin, M., Daum, P., Kleinman, L., Lee, J.H., Weinstein-Lloyd, J. (1998) Model correlations for ozone, reactive nitrogen and peroxides for Nashville in comparison with measurements: implications for VOC-NO_x-sensitivity. J. Geophys. Res. **103**, 22629-22644.

Sillman, S., He, D. (2002) Some theoretical results concerning O_3-NO_x-VOC chemistry and NO_x-VOC indicators. J. Geophys. Res. **107**, D22, 4659, doi:10.1029/2001JD001123.

Sillman, S., Vaudatard, R., Menut, L., Kley, D. (2003) O_3-NO_x-VOC sensitivity and NOx-VOC indicators in Paris: results from models and Atmospheric Pollution Over the Paris Area (ESQUIF) measurements. J. Geophys. Res. **108**, D17, 8563, doi:10.1029/20002JD001561.

Sosa, G., West, J., San Martini, F., Molina, L.T., Molina, M.J. (2000) Air Quality Modeling and Data Analysis for Ozone and Particulates in Mexico City. Rep. No. 15. MIT Integrated Program on Urban, Regional and Global Air Pollution. Cambridge, MS. October.

Staffelbach, T., Neftel, A., Blatter, A., et al., (1997) Photochemical oxidation formation over Southern Switzerland, part I: Results from summer 1994. J. Geophys. Res. **102**, 23345-23362.

Streit, G.E., Guzman, F. (1996) Mexico City air quality: progress of an international collaborative project to define air quality management options. Atmos. Environ. **30**, 723-733.

The Ohio Environmental Council (2000) Ohio Valley – Ozone Alley. The Ohio Environmental Council. Columbus, OH.

Tonnesen, G.S., Dennis, R.L. (2000) Analysis of radical propagation efficiency to assess ozone sensitivity to hydrocarbons and NO_x, 2, long-lived species as indicators for ozone concentration sensitivity. J. Geophys. Res. **105**, 9227-9241.

Trainer, M., Parrish, D.D., Buhr, M.P., et al., (1993) Correlation of ozone with NO_y in photochemically aged air. J. Geophys. Res. **98**, 2917-2926.

US EPA (1996) Air Quality Criteria for Ozone and Other Photochemical Oxidants. Vol. I. EPA-600/P-93/00bF. National Center for Environmental Research. U.S. Environmental Protection Agency. Research Triangle Park. NC27711.

US EPA (2004) OTAG Technical Supporting Document. Technology Transfer Network Ozone Implementation. EPA – TTN NAAQS OTAG. U.S. Environmental Protection Agency. Available at: http://www.epa.gov/ttn/naaqs/ozone/rto/otag/finalrpt.

Wierman, S. (2003) Will the 8-hr ozone standard finally get off the ground? EM, 20-28, September.

Chapter 2

EXPERIMENTAL METHODS

2.1 Measurement of Indicator Species

The program for the measurement of ambient air species in Cincinnati and Mexico City was designed to provide the aerometric databases needed to apply the photochemical indicators method (PIM) and to corroborate the consistency of the application of this method. Continuous measurements of O_3, NO, and total NO_y were made in the near-peak O_3 region of each of the two cities, while 1-hr H_2O_2 and HNO_3 measurements were made only in Cincinnati during the afternoon hours (13:00-17:00 hr). As a result of a review of previous studies on the dynamics of the photochemical air pollution in both cities (see chapter 3), it was assumed that the measurements done at only one site within the near-peak O_3 region of each of these urban areas would be representative of the O_3-NO_x-VOC chemistry of their airsheads.

The measurements were performed at the times of year in which ozone reached its highest levels (summer for Cincinnati and winter for Mexico City). The study and analysis of days with high O_3 concentrations provides elements appropriate to infer the interrelationship between precursor emissions and meteorology associated with the occurrence of these “event” days. In addition, the design of O_3 control strategies has been traditionally based on the selection of days with higher ozone concentrations (US EPA, 1996).

The selection of the methods for the continuous measurement of O_3 and NO_y species was done following the recommendations of Parrish and Fehsenfeld (2000) and of the US EPA (US EPA, 2001). Methods for the sampling and analysis of H_2O_2 and HNO_3 were selected after a review of the specialized literature (Sakugawa et al., 1990; US EPA, 1999; Parrish and Fehsenfeld, 2000). Table 2.1 shows a summary of the methods used for monitoring and sampling of the several indicator species.

The methods used by commercial analyzers for measuring O_3 and NO are well accepted to obtain ambient concentrations of these species (Parrish and Fehsenfeld, 2000). Therefore, the instruments used in the experiments did not require special considerations.

Table 2.1. Summary of monitoring and sampling methods for the measurement of indicator species.

Compound	Type of measurement	Method	References	Reported detection limit
NO	Continuous	Chemiluminescence	US EPA, 2001	15 ppt
NO_y	Continuous	Thermal conversion with converter located near the sample inlet/chemiluminescense	US EPA, 2001	15 ppt
O_3	Continuous	Ultraviolet absorption photometry	Parrish and Fehsenfeld, 2000	2-5 ppb
HNO_3	1-hr integrated sample	Na_2CO_3 coated annular denuder/analysis by ion chromatography	US EPA, 1999	0.78 ppb for 1-hr at a 10 L/min sampling
H_2O_2	1-hr integrated sample	Ti(IV)-H_2SO_4 coated annular denuders/analysis by spectrophotometry with a ferrous thiocyanate reagent at 475 nm	Possanzini et al., 1988	0.037 ppb for 1-hr at a 10 L/min sampling

However, measurement of NO_y species is not straightforward and requires of a number of special adaptations. As previously mentioned, NO_y species consist primarily of NO, NO_2, PAN, HNO_3, particulate nitrate (NO_3^-), and nitrous acid (HONO), roughly in that order of importance (Finlayson-Pitts and Pitts, Jr., 2000). NO_y is commonly measured by passing the airstream containing NO and the other oxides of nitrogen over a catalyst to convert the oxides into NO. Commercial heated molybdenum converters have been shown to readily reduce these species to NO, although the reduction efficiency for particulate nitrate may vary with the converter design (US EPA, 2001). The conversion is accomplished with the converter operating at 325 to 375°C. Above 375 degrees, the converter begins to convert other gases (e.g., ammonia), although the conversion has been reported at less than a few percent under typical operating conditions (Parrish and Fehsenfeld, 2000).

Plumbing changes or adaptations to standard NO_x sampling configurations in commercial NO_x analyzers allows one to maximize NO_y sample collection (Fitz, 2002). These alterations include external placement of the heated converter, shorter non-reactive sampling inlet lines to the converter, moving the location of the particle filter at the exit of the converter, and adding a larger capacity pump. Under this re-

arrangement of the measuring system, the HNO_3 and aerosol nitrate are not lost prior to the converter and they as well as other oxidized nitrogen species (i.e., PANs) are effectively reduced in the external converter to NO* (where NO* represents all of the NO_y compounds reduced to NO). Because the NO_x analyzer works on the principle that chemiluminescence emitted by NO_2 is directly proportional to its concentration, the measured NO* is taken as equivalent to the NO_y concentration. Results of an intercomparison of several NO_y measurement techniques conducted at a suburban site of Nashville, Tennessee (Williams et al., 1998), indicated that these instruments can reliably measure NO_y in typical urban and suburban environments (Parrish and Fehsenfeld, 2000). However, several concerns have been mentioned on the possibility of having measurement errors depending on the history of the converter's exposure (Fitz et al., 2003).

For the purposes of this research, NO_y converters were placed outside, leaving the instrument detector within the air-conditioned monitoring shelter. This was done to insure that the sampling lines did not absorb nitric acid (Fitz et al., 2003). In addition, the NO_y sampling was conducted using the shortest possible PFA Teflon line to the converter in order to prevent the adsorption (and loss) of nitric acid. The filters to protect the instruments of MoO dust were located at the exit of the converters insuring in this way the conversion of NO_3^- aerosols. In the Cincinnati and Mexico City monitoring campaigns, a commercial NO_x analyzer was adapted to the above specifications in order to measure the NO_y species.

The ideal method of measuring NO_y would be to measure each of the contributing species to the total expected NO_y. However, this effort requires specialized instruments currently only available in a few research centers. In several prior field studies, the sum of the concentrations of the individual NO_y species has been found to be less than the measured total NO_y using conversion to NO (Finlayson-Pitts and Pitts, Jr., 2000). A number of possible sources of error have been proposed to explain this negative difference; the most likely being the cumulative uncertainty resulting from taking successive small measurements.

NO_z species ($NO_z = NO_y - NO_x$) were not determined directly from the continuous measurement of the chemiluminescence NO_x analyzers because of the recognized difficulty this equipment has in accurately measuring NO_2 (US EPA, 2001). These kind of analyzers report NO_x as the sum of NO and

NO_2 detected by the instrument. However, the chemiluminescent NO_x analyzers not only measure NO_2 but also simultaneously respond to PAN and other organic nitrates (Winer et al., 1974; Grosjean and Harrison, 1985; Gerboles et al., 2003). As a result, routine NO_x measurements overestimate the actual NO_x and are not suitable for the calculation of indicators (US EPA, 2001).

Because of this operative deficiency of the NO_x analyzers, several empirical approaches were investigated to derive a surrogate concentration for the NO_z species. These included: use of direct NO_x measurements; a gross "corrected" estimation of NO_x from the sum of measured NO and an assumed measured-surrogate of the sum NO_2 + PAN; the estimation of NO_2 from the difference between the sum of estimated and measured individual contributions to the total measured NO_y; the empirical calculation of NO_x from the difference between the measured NO_y and an estimated fraction of the cumulative NO_y mass loss by deposition; the estimation of NO_2 from an empirical equation derived from selected ambient measurements of NO, NO_2, and NO_x; and the graphical interpolation of an uncertainty correction factor to NO_2 readings from measured NO and NO_x. Table 2.2 shows a summary of the general characteristics of the investigated approaches. All approaches shown in Table 2.2 were evaluated for consistency by means of several conceptual and graphical comparisons between the measured data and other information available in the literature. The BUWAL empirical equation ($NO_2 \cong 0.055[NO_x] + 55[1 - e^{-NO_x*0.01173}]$) was selected to calculate the surrogate NO_z. The criterion for its selection was that this relationship has been used by the European Environmental Agency to investigate the air quality trends of more than 200 cities in 15 countries of the European Union (de Leeuw et al., 2001).

Although the annular denuder methods have been tested in field measurements and have been suggested as appropriate for the determination of H_2O_2 and HNO_3 levels typical of urban areas (Possanzini et al., 1988; US EPA, 1999), there are several factors that may affect measured concentrations.

All the measured data were statistically analyzed in periods of 1-hr for their mean, standard deviation and range. An interpretation of the resulting average diurnal profiles was performed for each of the monitoring campaigns as an introduction for the subsequent analyses.

Table 2.2. Summary of empirical approaches investigated as alternatives to approximate concentration values of NO_x or NO_2 species useful for the estimation of NO_z concentrations.

Estimating approach	Equation/Basic procedure	Comments
NO_x as an upper limit of regular NO_x measurements[a]	$NO_x \cong NO + NO_2$ where: NO_x is the concentration measured by the chemiluminescent analyzer	The assumption that contributions of PAN and HNO_3 are minor and that they do not interfere may lead to important uncertainties in the calculation of NO_z.
NO_x as the sum of NO, and a surrogate of the sum of NO_2 and PAN	$NO_x \cong NO + NO_2$* where: NO is the measured concentration and NO_2* is the NO_2 reading from the instrument, which is then interpreted as a surrogate of the sum of the concentrations of NO_2 and PAN.	This approximation is based on the fact that PAN is quantitatively detected by the NO_x analyzer in the NO_2 mode and on the assumption that all of the HNO_3 is lost in the sample tubing during the transport of the air sample to the analyzer and that all the NO_3^- is retained on the filter of the air inlet sample to the analyzer.
NO_2 from the difference between measured and/or empirically derived NO_y species[b]	$NO_2 \cong NO_y - NO - HNO_3 - PAN^* - NO_3^-$ where: NO_y, NO and HNO_3 are the hourly average measured species; PAN is an estimated derived from a power regression[c] performed to reported concurrent measured PAN and O_3 data from urban and rural sites[d]; and NO_3^- is an estimated[e] from the reported ratio HNO_3/NO_3^- observed in a suburban site of Tennessee[f].	The assumptions that total NO_y is given by the sum of only the main nitrogen oxidized species ($NO_y = NO + NO_2 + PAN + HNO_3 + NO_3^-$); that PAN is related to the O_3 levels as reported for other regions; and that the ratio HNO_3/NO_3^- is universally constant, have not been tested for the Cincinnati and Mexico City regions.
NO_x from the hypothetical mass balance of the NO_x input and the NO_y deposition losses in the tropospheric regional airshed system from time zero (6:00 hr) to time t[g]	$NO_x(i) \cong NO_y(t) + DNO_y(t)$ where: $NO_x(i)$ is the hypothetical concentration at time t corresponding to the mass of NO_x input into the system from time zero to time t. $NO_y(t)$ is the measured concentration at time t. DNO_y is the cumulative deposition of NO_y at time t, and where the deposition term is a function of a time-varying deposition velocity and of the depth of the mixed layer in that region.	This empirical estimation is dependent on the accuracy of the measurement of the mixing layer, and on the assumption that the deposition coefficients required to obtain the deposition velocity are universal and do not change with time of the day.
NO_2 from NO_x measurements[h]	$NO_2 \cong 0.055[NO_x] + 55[1 - e^{-NO_x*0.01173}]$ where: NO_x are the readings reported by the chemiluminescent analyzer.	Empirical equation based on selected monitoring data in Germany, Austria and Switzerland. Used to estimate the air quality trends of a number of cities in the European Union.[i]
NO_2 uncertainty factor from measurements of NO, NO_2 and NO_x[j]	Graphical interpolation of the NO_2 relative expanded uncertainty using a standard graph of NO_x versus NO.	The interpolation is difficult to perform. It gives very approximated values particularly at low NO_x and NO concentrations.

[a] Chameides et al., 1992.
[b] For the Cincinnati case.
[c] $PAN = 0.0004[O_3]^{1.9524}$; $R^2 = 0.97$.
[d] Roberts et al., 1995.
[e] $.NO_3^- = 0.2489[HNO_3]$; $R^2 = 0.878$
[f] Williams et al., 1998.
[g] Blanchard et al., 1999.
[h] BUWAL, 1997.
[i] de Leeuw et al., 2001.
[j] Gerboles et al., 2003.

These factors include: the possibility of uptake and conversion of other nitrogen containing compounds in the HNO_3 sampling and artifact H_2O_2 formation from O_3 on denuder walls (Possanzini et al., 1988; Sakugawa et al., 1990; Finlayson-Pitts and Pitts, Jr., 2000; Saver et al., 2003).

The monitoring and sampling programs in Cincinnati and Mexico City were supported with tracking down procedures and data validation assessment recommendations taken from the US EPA (US EPA, 1994, 1998). Because in both cases the measurements of O_3, NO, and NO_y were conducted at official monitoring sites, the calibration and operation of the equipment was done under protocols of the US EPA by the personnel in charge of the monitoring stations (HCDOES, 2003; RAMA, 2004). These protocols include the accuracy evaluation between the field measurements and a quantitative transfer standard.

The adapted chemiluminescent NO_x analyzers (or NO_y* analyzers) were calibrated with the same protocol as used for typical NO_x analyzers. One standard gas was supplied at the inlet of the converters. The common calibrated audit systems consisted of zero air, NIST-traceable NO gas in a cylinder, and an ozone generator. The response of the molybdenum converter to convert NO_y species was verified through a response comparison of the NO_y* instrument with the concurrent measurements of NO_x from the analyzer that was measuring NO. Figure 2.1 shows a general scheme of the setup distribution of the different instruments in the monitoring sites.

An additional validation of the performance of the NO_y* analyzer in Mexico City was done through the evaluation of the statistical correlation between the NO_y concentrations and their concurrent CO levels. Because both CO and NO_y have the same origin, a good correlation should be observed between them under indirect evaluation (Sillman et al., 1997). The sampling and analysis of HNO_3 and H_2O_2 had their own quality assurance program. The procedures used were adapted from the original methods themselves and from general recommendations made by the US EPA (1998, 1999). Special emphasis was placed on sampling travel blanks and analytical calibration curves. The correlation between O_3 and ($2H_2O_2$ $+NO_z$) was used to indirectly evaluate the consistency of the NO_y measurements in Cincinnati (Sillman et al., 1997).

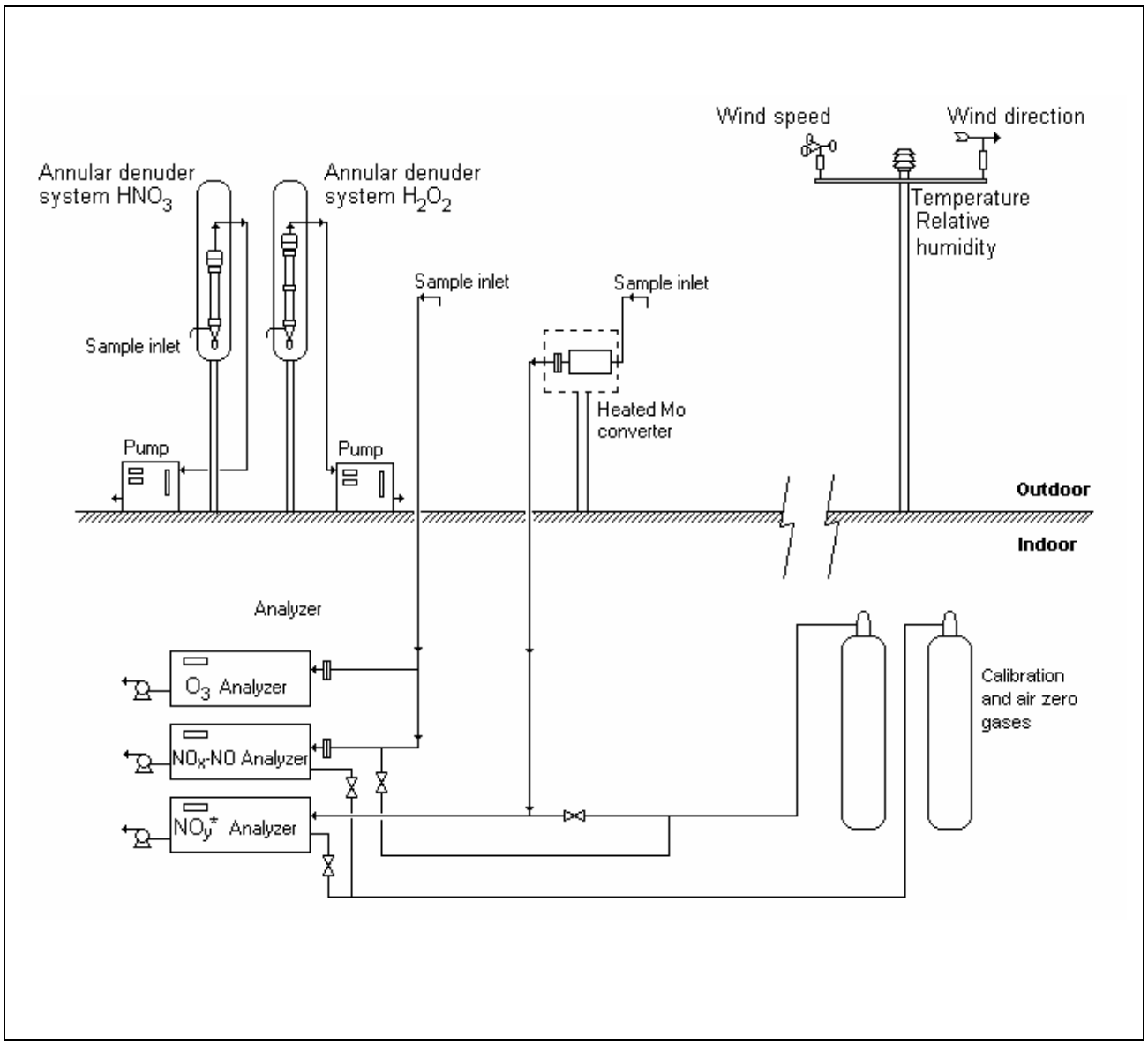

Figure 2.1. Schematic diagram of the general setting up of the instruments in the monitoring sites.

2.2 Photochemical Indicators Evaluation

Photochemical indicators consist of correlations and calculated ratios of secondary photochemical products. Because of the lack of a standard procedure for using PIM, however, the PIM, the consistency of the measurements must be validated. NO_y measurements were evaluated for two purposes: (1) to insure that HNO_3 was included in the measurement (section 2.1), and (2) to insure that ambient conditions were appropriate. Because the connection between NO_y and O_3-NO_x-VOC sensitivity is due primarily to HNO_3, rather than to other components of NO_y, it is not acceptable to substitute NO_x or the sum of NO_x and organic nitrates for NO_y in the PIM determinations (Sillman 1995; 2002). In addition, measurements affected by rainfall events (at the site or upwind) cannot be used as NO_y-VOC indicators because HNO_3 has been removed. Other suspicious conditions, such as the presence of high NH_3 concentrations in the location of the measurement, should be carefully evaluated, because the chemistry of aerosol formation acts as an important removal path for HNO_3.

The validity of the measurements performed during the monitoring campaigns was evaluated following the recommendations of Sillman (2002). These evaluations were done by examining scatterplot patterns of O_3 versus NO_y, as well as versus NO_z and HNO_3, and comparing them to previously measured and/or modeled correlations. According to Sillman, these scatterplots should be imposed on the pattern of research-grade measured and/or model correlations for well identified NO_y-sensitive and VOC-sensitive conditions. To be valid, measured values should fall within the broad range of model values. However, if a significant portion of the measurements fall outside of model values, then the measurements for the day in question should not be interpreted as NO_y-VOC indicators. In all cases, the evaluations must be done to measurements performed during afternoon hours (13:00 to 17:00 hr).

Figure 2.2 shows the scatterplots of measured correlations between O_3 and NO_y and NO_z obtained in several research experiments performed in regions previously identified with either VOC- or NO_x sensitive conditions. The overlapping of the measured values on these patterns should be interpreted as a preliminary identification of either NO_x- or VOC-sensitive conditions associated to each region.

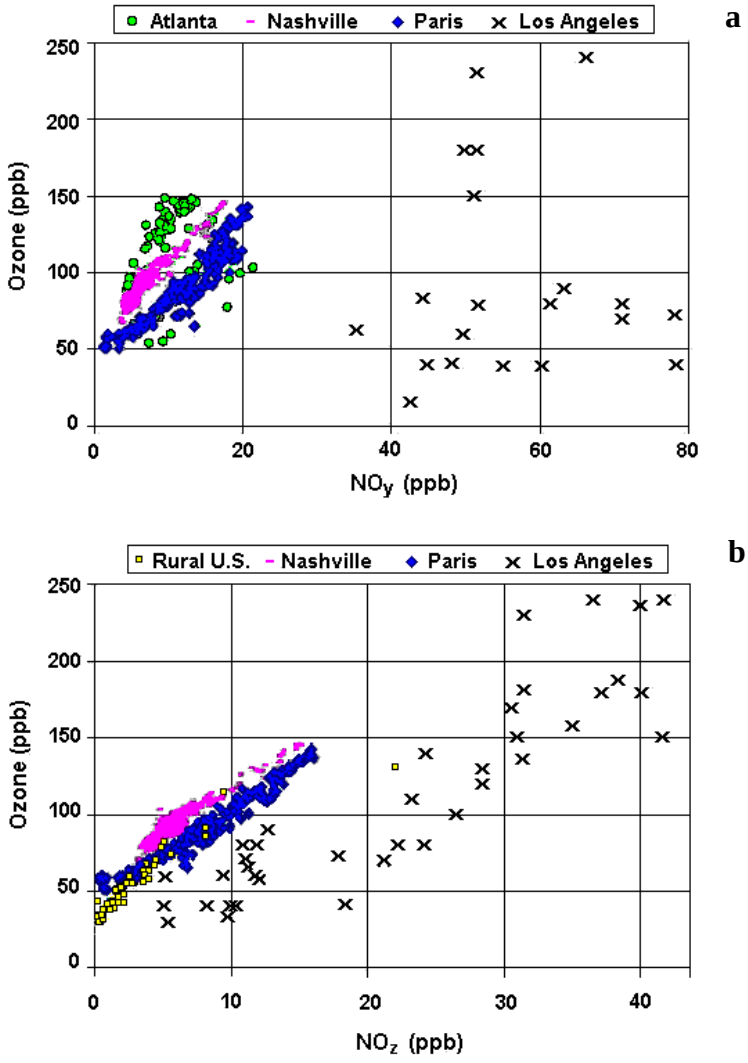

Figure 2.2. Measured scatterplot comparison between O_3 and NO_y in (**a**) Atlanta (circles), Nashville (dashes); Paris (diamonds) and Los Angeles (crosses); (**b**) measured correlation between O_3 and NO_z in Nashville (dashes), Paris (diamonds), Los Angeles (crosses) and from rural sites in the Eastern U.S. (squares), from measurements reported by Sillman et al. (1997, 1998, 2003) and Trainer et al. (1993). The identified conditions are: NO_x-sensitive in Atlanta, GA., mixed sensitivity in Nashville, TN. and Paris, France, and strongly VOC-sensitive in Los Angeles, CA. Figures adapted from Sillman 2002 and 2003.

Figure 2.3 shows the scatterplots of modeled O_3, NO_y, and NO_z correlations for VOC- and NO_x-sensitive conditions obtained from 3-D photochemical simulations of several representative regions in the U.S., performed by Sillman 2002; Sillman and He, 2002. These plots show four different pattern conditions: NO_x-sensitive, VOC-sensitive, mixed, and NO_x-titration. The interpretation of the first three conditions directly arises from the definitions previously mentioned in this dissertation. The NO_x-titration condition was included by Sillman, and Sillman and He, to consider that situation in which the locations under study are near large sources of NO_x. These locations typically have relatively low O_3. At the same time, O_3 has been affected primarily by the titration reaction ($O_3 + NO \rightarrow NO_2 + O_2$) in the presence of directly emitted NO, rather than by O_3 production mechanisms. This condition should be carefully evaluated. Appendix A presents the modeling-base definition of each of the conditions mentioned above.

Comparison with model correlations is considered important because the criteria for NO_x-sensitive and VOC-sensitive indicator ratios were based on models with specific scatterplot patterns. If measurements are not consistent with these model scatterplot correlations, the indicator ratios may not be valid. Sillman (2003) and Sillman and He (2002) have provided data files and plots of modeled values for the previously mentioned correlations that can readily be used for evaluation purposes.

It should be noted that several predicted NO_x-titration data points overlap other data points for other conditions. Therefore, at one extreme of Figure 2.3(b), there is the possibility that measured data points may fall within this zone of scatterplots patterns and create confusion in the interpretation of the data. To solve this problem, simple procedures that would identify when a value was associated with NO_x-titration conditions were investigated. The best approach resulted from the combination of photochemical age concept (Trainer et al., 1993) with the scatterplot patterns for each of the VOC-sensitive and NO_x-titration conditions (Sillman, 2002). As previously mentioned, the NO_x-titration is related to situations in which a given location is near the influence of relatively large sources of NO_x. Trainer et al. (1993) have suggested that to discriminate the influence of fresh emissions in the measurement of NO_y species in rural areas, a figure ≤ 0.6 for the ratio NO_x/NO_y could be indicative of the arriving of chemically aged air masses.

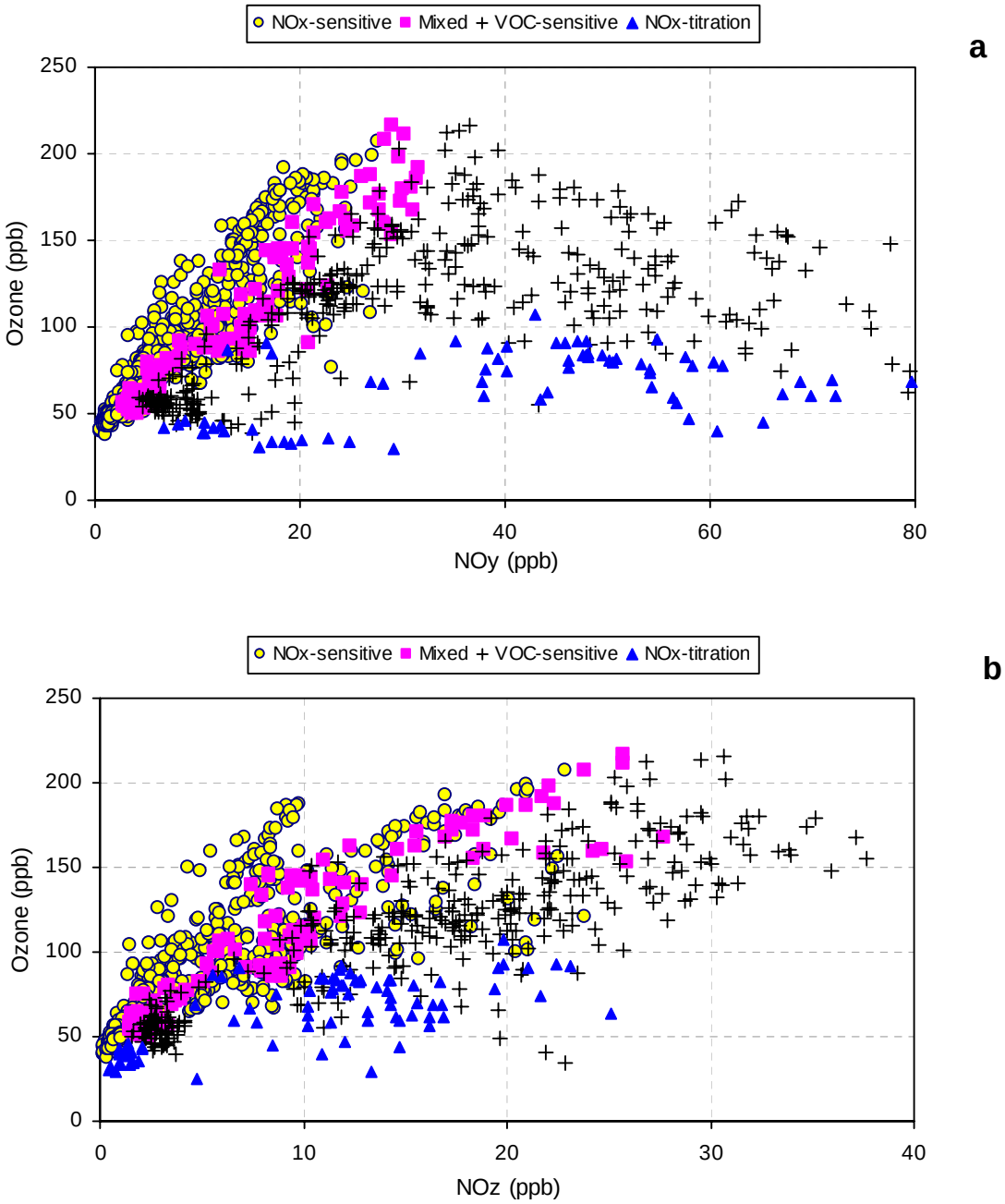

Figure 2.3. Predicted scatterplot patterns for (**a**) O_3 vs. NO_y, and (**b**) O_3 vs. NO_z from 3-D simulations listed in Table 1 in Sillman and He (2002). Each location is classified as NO_x-sensitive (circles), VOC-sensitive (crosses), mixed or with near-zero sensitivity (squares), and dominated by NO_x-titration. Scatterplots constructed from data file available from Sillman (2003).

However, in urban areas, this criterion could not be appropriate, because there is always the possibility that local traffic will cause fresh emissions. Sillman (2002) has suggested a limit value of 0.7 for this ratio. The correlation between O_3 and the corresponding ratios NO_x/NO_y for the VOC-sensitive and NO_x-titration conditions is shown in Figure 2.4.

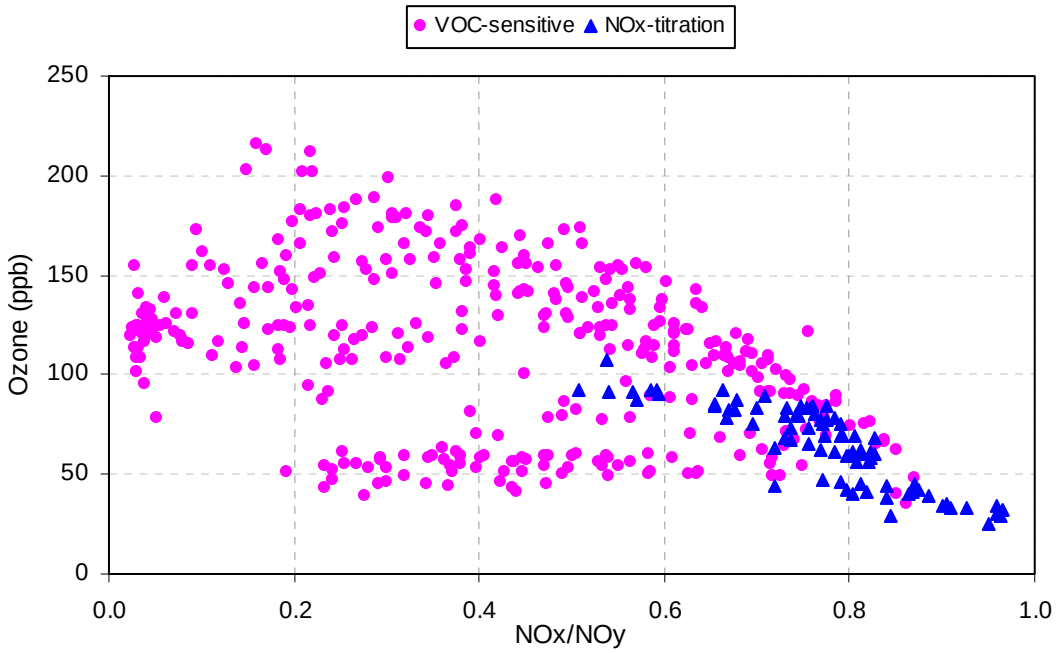

Figure 2.4. Scatterplot patterns for predicted O_3 vs. the ratio NO_x/NO_y from 3-D simulations listed in Table 1 in Sillman and He (2002). From data file available from Sillman (2003).

The idea behind this gross evaluation was simple. If the superimposing of the scatterplot correlation of measured O_3 vs. the estimated ratio NO_x/NO_y over the patterns clustered in Figure 2.4 matched the data points of the predicted O_3 vs. NO_x/NO_y correlation for the NO_x-titration condition, or if the measured NO_x/NO_y ratio was greater than 0.7, then this observation might not be appropriate for the indicator method application.

Two very important assumptions were made in the application of PIM. The first was that, due to the lack of photochemical modeling information for Cincinnati and of accurate simulated results for

Mexico City, the predicted correlation values of Sillman and He (2002) and Sillman (2003) would be valid for inferring the consistency of the indicator evaluations for the study cities.

The second assumption involved the fact that indicators were measured at only one representative site in both cities. Sillman (2002) suggested that measurements of indicators be made over a network broad enough to include most of the locations with elevated O_3 in the study region. If the latter were not possible, however, the selected site should be representative of the ozone air pollution situation in the region. The monitoring sites in Cincinnati (Taft monitoring station) and in Mexico City (Santa Ursula monitoring station) were selected for this very reason. It was also assumed that the single measurement site could be compensated for with the collection of data during a representative monitoring period. In this situation, the sampling would include air masses coming from the dominant sectors of the region and not from just one particular event. There was one attempt to measure O_3, NO_y, and HNO_3 species at a rural site of Mexico City, but several inconsistencies were observed in the measurements. Additional details regarding the experimental work are presented in chapter 4.

Once the consistency of the results was evaluated, the data were interpreted numerically and graphically. The afternoon species ratios of O_3/NO_y and O_3/surrogate NO_z (or NO_z*) and afternoon NO_y concentrations for both cities were directly compared with the original indicator transitional values shown in Table 1.1. Subsequently, the measured correlations of O_3 versus NO_y (and of measured O_3 vs. NO_z*) were superimposed over the respective simulated correlations for mixed sensitivity conditions given by Sillman (2003) and Sillman and He (2002). Measured data points close to the mixed values were identified as having mixed sensitivity, while O_3/NO_y (or O_3/NO_z*) ratios significantly above or below this correlation were interpreted as representing NO_x-sensitive or VOC-sensitive conditions, respectively.

2.3 Complementary Data Analysis Tests

Several additional approaches were used to validate and/or reinforce the findings of the O_3-NO_x-VOC sensitivity analysis in Cincinnati and Mexico City. The first approach was the investigation of the weekend/weekday effect on the peak O_3 concentrations. The basic assumption supporting this semi-

empirical evaluation was that, in NO_x-sensitive locations (i.e., locations with abundant VOC relative to NO_x), weekend O_3 peak should decrease significantly compared with the average weekday O_3 peak, as a consequence of the weekend reductions in NO_x emissions (i.e., reduction in diesel trucks and gasoline vehicles traffic) (right lower corner of EKMA diagram in Figure 1.1). In areas where ozone formation is VOC-limited (left upper corner of EKMA diagram in Figure 1.1), weekend O_3 peak should exhibit a significantly higher value relative to the average weekday O_3 peak due to the weekend reductions in NO_x emissions (Altshuller et al., 1995; Fujita et al., 2002; Heuss et al., 2003; Pun et al., 2003).

A two-tailed *t*-test was used to test the statistical significance of the mean differences. The *t*-test has been used to interpret weekend/weekday differences in ambient air (US EPA, 1979) and is appropriate for the analysis of small populations (Spiegel, 1961). The means tested were the weekend and weekday peak O_3 and mean weekend and weekday 6:00 to 9:00 hr (6-9 am) NO concentrations. The mean 6-9 am NO was assumed to be a surrogate of the NO_x morning emissions because the difficulty to know the exact uncertainty of the NO_x measurements. The test of hypotheses and significance were formulated based on the definition of NO_x- and VOC-sensitive conditions, as explained in chapter 1. Table 2.3 shows the main characteristics of the statistical tests. This evaluation was extended to the max 8-hr O_3 average.

The comparison of weekend/weekday differences in ozone and precursor species with OBM has been explored previously. Blanchard and Fairley (2001) investigated the use of the "extent of reaction" concept, which is based on the smog production (*sp*) algorithm, to strengthen the delineation of the NO_x- or VOC-limitation in urban areas. However, the strong dependence of the *sp* algorithm calculation on a relatively high number of empirical and practical assumptions seems to be associated to the uncertainty of the results.

Sillman and He (2002) have investigated the *sp* algorithm as a tool to delineate the NO_x-VOC sensitivity transition, in an approach similar to the PIM graphical concept using 3-D models, and found that, although there was a certain correlation with the NO_x-VOC sensitivity predicted with models, its behavior showed a systematic variation with O_3, making the identification of the transition range difficult.

Table 2.3. Statistical tests used to differentiate the weekend/weekday effect on maximum afternoon O_3.

Parameter	Hypothesis[a]	Implication
Maximum 1-hr and 8-hr O_3 concentration	H_0: $\mu_{O3WE} = \mu_{O3WD}$	The change in WE maximum O_3 is insignificant, likely to be caused by a VOC-sensitive condition provided that the reduction in morning WE-NO_x emissions is significant
	H_1: $\mu_{O3WE} < \mu_{O3WD}$	The decrease in maximum WE maximum O_3 is significant, likely due to a NO_x-sensitive condition on condition that morning WE-NO_x emissions is significant
Morning 6-9 a.m. NO average concentration	H_0: $\mu_{6\text{-}9am\ NO\ WE} = \mu_{6\text{-}9am\ NO\ WD}$	The reduction in morning WE-NO_x emissions is insignificant probably due to mere chance
	H_1: $\mu_{6\text{-}9am\ NO\ WE} < \mu_{6\text{-}9am\ NO\ WD}$	The reduction in morning WE-NO_x is significant likely due to the reduction in WE activities

[a] Two-tailed *t*-test assuming equal variances.

Several empirical evaluations based on the chemistry of tropospheric formation of O_3 were used for assessing the characteristics of the O_3-formation scenarios in Cincinnati and Mexico City. These evaluations consisted basically on the analysis of the average duration of O_3 accumulation and the average rate of O_3 accumulation following a procedure suggested by Fujita et al. (2002). These evaluations were complemented with the analysis of the average rate of NO depletion. The duration of O_3 accumulation was estimated by calculating the difference between the occurrence of maximum O_3 (t_{maxO3}) and the time in the morning when NO and O_3 crosses over ($t_{NO=O3}$). The NO-O_3 crossover time represents the end of the morning inhibition period in which fresh NO emissions effectively titrate O_3 and restrain radical formation. The rate of O_3 accumulation (in ppb/hr) is the ratio of the increase in O_3 from $t_{NO=O3}$ to t_{maxO3} and the duration of O_3 accumulation is the time from the end of the inhibition to the maximum O_3 concentration (Rate = $\{[O_3]_{max} - [O_3(t_{NO=O3})]\}/\{t_{O3max} - t_{NO=O3}\}$). The rate of NO depletion was assumed to be equivalent to the ratio of the difference in NO concentrations from the time of its morning peak to the time when the O_3 peak occurs (Rate = $\{[NO]_{max} - [NO]_{(t_{NO\ =\ O3\ max})}\}/\{t_{NO\ max} - t_{NO\ =\ O3\ max}\}$).

An empirical interpretation of the severity of the event suggested by Milford et al. (1994) and Sillman (1999) was used for the evaluation of the consistency of the NO_x-VOC sensitivity suggested by photochemical indicators results and by theoretical sensitivity determined by the ratio of initial VOC/NO_x emissions. These authors have suggested that environmental conditions prone to have higher ozone precursors can be associated with either higher emission densities (i.e., larger urban areas) or with more restricted meteorological conditions (i.e., light winds and low daytime vertical mixing) or with a combination of both. Sillman has proposed an explanation for the severity of event effect by doing an analogy with the theoretical concept of Kleinman (1991, 1994) that indicates that the split between the NO_x-sensitive and *NO_x-saturated* (or VOC-sensitive) regimes is related to the relative supply of NO_x (from emissions) in comparison with the supply of radicals generated by sunlight. Freshly emitted plumes of polluted air have an initial NO_x supply that greatly exceeds the supply of radicals. As the plume ages the total amount of radicals created during the process of photochemical evolution becomes equal with and eventually surpasses the initial NO_x-source, causing a switch from *NO_x-saturated* to NO_x-sensitive conditions. Under the analogy of Sillman, if the source of NO_x source per unit volume in an airbasin is high (after considering the effect of dilution through daytime vertical mixing), it will take more time for the accumulated source of radicals (from the VOCs) to become equal with and surpass the NO_x source. As a result, a *NO_x-saturated* (VOC-sensitive) condition will persist for a longer time. But, if the NO_x source is low, the accumulated radical source will exceed the NO_x source after a short period of photochemical aging and the system will shift to NO_x-sensitive conditions.

2.4 Intercomparison Tests

Sillman and He (2002) have suggested that their transition values for indicator ratios may not be valid for every region in the world. On the one hand, they are appropriate for the Cincinnati airshed region, because they were obtained from photochemical simulations in regions of the U.S. On the other, those transition values might not be adequate for airshed regions outside the geographic region of North America such as Mexico City.

One attempt was made to evaluate the consistency of the photochemical indicator method (PIM) to the Mexico City observations using a state-of-the-art photochemical model (the Multiscale Climatic and Chemistry Model (MCCM)). However, the lack of sufficient input data to the model for the measurement period limited its application.

As an alternative, a semi-quantitative evaluation of the consistency of the NO_x-VOC sensitivity diagnosed with the photochemical indicator approach in Mexico City was done through the intercomparison of the measured indicator results with the findings of a preliminary effort carried out by Sosa et al. (2000) to identify the local O_3-NO_x-VOC sensitivity, and with the results of a simple box model results by Gaffney et al., (1999) to simulate some secondary species indicators. The measurements used by Sosa et al. and Gaffney et al. were obtained from a research-grade campaign carried out in Mexico City during the winter of 1997 (Doran et al., 1998; Edgerton et al., 1999). In addition, the measured species indicators and indicators ratios from the present research monitoring campaign were intercompared with the results of a modeling experiment with the MCCM for a historical ozone event. A direct comparison between all the available information could not be performed because the data had different averaging times, different simulating days, and/or different approaches of estimation.

Sosa et al. (2000) attempted to apply the PIM of Sillman based on a compilation of measurements taken at three different locations in Mexico City over an 18-day period. The monitoring locations were: La Merced (close to the downtown), Azcapotzalco (~ 13 km northeast of La Merced), and IMP (~ 8 km north of La Merced). They studied the correlations O_3/NO_y*, O_3/NO_z*, and O_3/HNO_3^-* (where the asterisks indicates surrogates), but they could not arrive at conclusive results.

In addition to the above evaluation, Sosa et al. (2000) carried out a number of modeling experiments with the CIT 3-D photochemical model to study O_3 formation in MCMA and to diagnose the NO_x-VOC sensitivity. Although they could produce in a relatively good agreement the O_3 daily pattern with the observed O_3 measurements of one selected day, and found that all of the urbanized sites were roughly on the crest between NO_x-sensitive and VOC-sensitive regions, they could not confirm the consistency of these results. They arrived at their final conclusions after performing an artificial increment

(a factor of three) to the VOC emissions in the base emission inventory. They also reported that the CIT model had problems reproducing the vertical meteorology of the region. The available simulation data from the CIT study was limited to the Merced site (Sosa et al., 2000).

The modeling experiment with the MCCM was a simulation of the spatial distribution of indicator species and indicator ratios for one historical event (March 3, 1997 from 14:00-15:00) using a previously integrated input database. It covered the Mexico City's entire region, including parts of two neighboring states. The emissions for the simulation were taken from an ozone precursors official inventory for the year 1995 (GDF, 1995). The results of the modeling experiment were obtained after a number of preliminary evaluations and discussions of the most representative modeling scenario. A graphical interpolation software package (Surfer 7) was used to generate the approximate species concentrations for the different locations of interest. García (2002) implemented the MCCM to study air quality and meteorological impact for a project to restore an artificial lake in northeast Mexico City and to study the reduction of NO_x emissions from a power plant in the region. He found that the MCCM could better reproduce ozone concentrations with a ~ 40% reduction in the NO_x emissions of the official base inventory. Jazcilevich et al. (2003) used the same input database and MCCM to investigate the influence of wind patterns on the 3-D behavior of air pollutants in central Mexico. They concluded that MCCM was able to reproduce more accurately the meteorology of the region than other models, and, as a consequence, to better reproduce the dispersion of the low reactive air pollutants. These two studies did not investigate further the NO_x-VOC sensitivity of the region. Appendix B presents a summary of the main components of the MCCM.

Gaffney et al. (1999) used a simple box model approximation to predict the "average" concentrations of PAN, NO_y (as NO_y-NO), and O_3 for Mexico City on a typical smog-polluted day based on a set of data collected in March 1997. The results of the simple box modeling were assumed to apply to the entire Mexico City air basin. Because no attempt was done by Gaffney et al. to define a NOx-VOC sensitivity for Mexico City, the data were worked to obtain several different indicator species useful required for the intercomparison.

Additional details on the preparation of the CIT and MCCM 3-D models, are given elsewhere (Grell et al., 1994; García, 2002; Sosa et al., 2002; Jazcilevich et al., 2003). Gaffney et al. (1999) did not provide more details on the particular characteristics of their box model. Table 2.4 shows a summary of the type of data available to perform the intercomparison.

Table 2.4. Measured and simulated data available and characteristics of the information for the intercomparison of measured indicator results in Mexico City.

Approach	Species	Averaging time and site of measurement/simulation
Measurement approach[a] (March 2-19, 1997)	O_3	1-hr average at La Merced and Azcapotzalco sites[b]
	NO_x	1-hr average at La Merced and Azcapotzalco sites[b]
	O_3	6-hr average at La Merced and Azcapotzalco sites
	NO_x	6-hr average at La Merced and Azcapotzalco sites
	$HNO_3 + NO_3^-$	6-hr average at La Merced during IMADA-AVER[c]
	PANs	30-min and 6-hr average at IMP during IMADA-AVER[d]
	O_3/NO_y ratio	6-hr average at La Merced and Azcapotzalco sites
	O_3/NO_z ratio	6-hr average at La Merced and Azcapotzalco sites
CIT simulation[a] (Sunday, March 2, 1997)	O_3	Surface hourly modeled at La Merced position
	NO, NO_2	Surface hourly modeled at La Merced position
	PAN	Surface hourly modeled at IMP position
	HNO_3	Surface 6-hr average modeled at La Merced position
MCCM simulation[e] (Monday, March 3, 1997)	O_3	Surface 1-hr (14:00-15:00 hr) covering the MCMA region (~ 80 x 75 km in 3600 grid data points)
	NO, NO_2	
	PAN	
	HNO_3	
	NO_3^-	
	H_2O_2	
	HCHO	
Simple Box Model[d] (Winter, 1997)	O_3	Average for afternoon hours for the whole Mexico City region
	NO_y (as $NO_y - NO$)	
	PAN	

[a] Sosa et al., (2000).
[b] SMA historic data files. (Red Automatica de Monitoreo Atmosferico, SIMA, http://sma.df.gob.ma/simat/)
[c] Edgerton et al., (1999) and Chow et al., (2003).
[d] Gaffney et al., (1999).
[e] Obtained from García and Jazcilevich (2004).

2.5 References

Altshuller, S.M., Arcado, T.D., Lawson, D.R. (1995) Weekday versus weekend ambient ozone concentrations: discussion and hypothesis with focus on Northern California. J. Air & Waste Manage. Assoc. **45**, 161-180.

Blanchard, C.L., Fairley, D. (2001) Spatial mapping of VOC and NO_x-limitation of ozone formation in Central California. Atmos. Environ. **35**, 3861-3873.

Blanchard, C.L., Lurmann, F.W., Roth, P.M., Jeffries, H.E., Korc, M. (1999) The use of ambient data to corroborate analyses of ozone control strategies. Atmos. Environ. **33**, 369-381.

BUWAL (1997) NO_2 Immissione in der Scweiz 1990-2010. Schriftreihe Umwelt nr. 289, Bundesamt für Umwelt, Wald und Landschaft, Bem, Switzerland.

Chameides, W.L., Fehsenfeld, F., Rodgers, M.O., et al. (1992) Ozone precursor relationships in the ambient atmosphere. J. Gephys. Res. **97**, 6037-6055.

Chow, J.C., Watson, J.G., Edgerton, S.A., Vega, E. (2002) Chemical composition of $PM_{2.5}$ and PM_{10} in Mexico City during winter 1997. Sci. Total. Environ. **287**, 177-201.

de Leeuw, F., Moussiopoulos, N., Bartonva, A., Sahm, P., Pulles, P., Visschedijk, A. (2001) Air Quality in Larger Cities in the European Union. Topic Report 3/2001. Prepared to European Environmental Agency. Copenhagen, Denmark. February.

Doran, S.C., Abbott, J.L., Archuleta, J., et al., (1998) The IMADA-AVER boundary layer experiment in the México City area. Bull. Am. Meteor. Soc. **79**, 2497-2508.

Edgerton, S.A., Bian, X., Doran, J.C., et al., (1999) Particulate air pollution in Mexico City: a collaborative research project. J. Air & Waste Manage. Assoc. **49**, 1221-1229.

Finlayson-Pitts, B.J., Pitts, Jr., J.N. (2000) Chemistry of the Upper and Lower Atmosphere. Academic Press. San Diego, CA.

Fitz, D.R. (2002) Evaluation of NO_y and Nitric Acid Measurement Methods and Collection of Ambient Data. Final Report. 02-AP-18392-03-FR. Prepared for California Air Resources Board Monitoring and Laboratory Division. CERT, College of Engineering, University of California, Riverside, CA. May.

Fitz, D. R., Bumiller, K., Lashgari, A. (2003) Measurement of NO_y during the SCOS97-NARSTO. Atmos. Environ. **37** (Suplement No. 2), S119-S139.

Fujita, E.M., Campbell, D.E., Stockwell, W., Keislar, W., Zrelinska, R.E., Sagebiel, J.C., Goliff, W., Keith, M., Bowen, J.L. (2002) Weekend/Weekday Ozone Observations in the South Coast Air Basin: Volume II – Analysis of the Air Quality Data. Final Report. Contract No. ACI-0-29086-01. Coordinating Research Council. Alpharetta, GA. April.

Gaffney, J.S., Marley, N.A., Cunningham, M.M., Doskey, P.V. (1999) Measurements of peroxyacyl nitrates (PANS) in Mexico City: implications for megacity air quality impacts on regional scales. Atmos. Environ. **33**, 5003-5012.

García, J.A.R. (2002) Evaluación de Escenarios Utilizando el Modelo Regional de Calidad del Aire *Multiscale Climate Chemistry Model*. Tesis Doctorado. Universidad Nacional Autónoma de México. Mexico City, Mexico. May.

García, J.A.R., Jazcilevich, A. (2004) On-line collaboration. Center for Atmospheric Sciences, National Autonomous University of Mexico. Mexico City, Mexico.

GDF (1995) Inventario de Fuentes de Area Precursores de Ozono y Monóxido de Carbono para la Zona Metropolitana de la Ciudad de México, 1995. Subdirección de Inventario de Emisiones. Gobierno del Distrito Federal. Cd. de México. México.

Gerboles, M., Lagler, F., Rembges, D., Brum, C. (2003) Assessment of uncertainty of NO_2 measurements by the chemiluminescence meted and discussion of the quality objective of the NO_2 European Directive. J. Environ. Monit. **5**, 529-540.

Grell, G.A., Emeio, S., Stockwell, W.R., Schenemeyer, T., Forkel, R., Michalakes, J., Knoche, R., Seidl, W. (2000) Application of a multiscale, coupled MM5/chemistry model to the complex terrain of the VOTALP valley campaign. Atmos. Environ. **34**, 1435-1453.

Grosjean, D., Harrison, J. (1985) Response of chemiluminescence NO_x analyzers and ultraviolet ozone analyzers to organic air pollutants. Environ. Sci. Technol. **19**, 862-865.

HCDOES (2003) Air Quality Management División, Hamilton County Department of Environmental Services. Cincinnati, OH.

Heuss, J.M., Kahlbaum, D.F., Wolff, G.T. (2003) Weekday/Weekend Ozone Differences: What can we learn from them? J. Air & Waste Manage. Assoc. **53**, 772-788.

Jazcilevich, A.D., Garcia, A.R., Ruiz-Suárez, L.G. (2003) A study of air flow patterns affecting pollutant concentrations in the Central Region of Mexico. Atmos. Environ. **37**, 183-193.

Kleinman, L.I. (1991) Seasonal dependence of boundary layer peroxide concentration: the low and high NO_x regimes. J. Geophys. Res. **96**, 20721-20734.

Kleinman, L.I. (1994) Low and high-NO_x tropospheric photochemistry. Geophys. Res. **99**, 16831-16838.

Milford, J.B., Gao, D., Sillman, S., Blossey, P., and Russell, A.G. (1994) Total Reactive Nitrogen (NO_y) as an Indicator of the Sensitivity of Ozone to Reductions in Hydrocarbon and NO_x Emissions. J. Geophys. Res. **99**, 3533-3542.

Parrish, D.D., Fehsenfeld, F.C. (2000) Methods for gas-phase measurements of ozone, ozone precursors and aerosol precursors. Atmos. Environ. **34**, 1921-1957.

Possanzini, M., DiPalo, V., Liberti, A. (1988) Annular denuder meted for determination of H2O2 in the ambient atmosphere. Sci. Total Environ. **77**, 203-214.

Pun, B.K., Seigneur, C., White, W. (2003) Day-of-week behaviour of atmospheric ozone in three U.S. cities. J. Air & Waste Manage. Assoc. **53**, 789-801.

RAMA (2004) Red Automática de Monitoreo Atmosférico. Gobierno de la Ciudad de México. D.F. México.

Roberts, J.M., Tanner, R.L., Newman, L. (1995) Relationships between PAN and ozone at sites in Easthern North America. J. Geophys. Res. **100**, 22821-22830.

Sakugawa, H., Kaplan, I.R., Isai, W., Cohen, Y. (1990) Atmospheric hydrogen peroxide. Environ. Sci. Technol. **24**, 1452-1461.

Saver, C.G., Pisano, J.T., Fitz, D.R. (2003) Tunable diode laser absorption spectrometer measurements of ambient nitrogen dioxide, nitric acid, formaldehyde, and hydrogen peroxide in Parlier, California. Atmos. Environ. **37**, 1583-1591.

Sillman, S. (1995) The use of NO_y, H_2O_2, and HNO_3 as indicators for O_3-NO_x-VOC sensitivity in urban locations. J. Geophys. Res. **100**, 11497-11508.

Sillman, S. (1999) The relation between ozone, NO_x, and hydrocarbons in urban and polluted rural environments. Atmos. Environ. **33**, 1821-1845.

Sillman, S. (2002) Evaluation of Observation-Based Methods For Analyzing Ozone Production and Ozone-NO_x-VOC Sensitivity. Report to: National Exposure Research Laboratory. National Exposure Research Laboratory. Office of Research and Development. U.S. EPA. Research Triangle Park, NC 27711.

Sillman, S. (2003) Observation-Based Methods (OBMs) For Analyzing Urban/Regional Ozone Production and Ozone-NO_x-VOC Sensitivity. University of Michigan. Available at: http://www-personal.engin.umich.edu/~sillman.

Sillman, S., He, D., Cardelino, C., Imhoff, R.E. (1997) The use of photochemical indicators to evaluate ozone-NO_x-hydrocarbon sensitivity: case studies from Atlanta, New York and Los Angeles. J. Air & Waste Manage. Assoc. **47**, 1030-1040.

Sillman, S., He, D., Pippin, M., Daum, P., Kleinman, L., Lee, J.H., Weinstein-Lloyd, J. (1998) Model correlations for ozone, reactive nitrogen and peroxides for Nashville in comparison with measurements: implications for VOC-NO_x-sensitivity. J. Geophys. Res. **103**, 22629-22644.

Sillman, S., He, D. (2002) Some theoretical results concerning O_3-NO_x-VOC chemistry and NO_x-VOC indicators. J. Geophys. Res. **107**, D22, 4659, doi:10.1029/2001JD001123.

Sillman, S., Vaudatard, R., Menut, L., Kley, D. (2003) O_3-NO_x-VOC sensitivity and NO_x-VOC indicators in Paris: results from models and Atmospheric Pollution Over the Paris Area (ESQUIF) measurements. J. Geophys. Res. **108**, D17, 8563, doi:10.1029/20002JD001561.

Sosa, G., West, J., San Martini, F., Molina, L.T., Molina, M.J. (2000) Air Quality Modeling and Data Analysis for Ozone and Particulates in Mexico City. Rep. No. 15. MIT Integrated Program on Urban, Regional and Global Air Pollution. Cambridge, MS. October.

Spiegel, M.R. (1961) Statistics. Chapter 11. Small Theory Sampling. Schaum Publishing Company. Pp. 188-200.

Trainer, M., Parrish, D.D., Buhr, M.P., et al., (1993) Correlation of ozone with NO_y in photochemically aged air. J. Geophys. Res. **98**, 2917-2926.

US EPA (1979) Weekend/Weekday Differences in Oxidants and Their Precursors. EPA-450/4-79/013. Office of Air Quality Planning and Standards. U.S. Environmental Protection Agency. Research Triangle Park. NC27711. April.

US EPA (1994) Quality Assurance Handbook for Air Pollution Measurement Systems. Vol. I: A Field Guide to Environmental Quality Assurance. EPA/600/R-94/038a. Office of Air Quality Planning and Standards. U.S. Environmental Protection Agency. Research Triangle Park. NC27711. April.

US EPA (1996) Air Quality Criteria for Ozone and Other Photochemical Oxidants. Vol. I. EPA-600/P-93/00bF. National Center for Environmental Research. U.S. Environmental Protection Agency. Research Triangle Park. NC27711.

US EPA (1998) Quality Assurance Handbook for Air Pollution Measurement Systems. Vol. II: Ambient Air Quality Monitoring Program. EPA-454/R-98/004. Office of Air Quality Planning and Standards. U.S. Environmental Protection Agency. Research Triangle Park. NC27711. August.

US EPA (1999) Determination of Reactive Acidic and Basic Gases and Strong Acidity of Atmospheric Fine Particles (<2.5 μm). Compendium Method IO-4.2; EPA-625/R-96/010a; Center for Environmental Information. Office of Research and Development. U.S. Environmental Protection Agency, Cincinnati, OH.

US EPA (2001) Recommended Methods for Ambient Air Monitoring of NO, NO_2, NO_y, and Individual NO_z species. EPA-600/R-01/005. National Exposure Research Laboratory. U.S. Environmental Protection Agency. Research Triangle Park. NC27711.

Williams, E.J., Baumann, K., Roberts, J.M., et al., (1998) Intercomparison of ground based NO_y measurement techniques. J. Geophys. Res. **103**, 22261-22280.

Winer, A., Peters, J.W., Smith, J.P., Pitts, Jr., N. (1974) Response of commercial chemiluminescent NO-NO_2 analyzers to other nitrogen – containing compounds. Env. Sci. Technol. **19**, 862-865.

Chapter 3
CHARACTERIZATION OF THE METROPOLITAN AREAS

3.1 Greater Cincinnati

The Greater Cincinnati area is located in the American Midwest (39.8° North, 84.3° West) at the southwestern tip of Ohio. It is comprised of the urban and suburban settlements that have extended around the city of Cincinnati and cover parts of 12 counties of Ohio, Kentucky, and Indiana. The City of Cincinnati is a part of Hamilton County, OH. The city is located on the bank of the Ohio River and extends over two ranges of hills. The hill elevation is about 120 m above the river valley level. Although the valley is not very steep, it influences meteorological conditions and pollutant dispersion in the area (Martuzevicius et al, 2004). The climate of the region shows a wide range of temperatures through the year. Summers are warm and humid, while winters are cold and dry. The region is subject to frequent changes due to the passage of cyclonic storms in winter and spring and thunderstorms during summer. The average temperature is ~12°C and prevalent wind direction is from south-southwest (NCDC, 2003). As of the 2000 census, Cincinnati had a total population of around 332,000. However, the estimated population in the Greater Cincinnati area is nearly 2 million residents (US Census Bureau, 2004).

Greater Cincinnati is crisscrossed by a network of highways that leads to important traffic flow throughout the day, as well as during the peak rush hours. A recent study found that during the year 2000, an estimated 124,000 vehicles passed through a 17-mile stretch of I-75 (Martuzevicius et al, 2004). In addition to very intensive traffic, Greater Cincinnati hosts almost 1000 major and small industrial facilities that emit a number of air pollutants into its airshed. According to the US EPA (2004), the estimated anthropogenic emissions of VOC and NO_x for the years 2000-1 were 121,921 and 239,277 tons per year, respectively. These values include the emissions of five counties in Ohio, six counties in Kentucky, and 2 counties in Indiana. Table 3.1 shows a composite of the emission inventory for Greater Cincinnati.

Table 3.1. Cincinnati-Hamilton, OH-KY-IN Emissions Inventory (year 2000).

Source Category	Annual (tons per year)				
	VOC	NO_x	CO	SO_2	PM_{10}
Fuel Combustion Electricity Utilities	438	119,115	3,386	260,990	3,696
Fuel Combustion Industrial	308	17,832	3,353	55,447	1,530
Fuel Combustion Other sources	2,657	6,089	14,339	5,486	1,941
Chemical & Allied products	2,192	188	0	2,051	306
Metals processing	1,151	1,737	22,073	3,176	2,740
Petroleum & Related Products	490	64	105	170	252
Other Industrial Processes	1,850	1,469	1,319	372	458
Solvent Utilization	41,769	0	0	5	150
Storage & Transport (Petroleum products)	8,487	0	84	0	411
Waste Disposal & Recycling	3,677	820	14,658	234	2,501
Highway Vehicles	41,510	63,861	408,338	2,482	2,405
Off-Highway	17,327	28,089	185,820	4,051	2,322
Miscellaneous	65	11	408	0	73,605
Natural Emissions (Biogenic)	39,151[a]	0	0	0	0
Total	161,072	239,277	653,943	334,459	92,173
Percent of total	10.87	16.16	44.16	22.58	6.23

[a] Estimated as proportional to the total annual emissions of biogenic hydrocarbon emission inventory and total land area for the US EPA Region V (Lamb et al., 1993), for the 13 counties of Ohio, Kentucky and Indiana considered by US EPA for the emission inventory (US EPA, 2004).

Solvent utilization and highway vehicles categories account for 52% of the total VOC, while biogenic hydrocarbon emissions account for 24%. Power plants and highway vehicles account for ~ 77% of the total NO_x emissions. The estimated VOC/NO_x ratio for the Greater Cincinnati area is 0.67, expressed as total annual emissions. The tons VOC/tons NO_x ratio must be converted to ppmC VOC/ppm NO_x in order to compare the present approximation to previous VOC/NO_x ratio estimates for the area. Using the method suggested by Baughes (1991) and the average composition of ambient hydrocarbons in 39 U.S. cities (Seinfeld, 1989), the estimated VOC/NO_x ratio is ~ 1.9 ppmC/ppm.

This value contrasts with a previously reported VOC/NO_x ratios for Cincinnati from 6:00-9:00 hr Non Methane Hydrocarbons (NMHC) and NO_x monitoring readings of 3.8 in 1976 (OKI, 1979) and of 9.1 in 1984 (Baugues, 1986), and of 6.4 from 1988 emissions inventories (Carter, 1994). The measured values should be taken as indicative because measurements of NO_x were carried out with chemiluminescence analyzers and the NMHC with flame ionization analyzers. The NMHC analyzers were not explicitly for detecting aromatic compounds. However, the downward trend is in agreement with the trend observed in these ratios in several Northeast U.S. cities from 1986 to 1991 (Wolff, 1993). This trend can be attributed to the more reductions in VOC relative to NO_x that have occurred in the past 15 years. Theoretically, the estimated VOC/NO_x ratio of 1.9 for Greater Cincinnati implies that VOC controls should be more effective than NO_x reductions. However, the Ohio Environmental Council (2000) has stated that, based on photochemical modeling analysis, reduction of NO_x emissions from power plants in the Ohio Valley would prevent excessive formation of O_3 in the airshed.

O_3 formation in Greater Cincinnati is well correlated with ambient temperature and humidity (Jung, 2000). As a result, the smog season in this airshed is typically from April through October. However, there is evidence that the differences in anthropogenic weekday activities are correlated with the local O_3 formation. A statistical analysis of the frequency of days exceeding an assumed O_3 1-hr threshold value of 125 ppb during 1992-1999 showed that the lowest frequencies occur early in the week, with a gradual increase through the week towards the highest frequency on Sunday (Jung, 2000). A recent study of the photochemical system in this airshed showed that O_3 concentrations at all sites within the Greater Cincinnati domain are strongly linked dynamically (Kanda, 1997). This means that high O_3 concentrations measured at one site of the region lead to high O_3 concentrations at other sites and vice versa, indicating that O_3 is formed in a well-mixed large-scale air mass. Kanda has suggested that control of some VOCs at one point in the domain could reduce O_3 concentrations over the entire airshed.

Although Greater Cincinnati has maintained the 1-hour O_3 standard since 1996 and had obtained the designation of an attainment area, in June of 2003, the US EPA demoted the area to "nonattainment" status. This was a result of the Ohio EPA's failure to adopt the federal Reasonably

Available Control Technology (RACT) rules into the Ohio State Implementation Plan (SIP) (HCDOES, 2004a). In addition, preliminary analysis of O_3 monitoring data has shown that southwestern Ohio will be in nonattainment with the new 8-hour O_3 standard. Figure 3.1 shows the trends in 1-hr and 8-hr average O_3 exceedences to their respective US EPA ozone air quality standard in the period 1983-2003.

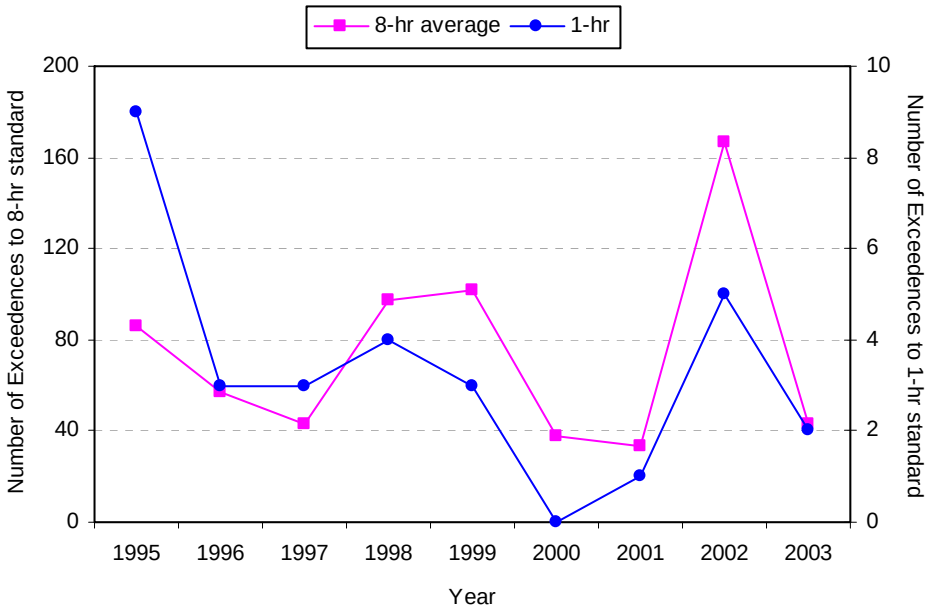

Figure 3.1. Trends in number of exceedences to the 1-hr and 8-hr average US EPA ozone air quality standards in Greater Cincinnati metropolitan area from 1995 to 2003. (US EPA 1-hr O_3 standard: 0.12 ppm max no to be exceeded more than three times over the three most recent years; 8-hr average O_3 standard: 0.08 ppmv max based on highest three-year average of the fourth highest 8-hour concentration). (Source: HCDOESa, 2004)

In addition, because Ohio is a part of the 22 states in the US within the US EPA's NO_x State Implementation Plan Call, it has the obligation to reduce ~ 33% of NO_x emissions to support the control of transported ozone in the region (68 FR No. 150 August 5, 2003). The most important O_3 control strategy has been the reduction of NO_x in electricity utilities. Other strategies that have been applied in Greater Cincinnati include reductions in VOC emissions from stationary sources and combined NO_x and VOC reductions from transportation activities. According to the Hamilton County Department of Environmental Services in Cincinnati (HCDOES, 2004b), from 1996 to 2002 there was a reduction of ~ 13% in VOC

emissions, as a result of stricter inspection and maintenance programs, vapor recovery systems on fuel pumps, and cleaner fuels.

According to a 1998 investigation into health effects, residents in the Greater Cincinnati area were exposed to higher levels of smog more often than residents in Boston and New York and had higher rates of smog-related respiratory hospital admissions, including asthma attacks and emphysema (The Ohio Environmental Council, 2000).

3.2 Mexico City Metropolitan Area

The Mexico City Metropolitan Area (MCMA) lies at a high altitude (2240 m) on an inland flat basin (~ 5,000 km^2) at a subtropical latitude (Lat. 19.5°N). Mountains to the east, south, and west, reaching to more than 2500 m above the basin floor, inhibit dispersion of air pollution and contribute to frequent wintertime thermal inversions that further trap pollutants near the surface (Bravo and Torres, 2002). Prevalent winds are from the NE and NW sector. Low-level regional winds during the cool season are usually not strong enough to provide ventilation of the air pollution in the basin. At other times, weak regional winds give way to cool, thermally driven down-slope winds that during the night reinforce the centripetal circulation, thus contributing to the lateral confinement of air pollutants (Jauregui, 2002).

The climate of the basin is wet-dry tropical in character, tempered by altitude, with a mean annual temperature of 16°C. During the dry season (November to April), clear skies and anti-cyclonic weather prevail with little rain. From May to October, the dry westerlies give way to moist trade winds that bring convective rain showers (Jauregui, 2002). The high elevation and latitude combine to provide plentiful sunshine, especially during the late winter, which in comparison to more northern latitudes, is enhanced by the UV radiation that drives atmospheric photochemistry to produce secondary pollutants such as O_3.

The MCMA consists of the 16 delegations of the Federal District (DF) and 17 municipalities of the State of Mexico, which border the DF. The population in the MCMA has grown rapidly, from 3 million in 1950 to nearly 20 million in 2000. The urbanized area of the region has reached an extension of

almost 1500 km^2. More than 40 million L of fuel are consumed per day, producing thousands of tons of pollutants. Table 3.2 shows the emission inventory for the MCMA that has been developed for the year 2000.

Table 3.2. Mexico City Metropolitan Area Emissions Inventory (year 2000).[a,b]

Source Category	Annual (tons per year)				
	VOC	**NO_x**	**CO**	**SO_2**	**PM_{10}**
Fuel Combustion Electricity Utilities	146	11,626	1,816	16	202
Fuel Combustion Industrial	7,876	6,155	3,594	5,130	1,071
Fuel Combustion Other sources	1,688	8,079	3,385	23	215
Chemical & Allied products	1,688	2,311	3,380	2,332	394
Metals processing	7,453	2,311	3,380	2,332	394
Petroleum & Related Products	5,159	2,563	2,371	1,588	887
Other Industrial Processes	1,515	4,586	964	1,237	447
Solvent Utilization	129,565	0	0	0	0
Storage & Transport (Petroleum products)	33,241	0	0	0	0
Waste Disposal & Recycling	0	0	0	0	0
Highway Vehicles & Off-Highway	194,517	157,239	2,018,788	4,348	5,287
Miscellaneous	33,170	33	1,127	7	1,838
Natural Emissions (Biogenic)	15,425	859	0	0	0
Total	429,755	193,451	2,035,425	14,681	10,341
Percent of total	16.05	7.2	75.8	0.55	0.4

[a] Includes 16 Delegations from the Federal District and 17 municipalities from the State of Mexico.
[b] Source: SMA (2003)

Fuel combustion in motor vehicles accounts for 81% of the total NO_x. Power plants contribute only with a 6% of the total. Most of the electricity consumed in MCMA is provided by a national interconnected network distribution from a number of power plants located across the country. Vehicles account for 45% of the total VOC, while solvent utilization accounts for 30% of VOC emissions. Leaks

from storage and distribution of Liquefied Petroleum Gas (LPG) account for 7.5% of the total VOC. The estimated VOC/NO_x ratio from the emission inventory is ~ 2.2. However, comparisons between measured VOC/NO_x ratio (as ppbC/ppm) and the equivalent ratio derived from emission inventories indicate a strong incongruence. Molina and Molina (2004) reported that, while the VOC/NO_x ratio derived from past inventories was ~ 3:1 (ppbC/ppm), the same estimation from measurements in representative locations were 15:1 or higher for the same period (1992-1997). These very high VOC/NO_x ratios have been extremely influential in past studies, which have concluded that ozone is likely to be NO_x-sensitive (MARI, 1994; Sosa et al., 2002).

The MCMA's large population, 35 000 industries, 3.5 million vehicles, complex topography, and meteorology cause high air pollution levels. Peak concentrations of O_3 are typically reached during the afternoon in the downwind southwest sector of the basin. One important effect of the regional meteorology of the Mexico Basin is the trapping of very high levels of aged O_3 aloft in the nocturnal mixing layer (Bravo and Torres, 2002). This aged O_3 may contribute effectively to the formation of new diurnal O_3.

The smog season in MCMA is typically between February and March, when the incoming UV radiation is larger and the sky is cleaner. During the wet summer months (June to September), clouds inhibit photochemistry and high O_3 episodes are less frequent.

Although significant improvement in ambient air quality in the MCMA has been reached in the past 12 years, levels remain high. In 2003, O_3 levels exceeded the local air quality standard (0.11 ppm 1-hr max. any day in the year) on 75% of days in the year. Figure 3.2 shows the trends in O_3 concentrations of the 1-hr max 95th percentile and 1-hr max annual average from data collected at five representative sites in the MCMA.

MCMA health studies indicate that most of the inhabitants in this area have been affected to some degree by the high levels of O_3 and high dosage of exposure (Calderón-Garcidueñas et al., 1992). Borja-Aburto et al. (1997) have demonstrated a statistically significant association between O_3 levels and cardiovascular mortality in inhabitants of the MCMA.

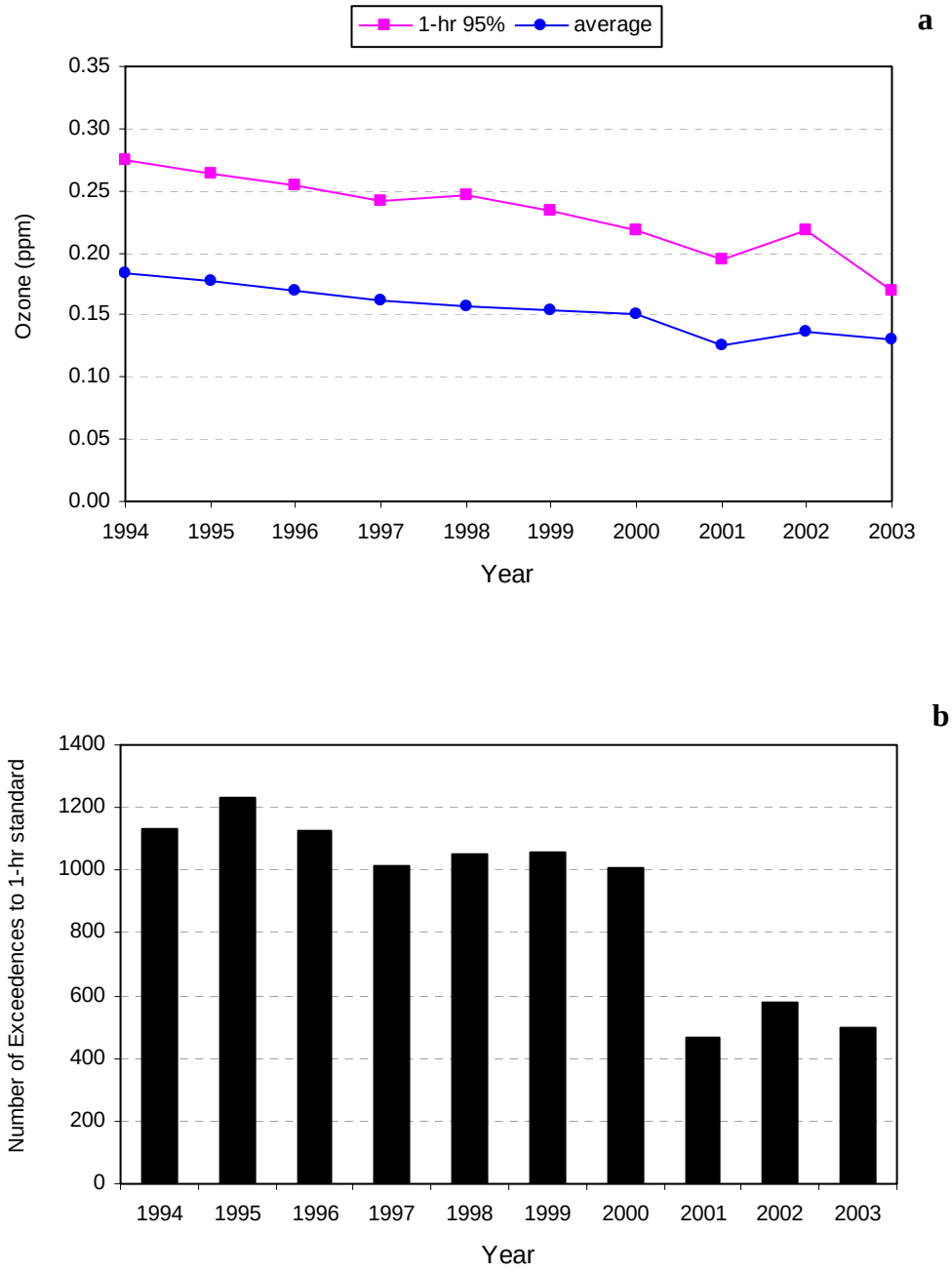

Figure 3.2. Trends in O_3 concentrations for (**a**) 1-hr max 95th percentile and 1-hr max annual average, and (**b**) number of exceedences to the 1-hr Mexican Ozone Air Quality Standard in MCMA from 1994 to 2003. (Mexican O_3 1-hr standard: 0.11 ppm max no to be exceeded any time in a year). (Source: SINAICA, 2004).

A new O_3 8-hr average standard (0.08 ppb) was approved in 2002 by the Mexican authorities. A preliminary analysis of the data indicates that since 1994, every year has not been below or not even close to this standard (SINAICA, 2004).

Historically, air quality management in the MCMA has focused on the whole local air pollution problem and not on one specific air pollutant. Most strategies from 1990-1995 were based on technological modernization and fuel improvement that had been demonstrated as useful in other countries (Molina et al., 2004). The most significant reductions in air pollution in that period, including ambient O_3 levels, can be attributed to the introduction of catalytic converters and the improvement in fuel quality.

In 1996, a five-year control program was initiated based on linear programming involving political and economical factors, as well as results from photochemical modeling efforts (Streit and Guzman, 1996). It is not clear if the concept of O_3-NO_x-VOC sensitivity was taken into account in this air quality management program. However, the authorities enforced a strong reduction in VOC emissions. For the period 2001-2010, a new control program was elaborated considering recommendations of a research group coordinated by Dr. Mario Molina at the Massachusetts Institute of Technology and modeling works done by the Fraunhofer Institute (CAM, 2002). The aim of this new plan was to reduce ambient O_3, PM_{10}, and $PM_{2.5}$ levels. Control strategies were based on NO_x reduction, although VOC reductions were also included. The MIT group concluded that, even though there is evidence from modeling and chamber experiments that O_3 formation in MCMA is likely NO_x sensitive, more research is needed to clarify this situation.

3.3 References

Baugues, K. (1986) A Review of NMOC, NO_x and NMOC/NO_x Ratios Measured in 1984 and 1985. EPA-450/4-86-015. U.S. Environmental Protection Agency. Office of Air Quality Planning and Standards. Research Triangle Park, N.C.

Baugues, K. (1991) Reconciling differences between ambient and emission inventory derived NMOC/NO_x ratios: implications for emission inventories. A&WMA Paper 91-67.5, presented at the 84th Annual Meeting of the Air & Waste Management Association. Vancouver, British Columbia, June.

Borja-Aburto, V.H., Loomis, D.P., Bangdiwala, S.I., Shy, C.M., Rascon-Pacheco, R.A. (1997) Ozone, suspended particulates, and daily mortality in Mexico City. Am. J. Epidemiol. **145**, 258-268.

Bravo, H. A., Torres, R.J. (2002) Air Pollution Levels and Trends in the México City Air Basin. Chapter 6. **In:** Urban Air Pollution and Forests. Resources at Risk in the Mexico City Air Basin. Fenn, M.E., de Bauer, L.I., Hernandez-Tejeda, T., Eds. Springer-Verlay, New York. Pp. 121-159.

CAM (2002) Programa para Mejorar la Calidad del Aire de la Zona Metropolitana del Valle de México 2002-2010. Coordinación: Comisión Ambiental Metropolitana. Secretaria de Ecología, Edo. de México; Secretaría de Medio Ambiente, Gobierno del Distrito Federal; Secretaría de Medio Ambiente y Recursos Naturales; Secretaría de Salud. México.

Calderón-Garcidueñas, A.L., Velásquez, O.A., Bravo-Alvarez, H., Delgado-Chávez, R., Barrios-Márquez, R. (1992) Histopathologic changes of the nasal mucosa in southwest Metropolitan Mexico City inhabitants. Am. J. Path. **140**, 225-232.

Carter, W.P.L. (1994) Development of ozone reactivity scales for volatile organic compounds. J. Air & Waste Manage. Assoc. **44**, 881-899.

HCDOES (2004a) Air Quality Data and Progress Report. Hamilton County Department of Environmental Services. Cincinnati, OH.

HCDOES (2004b) Emissions of Hydrocarbons and Oxides of Nitrogen in the Greater Cincinnati Area. Hamilton County Department of Environmental Services. Available at: http://www.hcdoes.org/air_quality/wepages/MAHOME.htm. Link: Emissions Presentation.

Jauregui, E. (2002) The Climate of the Mexico City Air Basin: Its Effects on the Formation and Transport of Pollutants. Chapter 5. **In:** Urban Air Pollution and Forests. Resources at Risk in the Mexico City Air Basin. Fenn, M.E., de Bauer, L.I., Hernandez-Tejeda, T., Eds. Springer-Verlay, New York. Pp. 86-117.

Jung, I. (2000) Evaluation of O_3 and Fine Particulate Matter Characteristics in Ohio. MS Thesis. Texas A&M University – Kingsville. December.

Kanda, R.V.S. (1987) Characterization of Ozone Dynamics in Urban Areas. MS Thesis. University of Cincinnati. May.

Lamb, B., Gay, D., Westberg, H., Pierce, T. (1993) A biogenic hydrocarbon emission inventory for the U.S.A. using a simple forest canopy model. Atmos. Environ. **27A**, 1673-1690.

MARI (1994) The Mexico City Air Quality Research Initiative. Los Alamos National Laboratory. Rep., LA-12699.

Martuzevicius, D., Grinshpun, S.A., Reponen, T., et al., (2004) Spatial and temporal variations of $PM_{2.5}$ concentration and composition through and urban area with high freeway density - The Greater Cincinnaty Study. Atmos. Environ. **38**, 1091-1105.

Molina, J.M., Molina, L.T. (2004) Megacities and atmospheric pollution. Critical Review. J. Air & Waste Manage. Assoc. **54**, 644-680.

Molina, J.M., Molina, L.T., Slott, R., et al., (2004) Critical Review Supplement :Air Quality in selected megacities and atmospheric pollution. J. Air & Waste Manage. Assoc. (online only). Available at: http://www.awma.org/journal.

NCDC (2003) National Climatic Data Center. Local Climatological Data. Available at: http://www.ncndc.noaa.gov/ncdc.html.

OKI (1979) Regional Air Quality Management Plan. Ohio-Kentucky-Indiana Regional Council of Governements. Cincinnati, OH. February.

Seinfeld, J.H. (1989) Urban air pollution: state of the science. Science. **243**, 745-752.
SINAICA (2004) Sistema Nacional de Información de la Calidad del Aire. Instituto Nacional de Ecología. SEMARNAT. México. Available at: http://sinaica.ine.gob.mx/construccion.html.

SMA (2003) Inventario de Emisiones a la Atmósfera del Valle de México, 2000. Secretaría del Medio Ambiente. Gobierno del Distrito Federal. Ciudad de México, D.F. México.

Sosa, G., West, J., San Martini, F., Molina, L.T., Molina, M.J. (2000) Air Quality Modeling and Data Analysis for Ozone and Particulates in Mexico City. Rep. No. 15. MIT Integrated Program on Urban, Regional and Global Air Pollution. Cambridge, MS. October.

Streit, G.E., Guzman, F. (1996) Mexico City air quality: progress of an international collaborative project to define air quality management options. Atmos. Environ. **30**, 723-733.

The Ohio Environmental Council (2000) Ohio Valley – Ozone Alley. The Ohio Environmental Council. Columbus, OH.

U.S. Census Bureau (2004) United States Census 2000. Available at: http://www.census.gov/main/www/cen2000.html.

US EPA (2004) Cincinnati-Hamilton, OH-KY-IN MSA. Technology Transfer Network Ozone Implementation.Envirofacts. U.S. Environmental Protection Agency. Available at: http://www.epa.gov/ttn/naaqs/ozone/areas/msaindex/htm.

Wolf, G.T. (1993) On a NO_x-focused control strategy to reduce O_3. J. Air & Waste Manage. Assoc. **43**, 1593-1596.

Chapter 4
RESULTS AND ANALYSIS

4.1 Greater Cincinnati

4.1.1 Indicator Species Measurements

Continuous measurements of O_3, NO_x, and NO_y were made from September 3-30, 2003 at the Taft monitoring station of the Hamilton County Department of Environmental Services (HCDOES) in the city of Cincinnati, Ohio (39.06°N, 84.3°W, 230 m.a.s.l.), ~ 5 km north of downtown (see Figure 4.1).

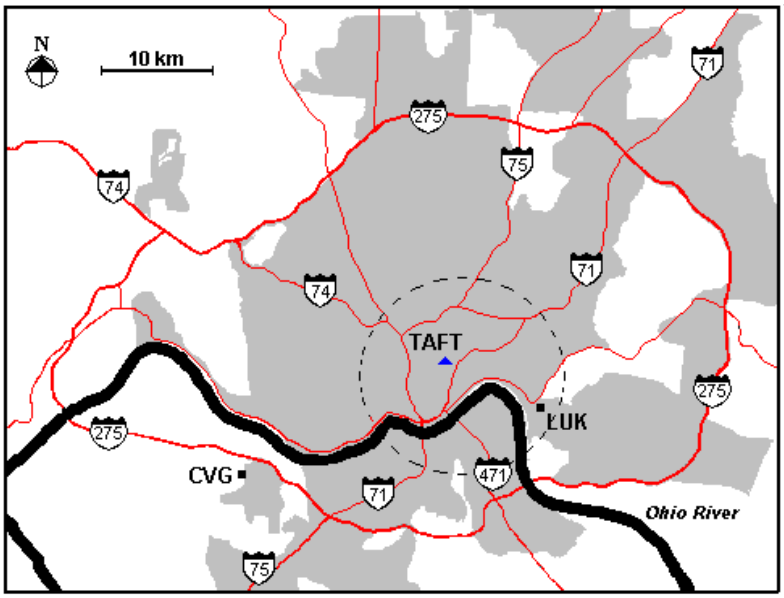

Figure 4.1. Map showing the Greater Cincinnati area and the location of the Taft Monitoring Station. The dashed circle encloses the approximate extent of the city while the remainder of the gray area outside of the circle shows the extent of the suburban area. LUK represents the Lunken Municipal Airport and CVG is the Cincinnati/Northern Kentucky International Airport.

The hourly average concentrations of O_3, NO_x, and NO_y were processed by HCDOES protocols. All species were sampled at ~ 6 m above ground level and all instruments were kept in a temperature-controlled room. O_3 measurements were made with a Dasibi Ozone Monitor model 1008-RS equipped with an internal O_3 generation system. NO_x (NO and NO_2) measurements were made with a Thermo

Environmental Instrument model 42C. NO_y measurements were taken with a chemiluminescent method, using a partially modified Columbia Scientific Instruments (CSI) model 1600 NO_x analyzer with an external heated converter mounted to the gas sample inlet. The external heated converter consisted of a molybdenum (Mo) converter assembly removed from a Monitor Labs 8840 NO_x analyzer. Energy to heat in the Mo converter was supplied by a cartridge heater. A type K thermocouple embedded in the assembly kept the temperature of the converter at approximately 365 ± 5°C. In order to insure that the measured total reactive nitrogen (NO_y) included gas-phase HNO_3 and aerosol nitrate, the inlet Teflon line to the external converter was cut as short as possible (~ 30 cm) to minimize the loss of nitric acid on the inlet. In addition, NO_y sampling was conducted without a particulate filter. NO_x and NO_y instrument calibrations were accomplished by the addition of a NBS standard reference material gas for NO_2 via a Sabio unit calibration system. Conversion efficiency of the Mo converter was calculated to be > 98%. Additional meteorological information was obtained from the Cincinnati Municipal Airport Lunke (NCDC, 2003).

Integrated 1-hour average samples (15:00–16:00 hr) of gas-phase H_2O_2 and HNO_3 were collected simultaneously on several weekdays between September 8-17 using two annular denuder systems (ADSs). The ADSs were located on the roof of the HCDOES laboratory; about ~ 20 m away from the inlet sampling of the monitoring equipment. After sampling, the denuders were sealed and kept in a dark enclosure immersed with blue-ice packs. The extractions were performed no latter than 30 min after the sampling. The analysis of the samples was performed in the Civil and Engineering Department of the University of Cincinnati.

H_2O_2 was collected in two Ti(IV)-H_2SO_4 coated URG annular denuders (3 channels x 30 mm O.D. x 150 mm length glass tubes) in series at a flow rate of 10 L/min (Possanzini et al., 1988). The leachates were then analyzed with a Hewlett-Packard UV-VIS Spectrophotometer Model 8453 using a ferrous thiocyanate reagent at 475 nm. The Ti(IV)-H_2SO_4 denuder based technique has a reported detection limit for H_2O_2 of 0.037 ppb (0.05 $\mu g/m^3$) for one hour of sampling. This technique does take into account a correction for possible O_3 interferences. Hydrogen peroxide content was calculated from a

calibration curve obtained with dilute solutions of H_2O_2, previously standardized with $KMnO_4$ solutions titrated against a sodium oxalate oximetric standard.

HNO_3 was collected in one Na_2CO_3 coated URG annular denuder (3 channel x 30 mm O.D. x 242 mm length glass tube) at a flow rate of 10 L/min. The aqueous extracts were analyzed by ion chromatography (US EPA, 1999). A Dionex DX-120 Ion Chromatograph equipped with an AS14A IonPack column was used for the analysis. The eluent consisted of a mix of sodium carbonate and sodium bicarbonate. The standard curve had a range of 0-100 mg/L and was constructed using several dilutions of sodium nitrate. The reported detection limit for HNO_3 with this method is 0.78 ppb (2.0 $\mu g/m^3$) for a 1-hour sampling at a flow rate of 10 L/min (US EPA, 1999).

As previously mentioned in chapter 2, an empirical model employed by the European Environmental Agency was used to determine the afternoon NO_2 concentrations from measured NO_x concentrations and to estimate "real" NO_2* concentrations (de Leeuw et al., 2001). The empirical model (BUWAL, 1997) has the form: $NO_2 = 0.055*NO_x + 55*(1-e^{-NO_x*0.01173})$.

In general, the calculated NO_2* value was ~ 65% of the measured non-corrected NO_2 value. This percentage was within to the operational uncertainty of chemiluminescent NO_x analyzers suggested by Gerboles et al. (2003) for this study's range of NO_x and NO concentrations. A surrogate NO_z* value was estimated from the measured NO_y and NO and the estimated NO_2* concentrations (ppb):

$$NO_z* = NO_y - NO - NO_2* \quad (13)$$

The estimations of NO_2* and, as a result, NO_z* were assumed valid only for the afternoon hours. It was also assumed that conversion efficiency of NO_y and NO was the unity.

4.1.2 General Findings

Hourly average concentrations of NO, NO_y, and O_3 from September 3-30, 2003 are shown in Figure 4.2. The basic statistical analysis of NO, NO_x*, NO_y, and O_3 data is presented in Table 4.1.

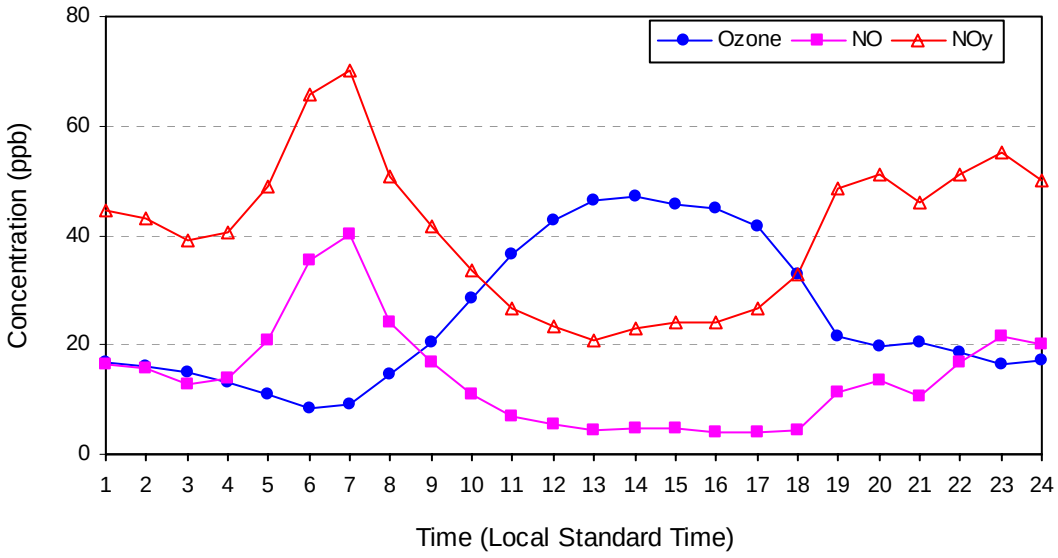

Figure 4.2. Composite diurnal profiles of hourly average NO, NO_y and O_3 concentrations measured at the Taft monitoring station in Cincinnati, September 3-30, 2003.

Table 4.1. Statistical summary of hourly NO, NO_x*[(a)], NO_y and O_3 and meteorological parameters[(b)] measured at the Taft monitoring station Cincinnati, OH (September 3-30, 2003).

Parameter	Unit	Mean	S.D.	Range	No. of Samples
NO	ppb	14.3	22.4	0.05-184	625
NO_x*	ppb	36.1	28.1	5-213	625
NO_y	ppb	41.2	29.1	10-213	625
O_3	ppb	24.8	17.4	1-73	621
Temperature	°C	18.1	5.3	3.9-28.9	626
Wind Speed	m/sec	1.8	1.7	0-8.75	626
Wind Direction	degrees	Dominant: 225 (10.4%)		0-360	593

(a) NO_x values as measured by the NO_x analyzer.
(b) Measured at the Cincinnati Municipal Airport Lunke.

Hourly average values of O_3 ranged from 1 ppb to 73 ppb—relatively low values. The dependence of "low" O_3 concentrations on "low" ambient temperature was clearly evident during the study period. According to historic mean temperature data from the Cincinnati-Northern Kentucky

Airport, the mean temperature during September 2003 had a 1.44°C difference less than the normal mean for this month (NCDC, 2003). As a consequence, the O_3 levels were relatively low. They were even below the O_3 8-hr standard of 0.08 ppm.

The hourly average O_3, NO, and NO_y diurnal profile showed the typical urban diurnal variation with a plateau of maximum O_3 concentrations in the afternoon between 13:00 and 15:00 hr and a minimum concentration early morning (~ 6:00 hr). The increase in O_3 during morning hours had a nearly constant positive slope that coincided with the decrease in NO concentrations. The net production (or accumulation) of O_3 started before 9:00 hr—once the equivalent concentration of NO titration was surpassed. The average rate of O_3 accumulation was ~ 5.3 ppb/hr, and the average duration of the ozone build-up was 5.2 hr. The "ridge" of average O_3 concentrations above the generally accepted O_3 background of 40 ppb extended from around 11:30 hr to shortly after 17:00 hr, with the average peak at 14:00 hr. The decrease in O_3 started at 16:00 hr as a result of the decreasing solar radiation and photochemical activity. After the evening, "fresh" NO emissions combined with other deposition mechanisms caused O_3 levels to fall.

The peak in the average hourly concentrations of NO and NO_y clearly coincided with the morning 5:00 to 8:00 hr traffic. These peaks were, in general, short—with their maximum levels (40 and 70 ppb respectively) around 7 hr. After a 6-hour period, both NO and NO_y reached a minimum plateau at around 13:00 hr. NO depletion rate after the start of the O_3 accumulation was ~ 3.3 ppb/hr. While the NO levels kept at a nearly constant level, a minimum of ~ 3 ppb from 13 to 18 p.m., NO_y concentrations showed a minimum (or background) average concentration of ~ 21 ppb by the early afternoon. After this, minimum NO_y levels showed a slight increasing trend, moving in the opposite direction of the trend for the O_3 concentrations. The difference in this pattern could be the result of regional contributions of HNO_3 and NO_3^- to the NO_y balance, because NO did not show a significant increase along this period. The constant levels of afternoon NO indicate that the Greater Cincinnati airshed was under the influence of constant NO_x emissions. Two additional NO and NO_y peaks were registered from late afternoon to

midnight, the first one associated with the evening rush hour and the second one to the resetting of the shallow nocturnal boundary layer. The reduction in NO_y levels between midnight and 3:00 hr followed the same reduction pattern as NO concentrations. Both moved in concurrence with a continuous nocturnal titration with O_3.

The set of data collected during the monitoring and sampling campaigns was statistically analyzed for the afternoon hours, as required by the PIM. Table 4.2 shows the mean, standard deviation of the mean, and range of afternoon NO, NO_y, and calculated values of NO_x* and NO_z* concurrent with $O_3 \geq$ 50 ppb (WE and WD, September 3-30, 2003). The limit of 50 ppb on O_3 concentrations was chosen arbitrarily to exclude days not representative of intense photochemical activity. Table 4.2 also gives the concurrent 15:00-16:00 hr measurements of O_3, NO_y, HNO_3, H_2O_2, and associated NO_x* and NO_z* (WD only, September 8-17).

Table 4.2. Statistical summary of average concentrations of measured NO, NO_y and estimated NO_x* and NO_z* levels concurrent with measured $O_3 \geq 50$ ppb between 13:00-17:00 hr (September 3-30, 2003), and hourly average of concurrent measured O_3, NO_y, HNO_3, H_2O_2 and estimated NO_x* and NO_z* between 15:00-16:00 hr (September 8-17) at the Taft monitoring station.

Period	Parameter	Mean (ppb)	S.D. (ppb)	Range (ppb)	N
13:00-17:00 hr (September 3-30)[a]	NO	2.9	1.3	1-6	44
	NO_y	21.6	4.6	13-30	44
	NO_x*	13.6	3.7	7-21	44
	NO_z*	7.9	1.8	5-12	44
	O_3	59.2	6.0	50-73	44
15:00-16:00 hr (September 8-17)[b]	NO_y	27.8	8.9	18-40	8
	HNO_3	6.8	0.59	6.24-7.08	8
	H_2O_2	1.4	0.76	0.30-2.46	7
	O_3	53.7	8.9	42-66	8
	NO_x*	18.9	4.9	14.5-27.9	8
	NO_z*	9.0	3.7	3.1-14.6	8

[a] Weekend and weekdays.
[b] Weekdays only.

In general, the concentrations of all the compounds measured during the afternoon hours did not have strong variation. The range of the NO_y average levels (13-30 ppb) was somewhat similar to reported afternoon NO_y values for a suburban site in Tennessee (13-27 ppb) (Williams, 1998). For comparison, the range of NO_y values reported for several sites of the Los Angeles Basin in 1987 were between 25 to 140 ppb (Sillman et al., 1997). The range of measured HNO_3 levels in Cincinnati (6.2-7.0 ppb) was slightly higher than that reported for a suburban site in Tennessee in the afternoon period (2.5-5.9 ppb) (Williams, 1998). However, it was approximately three times lower than the average of ranges reported for Claremont California from noon to 16:00 hr (11-18 ppb) (Hering, 1988). The range of measured H_2O_2 concentrations (0.30-2.4 ppb) was within the range of measurements reported for other locations in the Ohio region. For example, Daum (1990) reported a range of H_2O_2 concentrations of 0.2-6 ppb in Central Ohio for June 1987 and June 1988. Kok et al. (1978) reported a range of H_2O_2 concentrations from 10-30 ppb in the Los Angeles Basin during July 1977. The range of estimated NO_z* values of 5-12 ppb was also in agreement with the range reported for the suburban site in Tennessee (6-16 ppb) (Williams, 1998). The range of NO_z values reported for the Los Angeles Basin in 1987 was 3-52 ppb (Sillman et al., 1997).

4.1.3 Photochemical Indicators Evaluation

Figure 4.3 shows the comparison between hourly measured O_3 ($\geq$ 50 ppb) and both NO_y and estimated NO_z* afternoon concentrations in Cincinnati. Also shown are the reported O_3 and NO_y concentrations and the O_3 and NO_z concentrations measured in several representative sites of the U.S. and Paris (Sillman, 2002). This figure shows that the correlation patterns for Cincinnati tended to be more towards the VOC-sensitive conditions of the Los Angeles correlation pattern.

Figure 4.4(a) and 4.4(b) show, respectively, the comparison between the scatterplot correlation of measured $O_3 \geq 50$ ppb, NO_y, and estimated NO_z* from 13:00-17:00 hr and a composite of scatterplot patterns of predicted O_3 versus NO_y and NO_z afternoon values for mixed-, VOC-, and NO_x-titration conditions for several regions in the U.S. (Sillman and He, 2002).

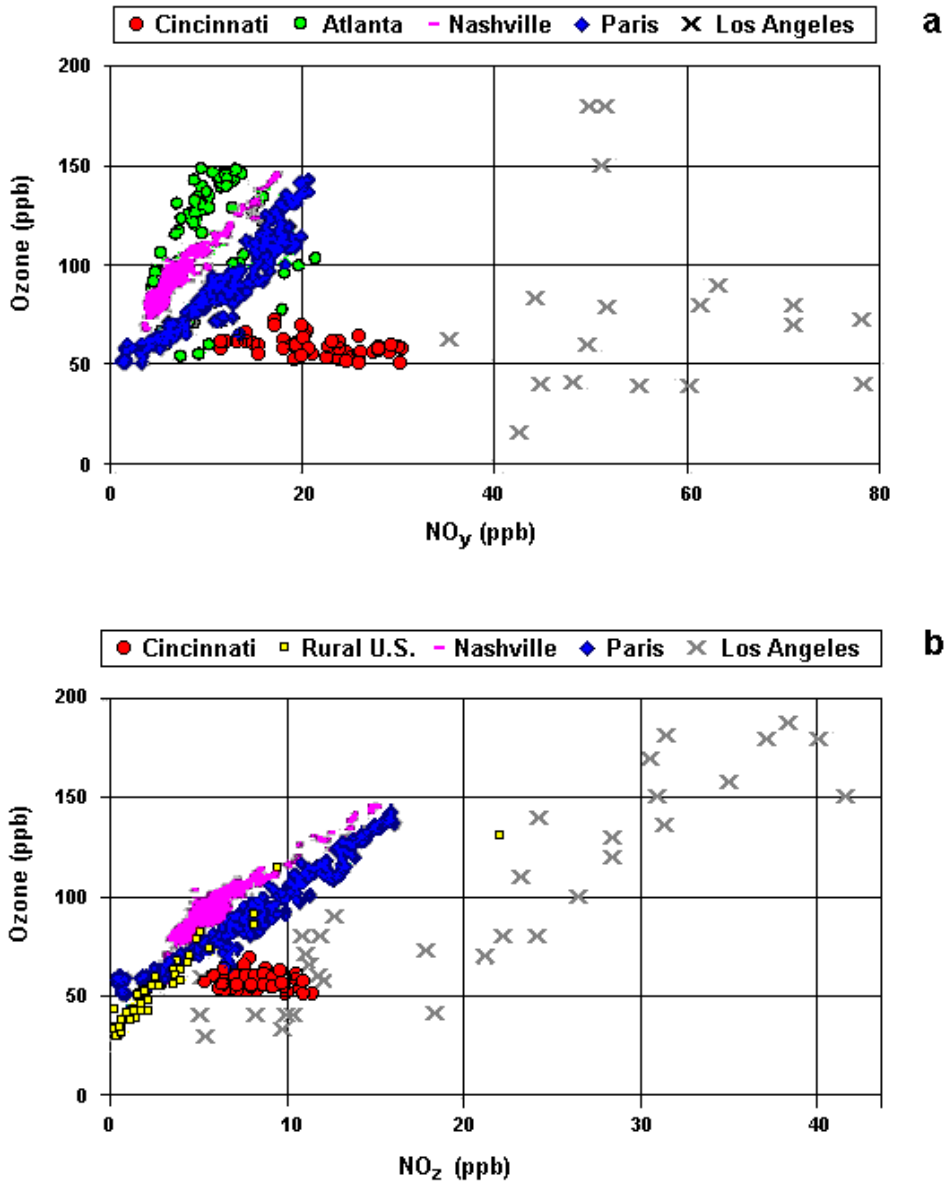

Figure 4.3. Scatterplot patterns of: (**a**) measured O_3 and NO_y, and, (**b**) measured O_3 and estimated NO_z* in Cincinnati compared with measured correlations of O_3 and NO_y and NO_z patterns for different locations identified as: NO_x-sensitive (Atlanta and Rural U.S.), mixed sensitive (Nashville and Paris), and VOC-sensitive (Los Angeles). Scatterplots adapted from Sillman (2002 and 2003).

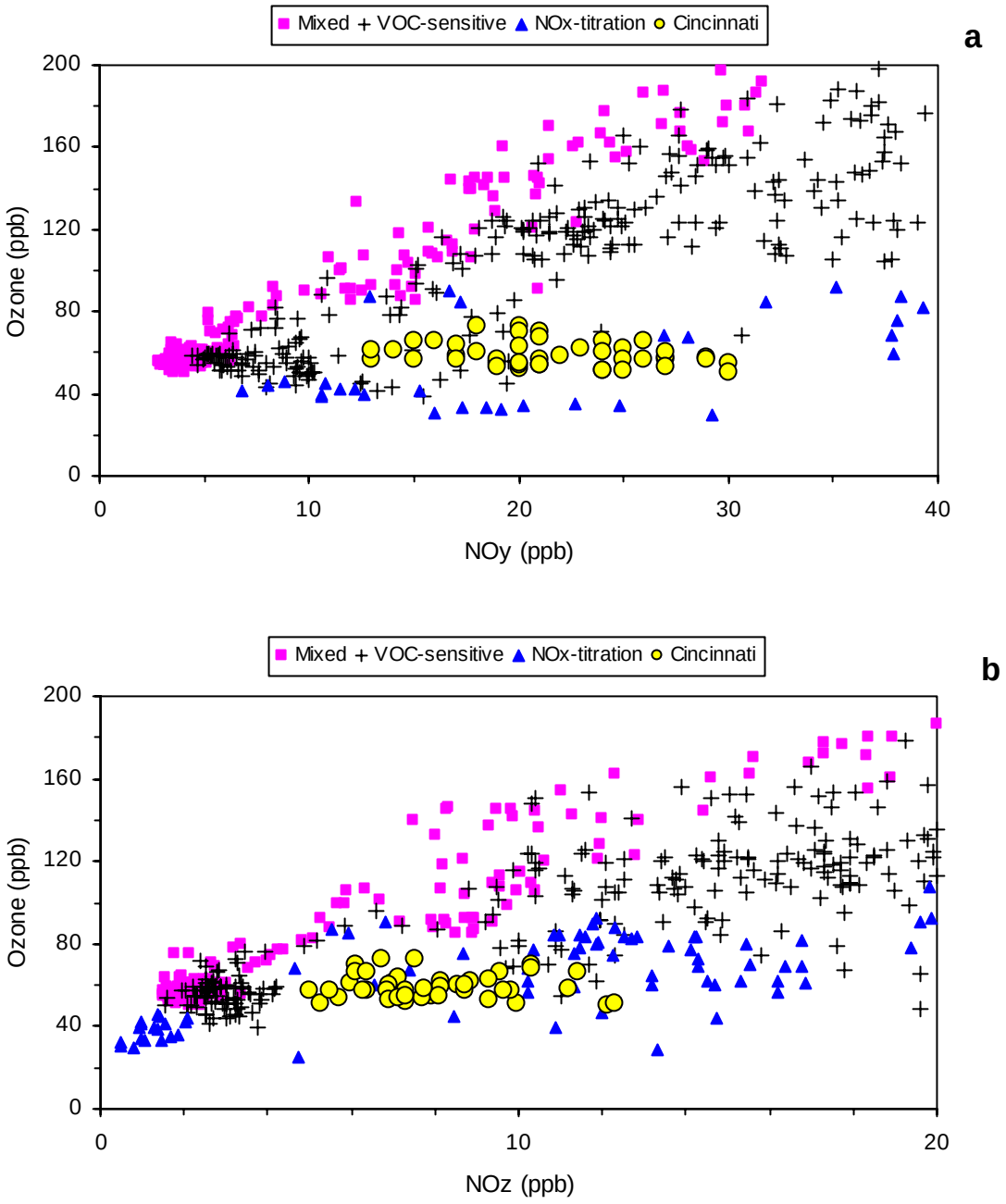

Figure 4.4. Scatterplot patterns of: (**a**) measured O_3 and NO_y, and (**b**) measured O_3 and estimated NO_z* at Cincinnati compared with 3-D model predicted O_3 and NO_y and NO_z patterns, respectively, for locations with mixed or with near-zero sensitive conditions (squares), VOC-sensitive conditions (crosses), and dominated by NO_x-sensitive titration (triangles). Simulation data obtained from data file available from Sillman (2003).

According to Figure 4.4(a), the O_3 vs. NO_y data points for Cincinnati matched with the predicted VOC-sensitive condition and a great portion of the NO_y data points were above 20 ppb (VOC-sensitive condition according Sillman, 1995). However, the outline of the O_3 vs. NO_z* scatterplot pattern, shown in Figure 4.4(b), suggests the possibility that the air masses sampled could be under conditions dominated by NO_x-titration.

Figures 4.5(a) and 4.5(b) show the results of the empirical procedure outlined in chapter 2 to identify VOC-sensitive conditions from those dominated by NO_x-titration environments, which involves the associated NO_x/NOy ratios. Figure 4.5(a) shows that most of the data points of the NO_x*/NO_y ratios for Cincinnati matched perfectly with a portion of the scatterplot pattern for locations with VOC-sensitive conditions. Figure 4.5(b) demonstrates that just a few of these data points overlapped the NO_x-titration pattern and had a NO_x*/NO_y ratio of less than 0.7.

Although the NO_x* values represented an approximation of the real NO_x concentrations, the results displayed in Figure 4.5 one could argue that the air masses that arrived at the monitoring site were not significantly impacted by local sources of NO and that, independent of origin and age, they were relatively homogeneous in their maximum O_3 concentrations.

On the other hand, one attempt was made to evaluate the consistency of the measurements of HNO_3 and H_2O_2 by a comparison of the correlations of measured O_3 versus $2H_2O_2 + NO_z$* with simulated values (as explained in chapter 2). However, the small number of observations (8 pairs) and the very low values of concurrent O_3 resulted in a small cluster located at the lower edge of the scatterplot. As an alternative, the $O_3/(2H_2O_2 + NO_z*)$ ratio was calculated, resulting in a value of ~ 4.7. This value was very close to the lower limit of the range (5-8) given by Sillman (2002).

Although, at the Taft monitoring site, there were no measurements of CO to verify the consistency of the registered NO_y levels, the ensemble of qualitative evaluations allowed one to conclude that the measurements of NO_y, the estimated NO_z*, and the HNO_3 and H_2O_2 indicator species were consistent with the indicator theory and that they could be used to evaluate the O_3-NO_x-VOC sensitivity of Cincinnati with the PIM.

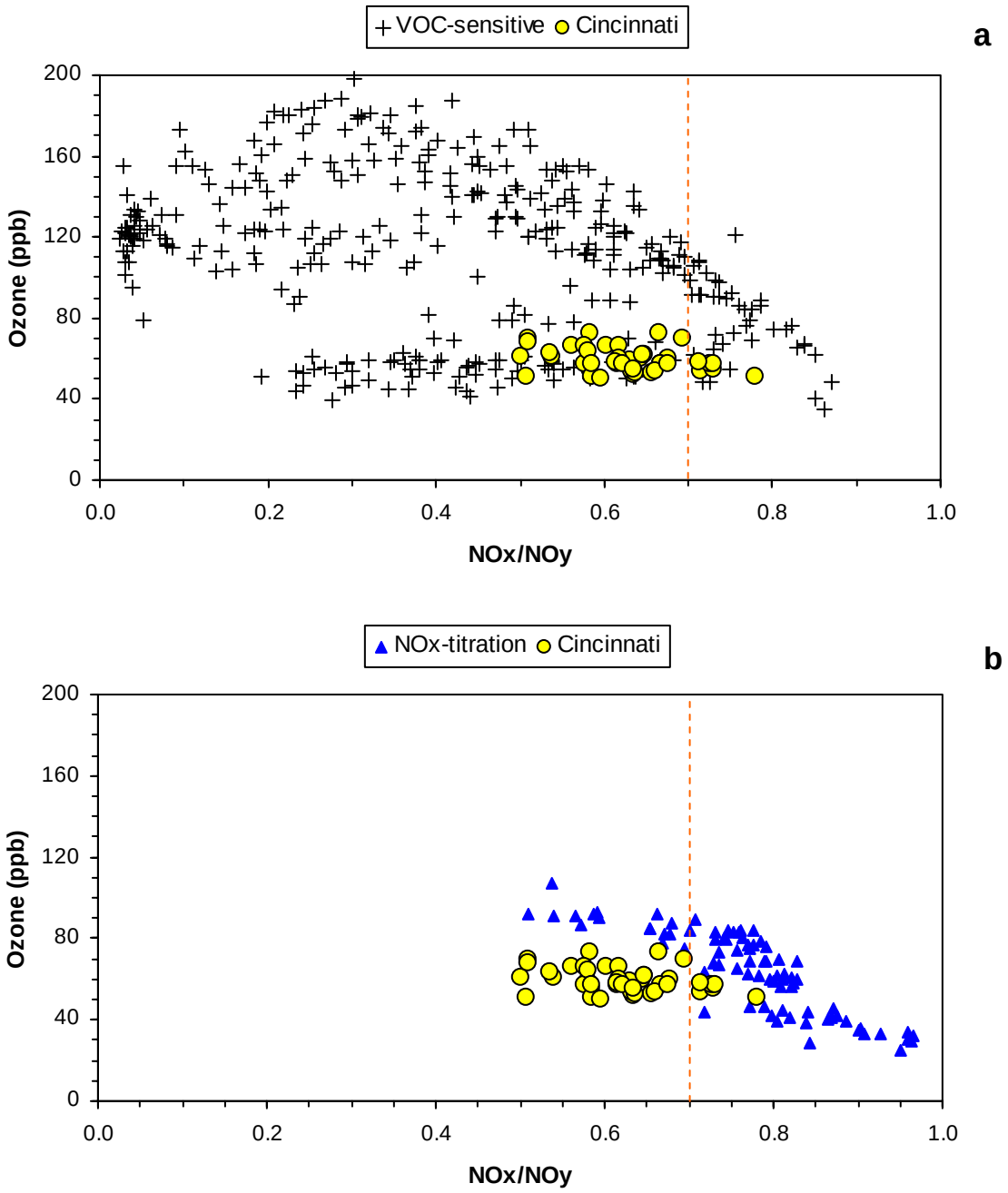

Figure 4.5. Scatterplot patterns for afternoon O_3 versus NO_x*/NO_y data for Cincinnati compared with the calculated NO_x/NO_y ratio from data results of 3-D model simulations for locations with: (**a**) VOC-sensitive conditions, and (**b**) dominated by NO_x-titration. The vertical dashed line represents the hypothetical limit for differentiating photochemically aged air parcels. Simulation data obtained from data file available from Sillman (2003).

In addition, the comparisons of the indicator data for Cincinnati with measured and predicted correlations for other locations were consistent with the identification of VOC-sensitive conditions.

Table 4.3 shows the comparison of the calculated photochemical indicator ratios from measurements performed in Cincinnati with the mean transition values proposed by Sillman (1995) and Sillman and He (2002). Figure 4.6 displays the scatterplots of measured O_3 versus NO_y and O_3 versus surrogate NO_z* in Cincinnati between 13:00 and 17:00 hr for late September 2003. It also compares them with the suggested mean transition lines for NO_x- and VOC-sensitive conditions for "clean" air conditions with O_3 maximum levels < 80 ppb, as is the case for Cincinnati. The combined results from Table 4.3 and Figure 4.6 provide a confirmation of the dominance of VOC-sensitive conditions in Cincinnati according to the PIM.

Table 4.3. Calculated average indicator ratios for data observed at the Taft Monitoring Station (Cincinnati) and transition ranges according to Sillman (1995) and Sillman and He (2002). Values of ratios lower than their transition ranges indicate VOC-sensitivity. Values of NO_y higher than the transition value indicate VOC-sensitive conditions.

Indicator	Taft average ratios	Transition range
O_3/NO_y	2.7[a]-1.93[b]	11–15[c]
O_3/NO_z	5.96[a]-5.92[b]	15–20[c]
O_3/HNO_3	7.89[b]	20–25[c,d]
H_2O_2/NO_y	0.05[b]	0.12-0.17
H_2O_2/NO_z	0.15[b]	0.20-0.25
H_2O_2/HNO_3	0.22[b]	0.25-0.35
NO_y	21.6[a]-27.8[b]	20

[a] From the whole monitoring period
[b] From the weekdays sampling period.
[c] Transition range for low ozone (< 80 ppb) polluted conditions.
[d] Interpolated from Figure 3 in Sillman and He (2002).

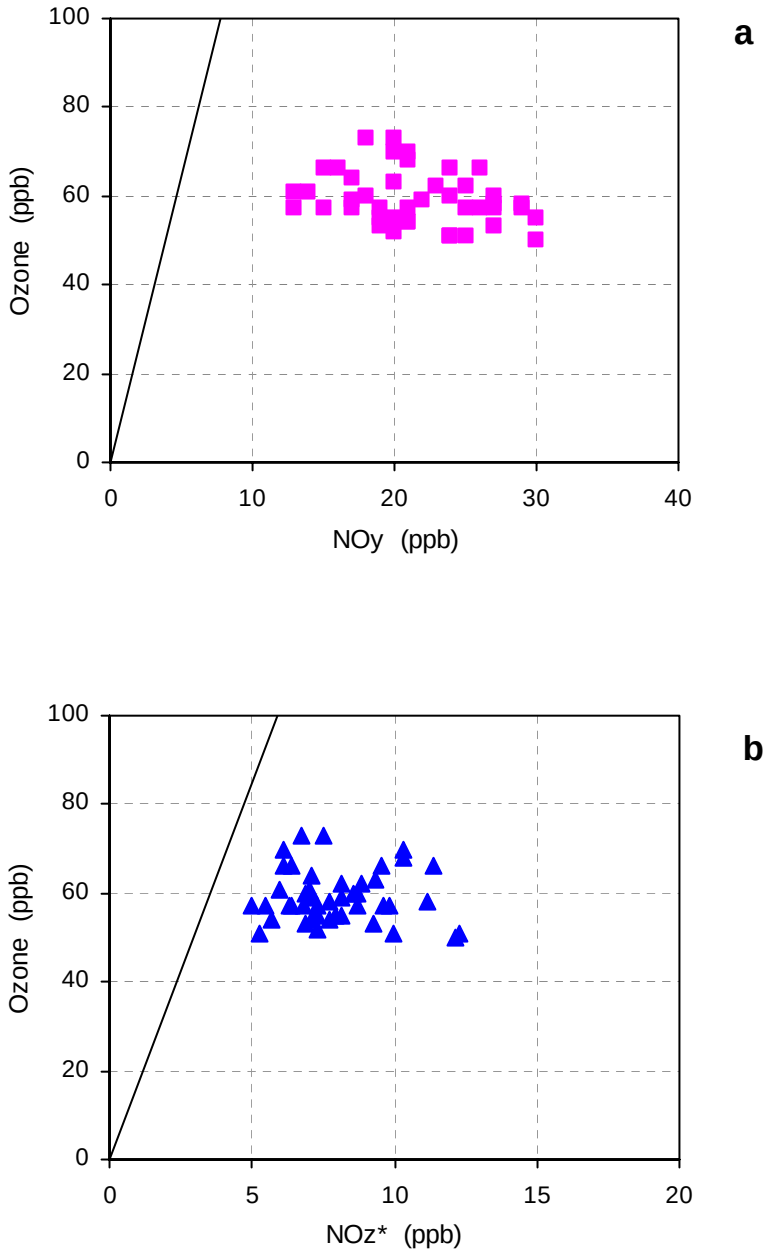

Figure 4.6. Scatterplot patterns of: (**a**) measured O_3 and concurrent NO_y and (**b**) measured O_3 and concurrent estimated NO_z* from 13:00 to 17:00 hr, September 3-30, 2003 at Cincinnati. The lines represent the transition between NO_x- and VOC-sensitive chemistry for O_3/NO_y and O_3/NO_z indicator ratios for low O_3 conditions (≥ 50 ppb) according to Sillman and He (2002).

4.1.4 Weekend/Weekday Effect Analysis

Figure 4.7 presents the average hourly diurnal weekend/weekday (WE/WD) variations of O_3 and NO from September 3-30, 2003. Table 4.4 presents the results of the tests for statistical significance in WE and WD for 1-hr O_3 maximum, 8-hr O_3 maximum average, and 6:00-9:00 hr NO average for the same sampling period.

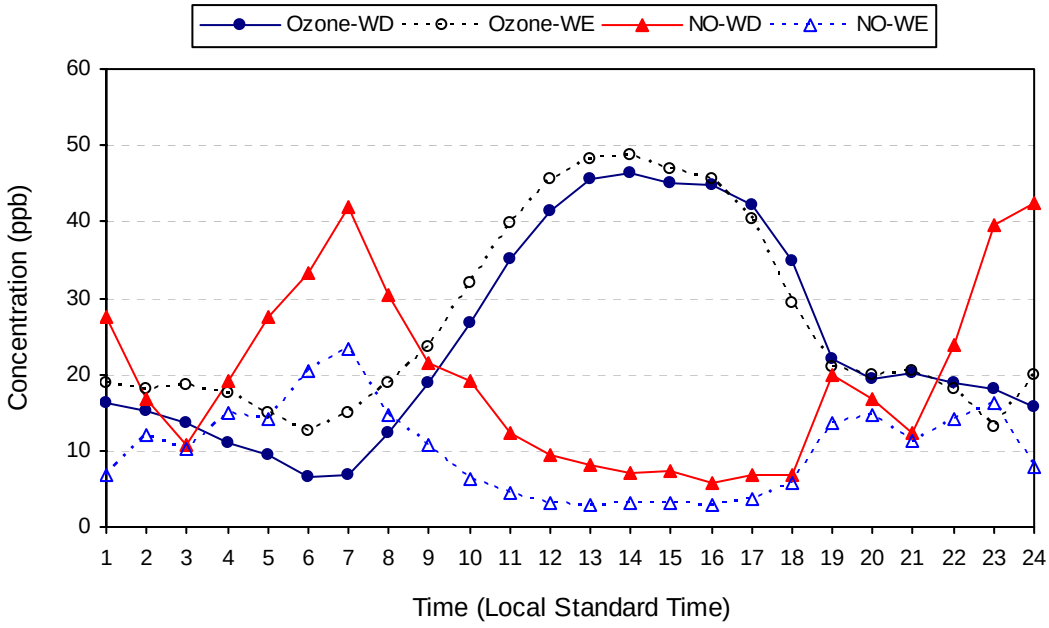

Figure 4.7. Average weekend and weekday hourly diurnal variations of O_3 and NO concentrations (September 3-30, 2003) measured at the Taft monitoring station, Cincinnati.

Average O_3 concentrations were lower during WD morning rush hours than in WE. This likely caused by the O_3 titration resulting from NO emitted by the heavy traffic during WDs. However, WE O_3 morning concentrations were around 7 ppb higher than those on WDs. Reduced diesel truck and gasoline vehicles traffic in WE could be associated with the reduction in NO_x emissions leading to a short supply of NO for morning titration. Accordingly, the average NO-O_3 crossover time in WE occurred about 1-hr earlier than in WD, and the duration of the build-up and accumulation of O_3 was also higher in WE (~ 6.3 hr) than in WD (~ 4.7 hr). The average WE/WD rate of accumulation of O_3 was also somewhat different.

It was a little faster in WE (5.8 ppb/hr) as compared with WD (5.1 ppb/hr). This change in efficiency and rate of WE /WD O_3 formation was probably due to reduced WE NO_x emissions and the associated higher WE VOC/NO_x ratio. This same phenomenon has been identified in California, where O_3 formation is dominated by VOC-sensitive conditions (Fujita et al., 2002).

Table 4.4. Results of the tests for statistical significance for WE/WD differences of maxima 1-hr and 8-hr average O_3 concentrations and 6:00-9:00 hr NO average levels for data registered between September 3-30, 2003, at the Taft monitoring station, Cincinnati.

Parameter	Mean (S.D.) ppb	No. of samples	Results of tests of significance	Interpretation
WE max 1-hr O_3	48.6 (14.4)	8	$p = 0.721$	H_0[b]: $\mu_{1\text{-hr O3WE}} = \mu_{1\text{-hr O3WD}}$ Accepted
WD max 1-hr O_3	46.4 (14.8)	17		H_1[c]: $\mu_{1\text{-hr O3WE}} < \mu_{1\text{-hr O3WD}}$ Rejected
WE max 8-hr O_3	43.3 (25.4)	8	$p = 0.739$	H_0[b]: $\mu_{8\text{-hr O3WE}} = \mu_{8\text{-hr O3WD}}$ Accepted
WD max 8-hr O_3	41.6 (11.6)	17		H_1[c]: $\mu_{8\text{-hr O3WE}} < \mu_{8\text{-hr O3WD}}$ Rejected
WE 6-9 a.m. NO	16.1 (25.4)	54	$p = 0.021$	H_0[d]: $\mu_{6\text{-9am NO WE}} = \mu_{6\text{-9am NO WD}}$ Rejected
WD 6-9 a.m. NO	31.7 (27.5)	24		H_1[e]: $\mu_{6\text{-9am NO WE}} > \mu_{6\text{-9am NO WD}}$ Accepted

[a] If $p \leq 0.05$, the difference is significant; if $0.05 \leq p \leq 0.10$ the difference between the means is marginally significant, if p>0.10, the difference is insignificant.
[b] H_0: The change in WE maximum O_3 is insignificant, likely to be caused by a VOC-sensitive condition provided that the reduction in morning WE-NO_x emissions is significant.
[c] H_1: The decrease in maximum WE maximum O_3 is significant, likely due to a NO_x-sensitive condition on condition that morning WE-NO_x emissions is significant.
[d] H_0: The reduction in morning WE-NO_x emissions is insignificant probably due to mere chance.
[e] H_1: The reduction in morning WE-NO_x is significant likely due to the reduction in WE activities.

The higher WE O_3 morning levels converted into higher afternoon levels relative to the WD O_3 peak levels. The difference between the average 13:00-15:00 hr WE/WD O_3 values was on the order of 2 ppb. As shown in Table 4.4 however, the difference in the 1-hr maximum WE/WD O_3 was not statistically

significant at a 95% confidence level. Shortly after 16:00 hr, average WE and WD O_3 concentration profiles crossed over and had a strong decreasing that suddenly ceased around 19:00 hr when both WE and WD O_3 were almost equal. From midnight to predawn, WE O_3 had a higher concentration than in WD.

The most obvious variation, shown in Figure 4.7, was in the NO WE/WD hourly average profile. Although the morning WE and WD NO peaks occurred at the same hour (~ 7 a.m.), the WD NO peak was almost 1.8 times higher than the WE NO peak. The previously suggested association between the reduction in WE NO_x emissions and the reduction in traffic seems to be confirmed by this difference.

Moreover, the importance of morning WE NO_x emissions reduction for afternoon WE O_3 concentrations is confirmed by the results shown in Table 4.4. The reduction in 6:00-9:00 hr average WE NO levels compared to the respective morning WD NO average concentration was statistically significant at a 95% confidence level. After the occurrence of the NO morning peaks, the diurnal NO levels were dominated by the WE levels. This difference converged around 19:00 hr. There was a second short NO peak in the evening, due likely to evening traffic. This peak was higher for WE compared to WD. A third nocturnal NO peak was observed in average WD NO concentrations equivalent in level to the WD morning peak but longer in duration. A careful examination of the hourly data indicated that, although the occurrence of very high NO concentrations around midnight did not follow a constant pattern, the measured values affected the calculated hourly averages. It is possible that the combination of a strong reconstruction of the shallow boundary layer with the typical nocturnal NO_x emissions could lead to such accumulation in the NO levels.

Because in the statistical analysis results showed in Table 4.4 one sample (WD) was almost 2.5 times as large as the other (WD), two additional evaluations were performed to corroborate these results. One was the use of a stricter two-tail *t-test* with unequal variances and another was the testing of the differences in the WE and WD means from a matrix of 2 days from the weekdays data set in order to have the closest population numbers (equal variances). In all cases the results of the tests were the same as those shown in Table 4.4. Appendix C presents a summary of the set of two WE/WD combinations.

The O_3 8-hr average diurnal WE/WD patterns (see Figure 4.8) followed the same outline as those for the O_3 1-hr patterns. They evidenced higher levels on WE than on WD during the daytime. The highest difference of ~ 6 ppb occurred at 11:00 hr. The WE O_3 8-hr average peak occurred at 17:00 hr with a difference of less than 2 ppb with respect to the respective WD average. Testing the results of the WE/WD O_3 8-hr average peaks showed that there was not a statistically significant difference between the peaks.

The statistical analyses of the WE/WD differences suggest that, even though the reduction in WE NO_x emissions (represented by the morning average NO concentrations) was significant, both average maximum 1-hr and 8-hr WE O_3 average concentrations were not significantly lower than the respective WD averages, as would be expected in dominant NO_x-sensitive conditions. On the contrary, the 1-hr and 8-hr WE O_3 peaks were somewhat higher than the respective WD averages, although not statistically significant resembling a situation somewhat similar of VOC-sensitive conditions.

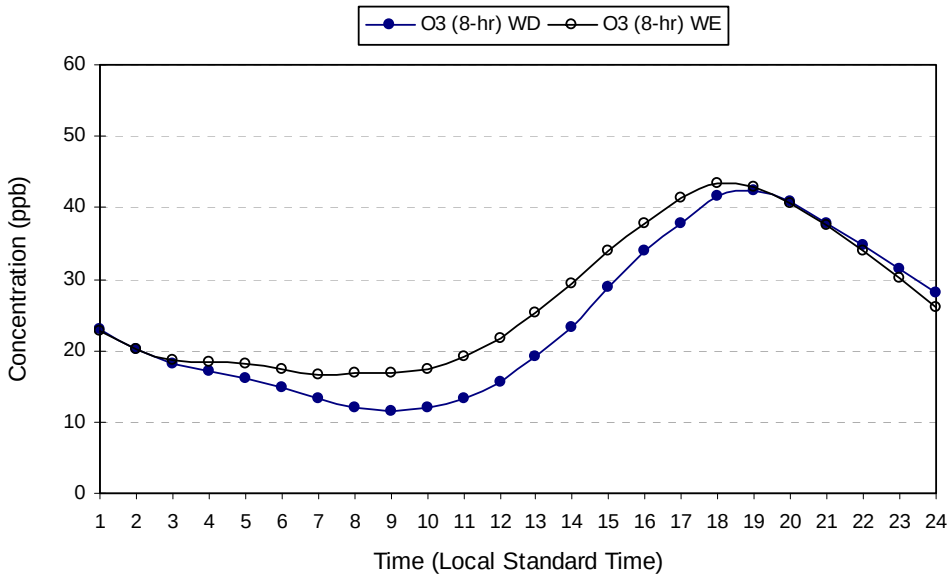

Figure 4.8 Average weekend and weekday 8-hr diurnal variations of O_3, September 3-30, 2003, for O_3 data registered at the Taft monitoring station, Cincinnati.

4.2 Mexico City Metropolitan Area

4.2.1 Indicator Species Measurements

Two monitoring campaigns were carried out from mid-February to mid-April 2004. The longest one was conducted at the urban smog-receptor site of Santa Ursula (19.3° N; 99.14° W, 2300 m.a.s.l.) in the south of Mexico City. The shortest was carried out at the downwind rural reference site of the Instituto Nacional de Investigaciones Nucleares (ININ) (Lat. 19.28° N; 99.38° W; 3119 m.a.s.l.) in the southwest mountains of the MCMA region (Figure 4.9).

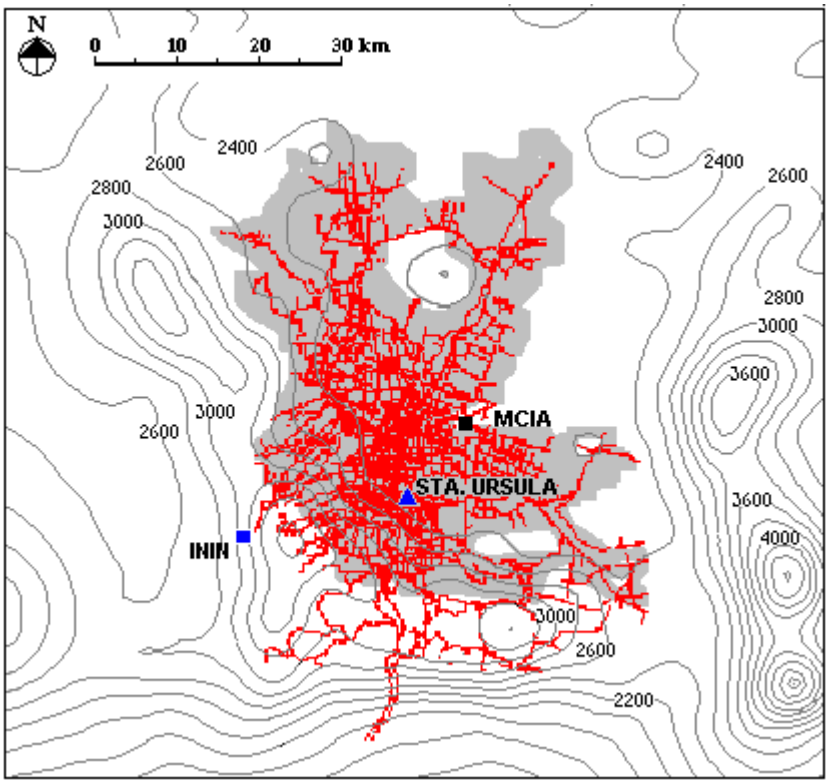

Figure 4.9. Map showing the Mexico City Metropolitan Area (MCMA) and the location of the Santa Ursula and the ININ monitoring sites. The gray area shows the approximate extent of the MCMA. MCIA represents the Mexico City International Airport. The dark-gray lines show the approximate elevation curves in the region. (Adapted from García, 2002).

4.2.1.1 Santa Ursula Monitoring Site

The Santa Ursula monitoring site (SUMS) is a typical urban-representative monitoring station of the official Automated Air Monitoring Network of the Government of Mexico City (RAMA). The SUMS is located within a typical low-medium income urban neighborhood of Mexico City. The site is not affected by any important fixed emission source and receives only the influence of the local traffic. The station is equipped with the following instruments: a $NO/NO_2/NO_x$ API Model 200 Chemiluminescent Analyzer, an O_3 API Model 400 Photometric Analyzer, a CO API Model 300 Infrared Analyzer, a SO_2 API Model 300 Fluorescence UV Analyzer, and a PM_{10} Rupprecht and Patashnick Model 1400 TEOM Analyzer. This station also measures other meteorological parameters. NO_y measurements were made with a chemiluminescence method using the NO_2/NO_x NO_x API Model 200 analyzer (or NO_y* analyzer) with an external heated converter mounted at the gas inlet. Personnel of the RAMA routinely calibrated the instruments following US EPA standard procedures.

The heated converter used in the SUMS consisted of a catalytic stainless steel (SS) converter assembly removed from a Columbia Scientific Industries Chemiluminizer Model NA510-2 NO_x analyzer. The SS tube was packed with ~ 1 g of molybdenum screen (12 x 12 wires cm^{-1}) (ThermoShield, Los Altos, CA). The converter was temperature controlled with a thermocouple embedded in the assembly and connected to a separate lab-made temperature controller. The temperature controller kept the temperature of the converter at approximately 370-385°C. Both the converter assembly and the temperature controller were located inside a small shelter that was mounted on the SUMS roof.

A Teflon tube (0.6 cm OD x 25 cm from the tip to heated converter) was used as the inlet line to the converter, while a ~ 3.5 m long Teflon tube connected the outlet of the converter to the NO_y* analyzer located inside the air-conditioned monitoring shelter. The NO_y* inlet tubing was not heated. A 47 mm Teflon filter pack located at the sampling inlet of the NO_y* analyzer protected the instrument from MnO dust. With the aim of keeping a relatively constant flow through the converter, a bypass pump was located ~ 0.8 m from the sample inlet of the instrument. The flow through the converter was ~ 1.5 L/ min. A number of tests (with- and without the Mo mesh packing) were carried out in the field to investigate the

converter configuration and operating conditions. The NO_y* analyzer was operated without any plumbing modification and with the original cycling sampling modes (NO/NO_x). The NO_x signal from the NO_y* analyzer was taken as the NO_y final reading. The conversion efficiency of the external converter was checked indirectly by comparing the NO_2 output reading of the NO_y* analyzer with the concurrent NO_2 reading of the other NO_x API 400 instrument dedicated to measuring NO_x species. Both the NO_y* and NO_x analyzers were periodically calibrated according to the US EPA NO_x calibration method. The NO_x analyzer sample inlet was connected to the common manifold of the monitoring shelter. The converter efficiency of the packed SS converter was calculated to be > 95%.

In order to estimate the NO_z* concentrations, the empirical model (BUWAL, 1997) was applied to the SUMS NO_x data. Due to technical difficulties, it was not possible to operate denuder samplers to collect H_2O_2 and HNO_3 at this site. Additional meteorological information was obtained from the Preparatoria 5 Meteorological Station located ~ 5 km to the east of the SUMS.

4.2.1.2 ININ Site

The ININ site is a research institute facility, about 35 miles southwest of downtown Mexico City, located in a semi-forested area partially insolated by a series of mountains. Because of its location downwind of the MCMA, the site is ideally suited for monitoring of the transport of air masses from the MCMA. The closest source of emissions to this site is a highway located ~ 3 miles to the north.

An equipped monitoring trailer belonging to the Atmospheric Physical-Chemical Group of the Center for Atmospheric Sciences (APC-CAS) was located in an insolated part of the ININ facility. The monitoring trailer was equipped with the following instruments: a $NO/NO_2/NO_x$ TEI Model 42C Chemiluminescent analyzer, an O_3 API Model 400 Photometric Analyzer, a CO TEI Model 48C Infrared Analyzer, and a Non-Methane HC TEI Model 55C, as well as a URG Annular Denuders System for HNO_3 integrated sampling. NO_y measurements were carried out with the $NO/NO_2/NO_x$ TEI 42C analyzer with an external heated catalytic converter (molybdenum). Calibration of all the instruments was carried out at

the site using standard gases and US EPA protocols. Meteorological parameters were measured with a Davis Weather Monitor III station.

The external converter consisted of an experimental prototype constructed in the electronics workshop of the Center for Atmospheric Sciences. It was made up of a straight stainless steel (SS) tube (0.6 cm x 25 cm) loosely packed with approximately 1 g of molybdenum screen (12 x 12 wires cm^{-1}) (Thermoshield, Los Altos, CA). The tube was placed in the center of two-channeled aluminum heating plates (12 cm x 10 cm x 2.5 cm each). This "oven" was heated by four concentrically separated tube-type heating cartridge elements (~ 10 cm long) inserted in each of plates. A thermocouple was inserted parallel to the SS tube in one of the two plates. The oven was inserted into a box made of ~ 5 cm thick solid insulating material. A Met-One data logger connected to a Campbell CR10X-console controlled the temperature of the converter. The operating temperature of the SS converter was set at 375°C.

The converter assembly was located inside a small metallic housing on the roof of the monitoring trailer, a configuration similar to the Santa Ursula site. The temperature controller system was placed inside a separated polypropylene-shelter box that was itself placed underneath the converter assembly. The inlet line to the converter consisted of a ~ 20 cm Teflon tube (0.6 cm OD). Another ~ 3 m Teflon tube (~ 0.6 cm OD) was extended from the outlet of the converter assembly to one of the inlets of an air sample diverter (a 3-way solenoid) connected directly to the NO_x analyzer. The other inlet of the 3-way solenoid valve was connected to a Teflon tube (~ 0.6 cm OD x 50 cm) that was inserted into the common manifold of the monitoring trailer. The purpose of this diverter was to allow the same NO_x instrument the measuring of both NO_y (from the external converter) and $NO/NO_2/NO_x$ (from the common manifold) concentrations in alternate equal short time cycles. A timer that switched the pass of the air sample to the analyzer every five minutes controlled the diverter. The out sample of the diverter was connected to a 47 mm diameter filter pack located at the sampling inlet of the analyzer to protect the instrument from MnO dust. In order to keep a constant flow of air through the converter during the "common manifold" diverter mode, an additional pump pulled the NO_y sample outside of the trailer at the same flow rate as the instrument.

The conversion efficiency of the external Mo converter was checked indirectly by comparing the NO_2 readings from the two inlet air sampling modes (i.e., external converter and common manifold flows). If the converter was operating correctly, under the "external converter" sampling mode, the NO_2 readings in the instrument should be "zero", because all the NO_2 that had passed previously across the external Mo converter had been reduced to NO. The NO_2* concentrations for the estimation of NO_z* were derived using the BUWAL equation and the NO_x readings taken from the "common manifold" air sampling mode.

Several attempts were made for sampling HNO_3 at this site. Instead of the typical 1-hr sampling period, the annular denuder system was operated for two hours in order to enhance the capture of gaseous HNO_3. Nitric acid was collected in one Na_2CO_3 coated URG annular denuder (3 channel x 30 mm O.D. x 242 mm length glass tube) at a sampling flow rate of 10 L/min. The extractions were done in the following 24 hours. The aqueous extracts were analyzed with a Perkin Elmer Liquid Chromatograph (Isocratic LC Pump 250) conductivity detector equipped with a Hamilton PRP-X100 IC anion column. The extractions and the analysis were performed at the APC-CAS laboratories. As well as in the SUMS gaseous hydrogen peroxide could not be sampled in this site.

4.2.2 General Findings

4.2.2.1 Santa Ursula Monitoring Site

The monitoring campaign at SUMS consisted of two stages: the first from February 18 to March 11, 2004, with the objective of testing the converter configurations; and the second from April 14 to 25, 2004 to measure, O_3, NO_y, NO and NO_x concentrations. Only the results of the measurement campaign are presented in this dissertation. Figure 4.10 shows the hourly average diurnal profiles of O_3, NO_y, and NO concentrations measured at SUMS from April 14-25. Table 4.5 presents the general statistical summary of the hourly measurements for the same monitoring period including the statistical summary of 30-min measurements of some meteorological parameters.

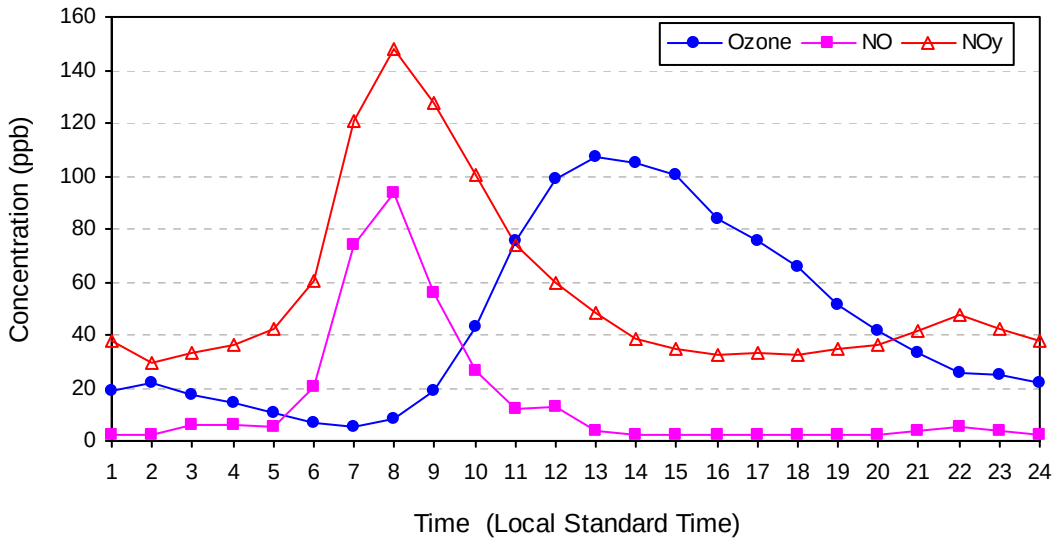

Figure 4.10. Composite diurnal profiles of hourly average NO, NO_y and O_3 concentrations measured at the Santa Ursula monitoring station in Mexico City, April 14 to 25, 2004.

Table 4.5. Statistical summary of hourly average NO, NO_x*[(a)], NO_y and O_3 concentrations and meteorological parameters[(b)] measured at the Santa Ursula monitoring station, Mexico City (April 14-27, 2004).

Parameter	Unit	Mean	S.D.	Range	No. of Samples
NO	ppb	14.8	29.8	0.05-183	271
NO_x*[(a)]	ppb	45.3	38.2	11-226	271
NO_y	ppb	54.7	39.0	16-228	243
O_3	ppb	44.7	37.1	4-172	286
Temperature	°C	19.7	4.86	9.1-28.2	491[c]
Wind Speed	m/sec	1.57	1.64	0-7.2	480[c]
Wind Direction	degrees	Dominant: 360 (22.12%)		0-360	480[c]

a NO_x values as measured by the NO_x dedicated instrument.
b Measured at the "Preparatoria 5" High School.
c 30-min average

Diurnal average ozone concentrations followed the typical urban pattern, with the peak between 12:00 to 15:00 hr and the lowest levels during the morning rush hours (6:00-8:00 hr). Average O_3 photochemical production started around 7:00 hr, shortly after the occurrence of the NO peak (~ 92 ppb),

and reached its maximum (~ 107 ppb) when NO levels dropped to their minimum (~4 ppb). The net build-up of O_3 started before 10:00 hr and the duration of effective ozone accumulation lasted around 3.3 hrs. The average rate of accumulation was ~ 21.4 ppb/hr. The ridge of levels above 80 ppb extended for approximately 5 hr. The period with O_3 peak was relatively short and, after 14:00 hr, ozone levels started to decrease, following a smooth slope. The mean of O_3 concentrations was 44.7 ppb and hourly average values ranged from 4 to 172 ppb. A detailed review of the data showed that the Mexican Ozone Air Quality Standard (0.12 ppm max 1-hr) was exceeded 17 times during this 12-day monitoring period.

On the other hand, the diurnal average NO concentrations pattern showed one peak between 6:00-9:30 hr. The NO raised and reached a maximum around 8:00 hr (~ 92 ppb) that coincided with the maximum emissions of NO during the day, in this case, morning peak vehicle traffic. Subsequently, NO concentrations dropped at an average rate of ~ 17 ppb/hr, reaching a low level plateau of less than 10 ppb for the rest of the day. Average NO_y concentrations had a pattern similar to the NO levels but with a second small peak around 22:00 hr. There was a longer "valley" of NO_y average concentrations (between 38 and 32 ppb) from 14:00-18:00 hr, before the occurrence of the second evening peak (~ 45 ppb). The meteorological conditions during this campaign were typical for this time of the year, with predominantly light winds coming from the north and, with less frequency, from the northeast. The afternoon hourly concentrations of NO, NO_y, and O_3, as well as estimated NO_x* and NO_z* values were statistically analyzed with the same method as the Cincinnati data (Table 4.6).

Table 4.6. Statistical summary of hourly average concentrations of measured O_3, NO, NO_y and estimated NO_x* and NO_z* between 13:00-17:00 hr (April 14-25, 2004) at the Santa Ursula monitoring station, Mexico City[a].

Parameter	**Mean (ppb)**	**S.D. (ppb)**	**Range (ppb)**	**N**
NO	2.6	1.2	1-7	54
NO_y	37.3	10.0	21-69	54
NO_x*	16.3	5.5	10-35	54
NO_z*	21.0	5.7	9-33	54
O_3	94.0	26.5	50-172	54

[a] Weekend and weekdays.

The range of NO_y concentrations measured at the Santa Ursula site (21-69 ppb) was significantly lower than the range of NO_y afternoon levels (10-240 ppb) reported by Sosa et al. (2000) for two sites in Mexico City close to downtown in March 1997. Although care should be taken when comparing the NO_y values reported by Sosa et al. (2000), because they based their analysis on a composite of measurements of NO_x, PAN, HNO_3, and NO_3^- that were not taken simultaneously, were not corrected for known interferences (NO_x measurements), and, in some cases, were not measured at the same site. However, the range of concurrent calculated NO_z* for the Santa Ursula site (9-33 ppb) was very similar to the range of NO_z values (as the sum: PAN + HNO_3 + NO_3^-) reported by these authors (1-35 ppb). In comparison, the ranges of the measured O_3 and NO_y concentrations and estimated NO_z* values in Santa Ursula were below the ranges of the respective measurements reported for the Los Angeles Basin during August 1987. The Los Angeles measurements were ~ 20-240 ppb for O_3; ~ 25-140 ppb for NO_y; and ~ 2-55 ppb for NO_z (Sillman et al, 1997).

4.2.2.2 ININ Site

Although the monitoring campaign at the ININ site extended from April 1-20, 2004, effective measurements of NO_y were possible only from April 16-19. Before April 16, cold weather, cloudy conditions, and continuous rain kept the NO_y measurements at a very low level and without variation. There was evidence that the low temperatures (median ~ 9.5°C and lows ~ 2°C) affected the conversion efficiency of the external converter. This situation changed during the week of April 15 when micro-regional weather conditions changed and ambient temperatures rose, coinciding with several smog events in Mexico City. Figure 4.11 shows the hourly average diurnal profiles of O_3, NO_y, and NO concentrations from April 16-19 at the ININ site. Table 4.7 presents a statistical summary of the measurements, including meteorological information for this period. According with Figure 4.11, nocturnal and early morning O_3 levels remained almost at a background level (~ 40 ppb), due to the lack of sufficient NO concentrations to titrate the ozone concentrations.

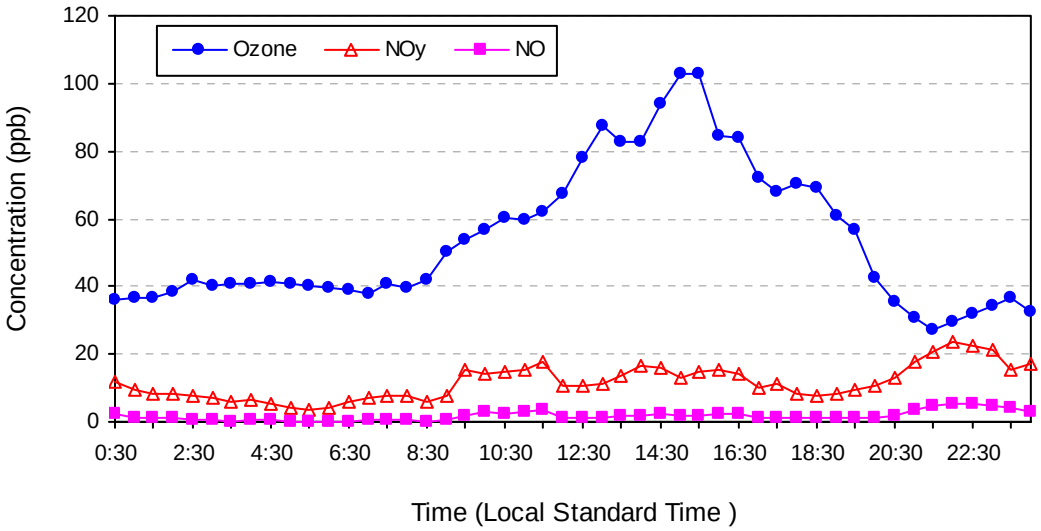

Figure 4.11. Composite diurnal profiles of 30-min average O_3, NO_y, and NO concentrations measured at the ININ site in southwest Mexico City, April 16 to 19, 2004.

O_3 production started after sunrise and was a result primarily of NO_x emitted in the nearby area. The average rate of O_3 accumulation was ~ 7.2 ppb/hr, once the ozone levels began to increase. The average time of O_3 build-up was around 7 hrs and the average time with ozone concentrations above 80 ppb was 4 hrs. The O_3 peaks occurred in the afternoon hours when the mixing layer reached its maximum development in region. The pass of air parcels coming from the urban area was registered with the occurrence of high ozone levels several hours after the maximum solar radiation. O_3 reached its maximum around 17:00 hr when solar radiation was at a minimum. NO and NO_y concentrations were in general low and did not show the typical morning peak observed in urban areas. From ~ 9:00 to ~ 17:00 hr, the NO_y concentrations rose and fluctuated between 10 and 20 ppb. A peak in NO_y levels occurred after sunset in concert with a decrease in O_3 concentrations. This effect could be a result of the movement of air parcels containing "fresh" NO_x from nearby locations. During the four-day smog-event period, one exceedence to the Mexican Ozone Air Quality Standard was observed. The NO levels did not equal the lowest O_3 concentration along the entire monitoring period. The diurnal NO_y average was 12.1 ppb, which was almost 4.5 times lower than the same average for the Santa Ursula site.

Table 4.7. Statistical summary of daily 30-min average NO_x*[(a)], NO_y and O_3 concentrations and 1-hr average meteorological parameters measured at the ININ site in southwest Mexico City (April 16-19, 2004).

Parameter	Unit	Mean	S.D.	Range	No. of Samples
NO	ppb	1.6	1.6	0.01-9.54	151
NO_x*[(a)]	ppb	10.7	6.69	1.0-41.5	155
NO_y	ppb	12.1	6.6	1.3-35.7	135
O_3	ppb	52.2	23.7	17.6-125.8	161
Temperature	°C	13.1	7.37	3.2-25.6	109
Wind Speed	m/sec	0.97	0.62	0-2.2	109
Wind Direction	degrees	Dominant: 202.5 (28.5%)		0-360	109

(a) NO_x values as measured by the instrument.
(b) 30-min average

Table 4.8 presents a basic statistical analysis of the 30-min average NO, NO_y, and O_3 measured concentrations for the afternoon hours (13:00-17:00 hr) from April 16-19, 2004. This table also shows the estimated NO_x* and NO_z* values at the ININ site.

Table 4.8. Statistical summary of 30-min average concentrations of measured NO, NO_y and estimated NO_x* and NO_z* between 13:00-17:00 hr (April 16-19, 2004) at the ININ site in southwest Mexico City.

Parameter	Mean (ppb)	S.D. (ppb)	Range (ppb)	N
NO	1.9	0.85	0.56-3.5	25
NO_y	14.6	4.16	7.7-22.3	25
NO_x*	9.67	2.88	5.0-15.0	25
NO_z*	2.2	0.41	1.6-3.1	25
O_3	87.5	19.4	56.3-125.8	26

The NO_y average afternoon level was 2.5 times lower than the same average in Santa Ursula, and the average afternoon NO_z* value was around 10 times lower than that at Santa Ursula. However, the average afternoon O_3 concentration was very close to that of the Santa Ursula site for the same dates.

Several samples of gaseous HNO_3 were collected with an annular denuder system at the ININ site. Table 4.9 presents the results of an analysis of the aqueous extracts from samples taken between April 13-19, 2004.

Table 4.9. Statistical summary of the analytical results for aqueous extracts of samples of HNO_3 collected with an annular denuder system at the ININ site from April 13 to 19, 2004.

Date	**Sampling period**	**Concentration (μg/mL)**	**Comment[a]**
April 13	10:00-11:07 hr	0.0440	< Detection limit
April 13	11:00-14:13 hr	0.0080	< Detection limit
April 16	12:00-14:00 hr	0.0296	< Detection limit
April 16	9:54-11:54 hr	0.0133	< Detection limit
April 19	11:56-13:53 hr	0.0310	< Detection limit
April 19	Transport blank	0.0032	-

[a] Detection limit = 0.07 μg/mL

As shown in Table 4.9, however, the amount of HNO_3 collected in all the samples was insufficient to reach the detection limit of the analytical method. The very low concentrations of HNO_3 encountered at the ININ site suggested that mechanisms were removing the HNO_3 from the air parcels before they reached this area.

4.2.3 Photochemical Indicators Evaluation

4.2.3.1 Santa Ursula Monitoring Site

Figure 4.12 shows the comparison between measured afternoon hourly averages of O_3 and NO_y and measured O_3 and estimated NO_z* in Santa Ursula and these parameters reported at several sites in the U.S. and in Paris, France (Sillman 2002). Figure 4.12 demonstrates that the measured data points from Santa Ursula matched the pattern of measured data from Los Angeles. Figure 4.13 presents a comparison of the scatterplot patterns of measured afternoon O_3, measured NO_y, and estimated NO_z* at Santa Ursula with a composite of scatterplot patterns of predicted O_3 versus NO_y and NO_z afternoon values for mixed-, VOC-, and NO_x-titration conditions for several regions in the U.S. (Sillman and He, 2002).

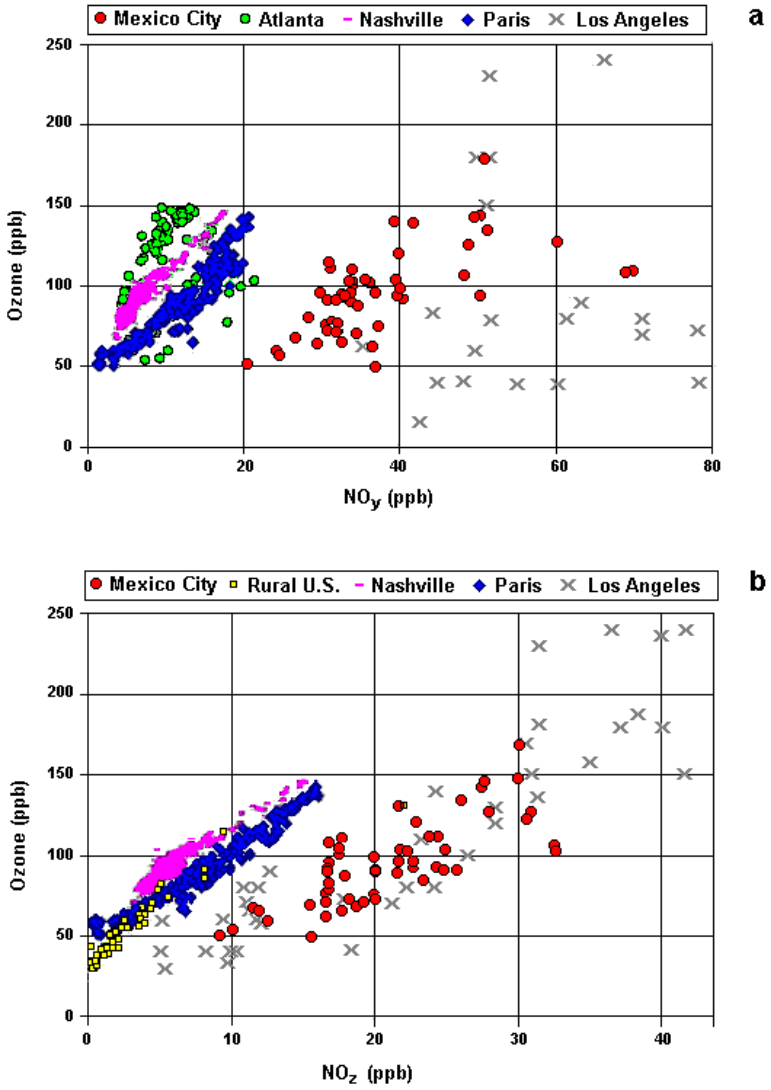

Figure 4.12. Scatterplot patterns of: (**a**) measured O_3 and NO_y, and, (**b**) measured O_3 and estimated NO_z* at Santa Ursula, Mexico City, compared with measured correlations of O_3 and NO_y and NO_z patterns for different locations identified as: NO_x-sensitive (Atlanta and Rural U.S.), mixed sensitive (Nashville and Paris), and VOC-sensitive (Los Angeles). Scatterplots adapted from Sillman (2002 and 2003).

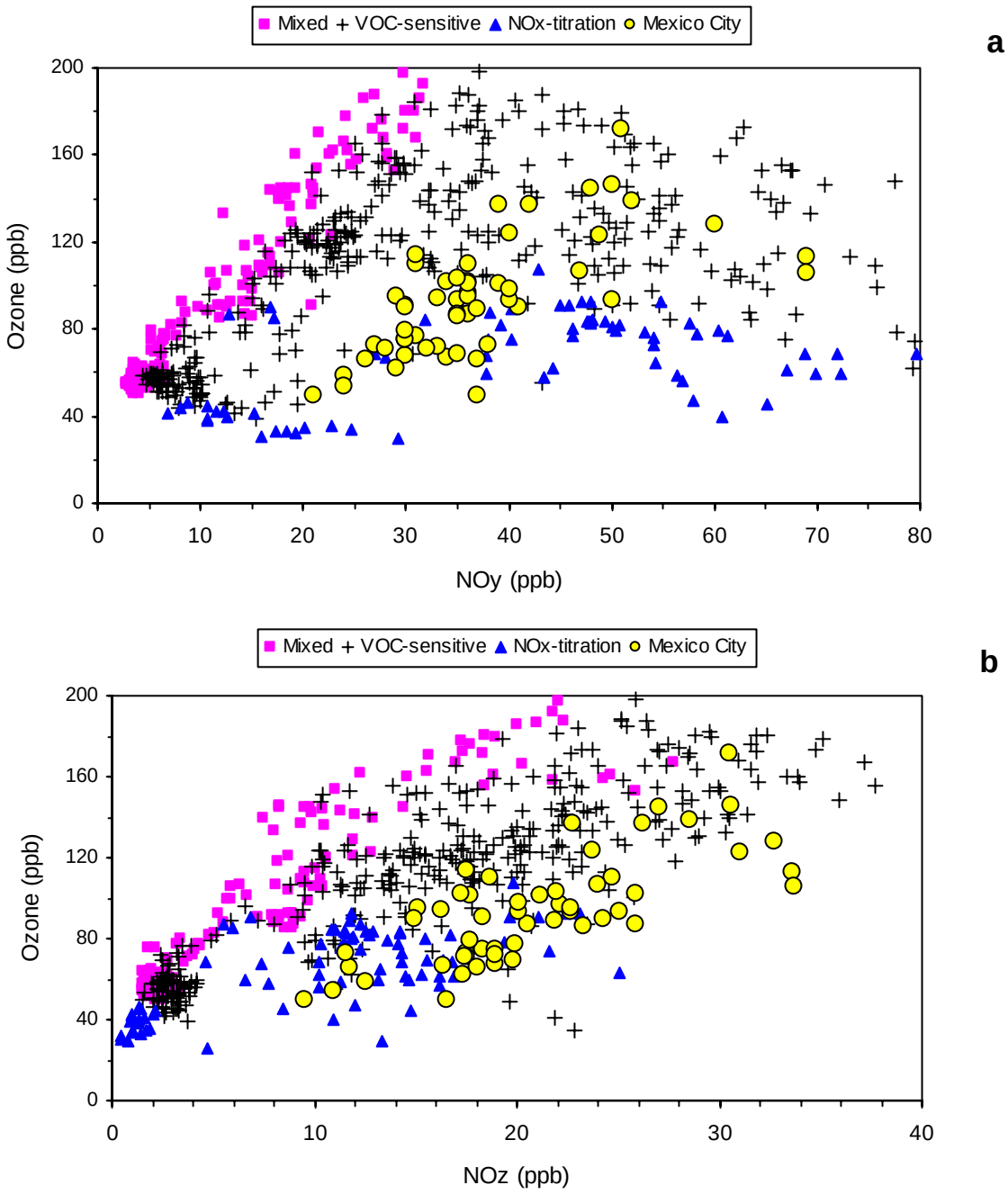

Figure 4.13. Scatterplot patterns of: (**a**) measured O_3 and NO_y, and (**b**) measured O_3 and estimated NO_z* at Santa Ursula, Mexico City, compared with 3-D model predicted O_3 and NO_y and NO_z patterns, respectively, for locations with mixed or with near-zero sensitive conditions (squares), VOC-sensitive conditions (crosses), and dominated by NO_x-sensitive titration (triangles). Simulation data obtained from data file available from Sillman (2003).

According to Figure 4.13(a), the O_3 versus NO_y scatterplot correlation for the Santa Ursula data practically superimposed one important segment of the respective simulated correlation for VOC-conditions. However, some data points of the O_3 versus estimated NO_z data points for Santa Ursula, seen in Figure 4.13(b), overlapped with the pattern for simulated conditions dominated by NO_x-titration.

Following the procedure used to clarify this same contradiction observed in the data for Cincinnati, Figure 4.14 shows the scatterplot correlation for O_3 versus the ratio NO_x^*/NO_y for Santa Ursula superimposed on the simulated O_3 versus NO_x/NO_y ratios for VOC-sensitive and NO_x-titration conditions. This figure clearly shows that the measured indicator species at Santa Ursula were strongly associated with VOC-sensitive conditions, as predicted.

The estimated afternoon average NO_x^*/NO_y ratio for the Santa Ursula data was ~ 0.44, suggesting that the air masses that passed over this site during the monitoring campaign were "middle-aged" parcels. Table 4.10 shows the comparison between the calculated average indicator ratios and the average NO_y concentration from the measurements carried out at Santa Ursula and the transition values suggested by Sillman (1995) and Sillman and He (2002) for moderately O_3 polluted sites. According to this table, the three indicator ratios O_3/NO_y, O_3/NO_z^*, and NO_y pointed to VOC-sensitive conditions.

Figure 4.15 presents the scatterplot of measured afternoon O_3 versus concurrent NO_y and of measured O_3 versus concurrent estimated NO_z^* at Santa Ursula, compared with the mean transition lines for NO_x- and VOC-sensitive conditions for moderately polluted conditions (80 ppb < $[O_3]$ < 200 ppb).

Table 4.10. Calculated average indicator ratios observed at the Santa Ursula Monitoring Station (Mexico City) and transition values for moderately ozone (80 to 200 ppb) polluted conditions according to Sillman (1995) and Sillman and He (2002). Values of ratios lower than their transition ranges indicate VOC-sensitivite conditions. Values of NO_y higher than the transition value indicate VOC-sensitive conditions.

Indicator	Santa Ursula average ratios	Transition range
O_3/NO_y	2.5	6-8
O_3/NO_z	4.47	8-10
NO_y	37.3	20

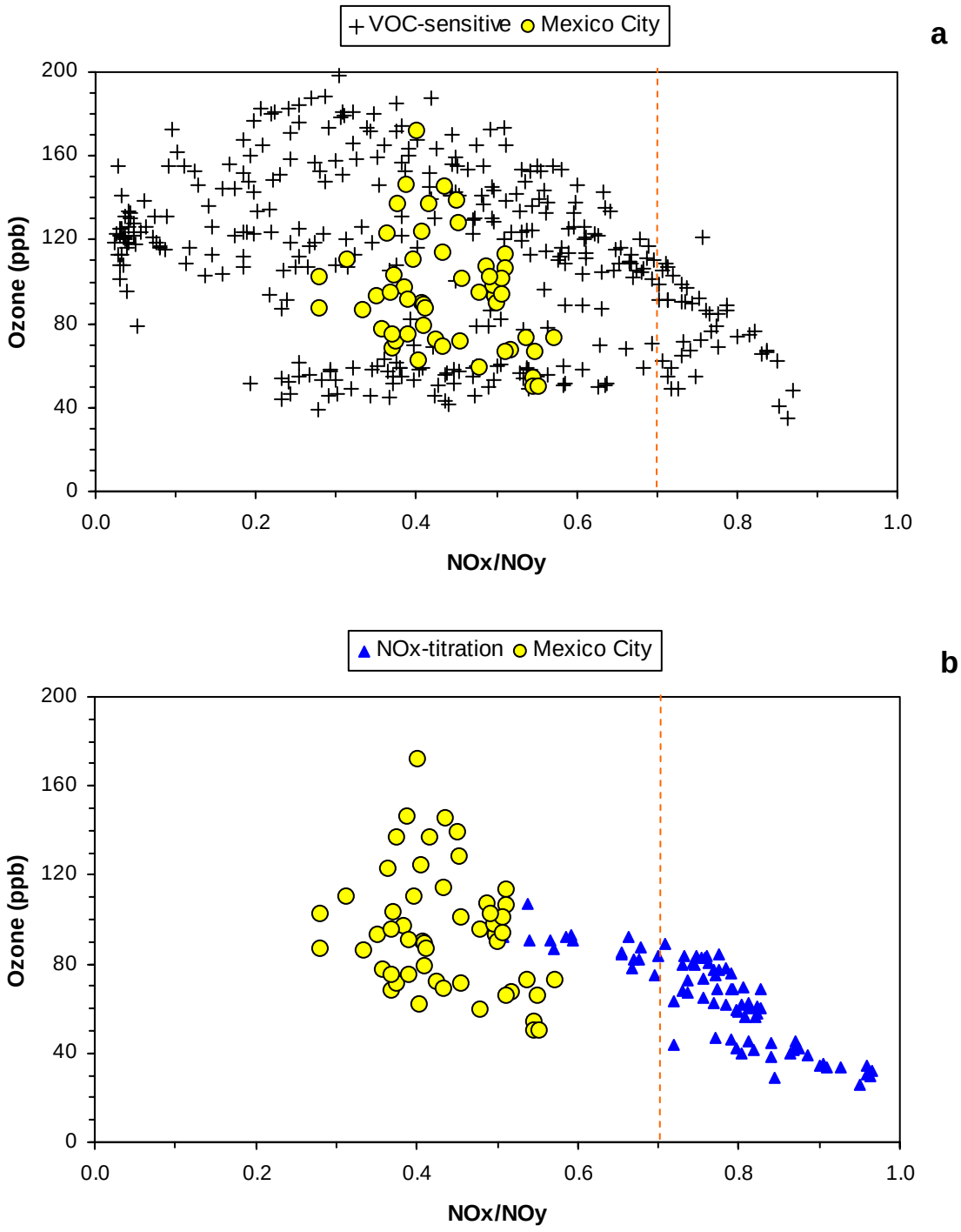

Figure 4.14. Scatterplot patterns for afternoon O_3 versus NO_x*/NO_y data for Santa Ursula, Mexico City, compared with the calculated NO_x/NO_y ratio from data results of 3-D model simulations for locations with: (**a**) VOC-sensitive conditions, and (**b**) dominated by NO_x-titration. The vertical dashed line represents the hypothetical limit to differentiate photochemically aged air parcels. Simulation data obtained from data file available from Sillman (2003).

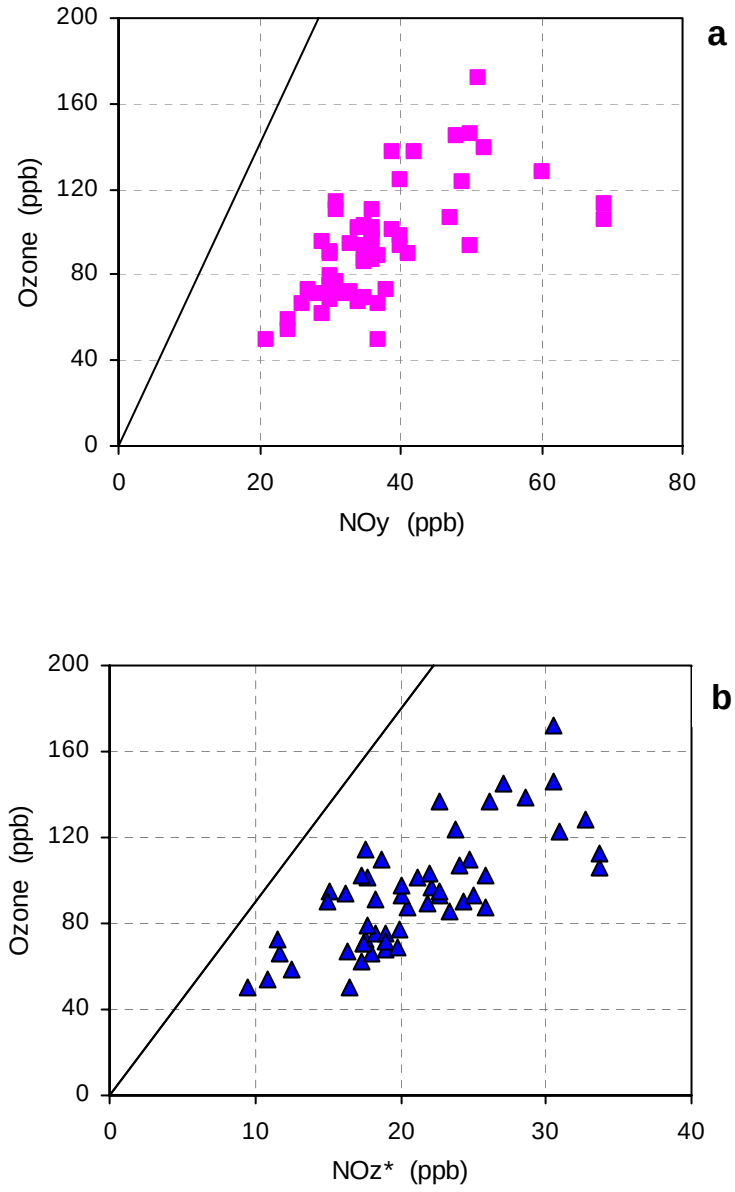

Figure 4.15. Scatterplot patterns of: (**a**) measured O_3 and concurrent NO_y, and (**b**) measured O_3 and concurrent estimated NO_z* from 13:00 to 17:00 hr, April 14-25, 2003 at Santa Ursula, Mexico City. The lines represent the transition between NO_x- and VOC-sensitive chemistry for O_3/NO_y and O_3/NO_z indicator ratios for moderately O_3 conditions (80 ppb ≤. $[O_3]$ ≤ 200 ppb) according to Sillman and He (2002).

The evaluation of the consistency of the NO_y measurements through the correlation between O_3 and the sum ($2H_2O_2$ + NO_z) could not be performed in this site because H_2O_2 measurements were not available. Two indirect alternative approaches were used for this evaluation. The first consisted in the regression analysis of CO concurrent with the NO_y monitoring data. As previously indicated, an acceptable correlation coefficient would be indicative that NO_y measurements were reliable. The second approach consisted in the empirical scatterplot comparison of the NO_y values versus the O_3/NO_z* ratio. The criterion applied was that, if the suggested sensitivities shown simultaneously for the indicators NO_y and O_3/NO_z* were consistent among them, that would be an indication that the NO_z* values were within reasonable values.

Figure 4.16 shows the correlation between hourly measurements of CO and NO_y at SUMS from April 14-25, 2004 and the NO_y-O_3/NO_z* correlation for the same data period. As shown in Figure 4.16(a) the correlation between CO and NO_y concentrations resulted in an R^2 = 0.88. The losses in some NO_y species by deposition mechanisms could be associated with the withdrawal of the data points from the ideal correlation.

In Figure 4.16(b), all the data points of the NO_y-O_3/NO_z* correlation fell in the upper left quadrant (NO_y > 20 ppb and O_3/NO_z* < 7 for moderate ozone conditions). The measured indicators were consistent with each other simultaneously.

4.2.3.2 ININ Site

Figure 4.17 shows the correlations patterns of measured O_3 (≥ 50 ppb) versus measured NO_y and estimated NO_z* for the ININ site with 3-D model predicted O_3, NO_y, and NO_z patterns, respectively. The model predictions are for locations with mixed or with near-zero sensitive conditions. Figure 4.17 reveals a contradiction in the PIM theory. While the correlation of O_3 versus NO_y suggests that VOC-sensitive conditions were prevalent at the ININ site, the correlation of O_3 versus NO_z* indicates that relatively strong NO_x-sensitive conditions could dominate this site during smog-events.

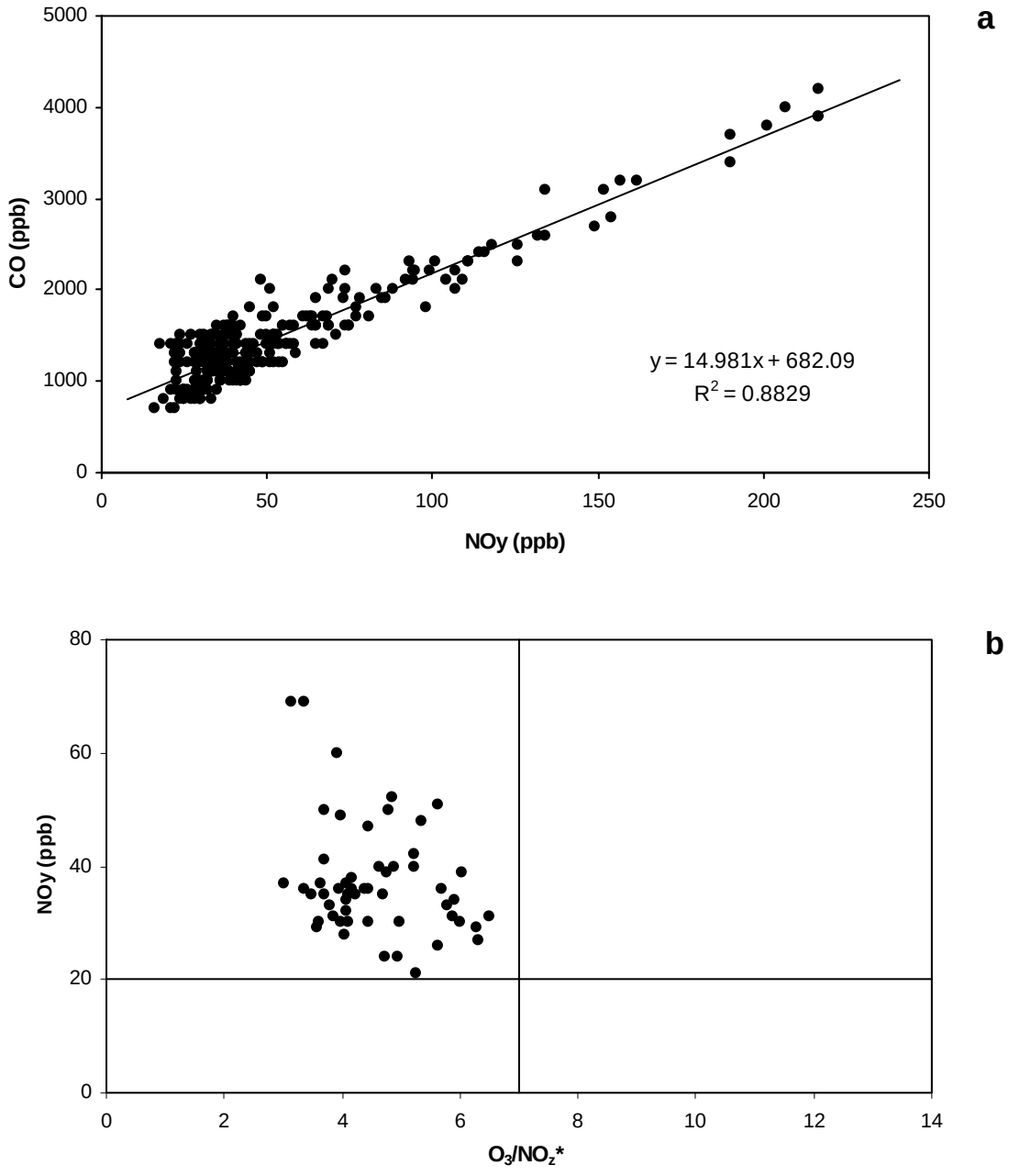

Figure 4.16. Scatterplot patterns between: (**a**) diurnal CO and concurrent NO_y hourly concentrations, and, (**b**) correlation between afternoon NO_y concentrations and O_3/NOz^* ratios for measurements carried out at the Santa Ursula Monitoring Station from April 14 to 25, 2004.

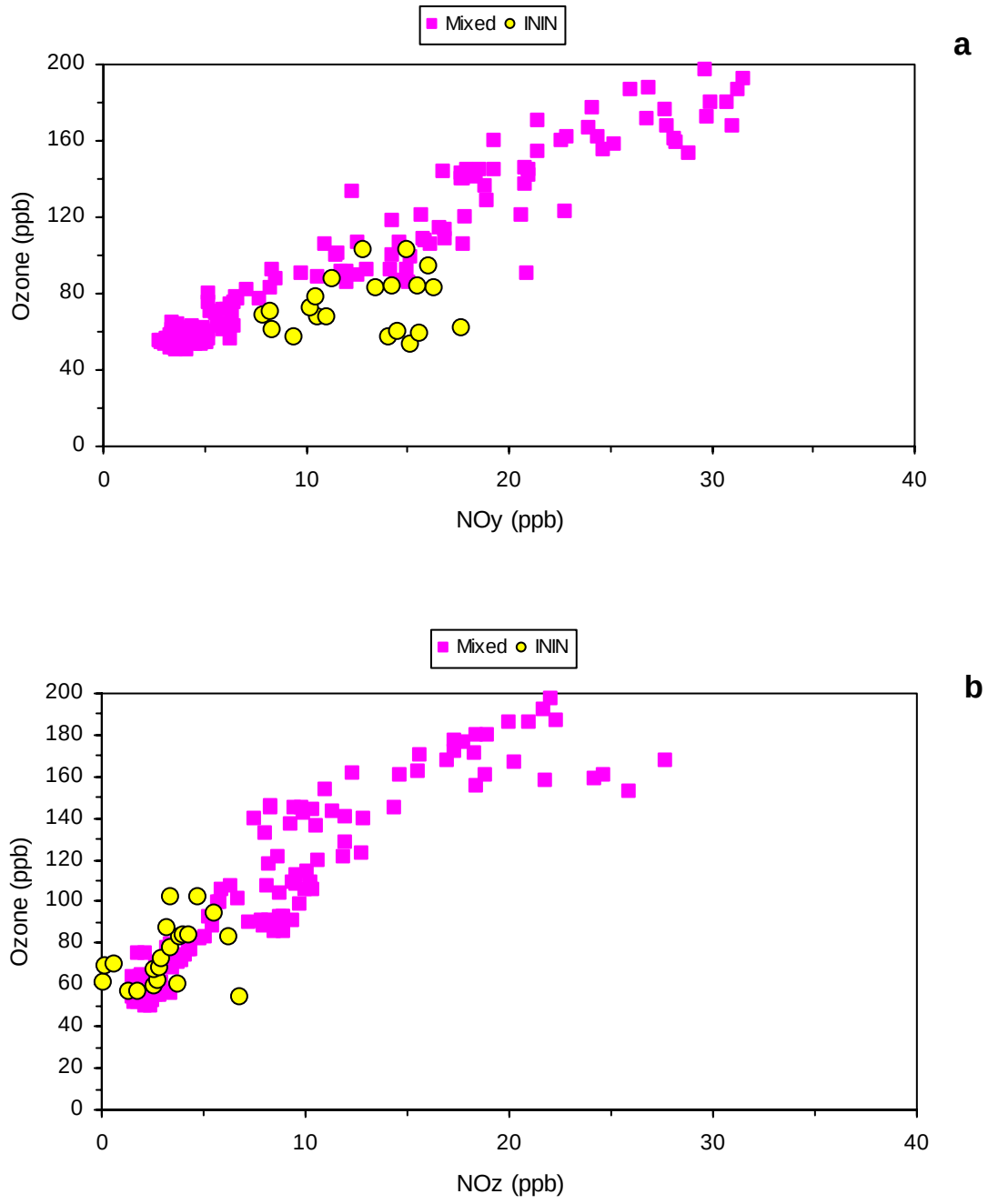

Figure 4.17. Scatterplot patterns of: (**a**) measured O_3 (≥50 ppb) and NO_y, and (**b**) measured O_3 (≥ 50 ppb) and estimated NO_z* at the ININ site south west Mexico City, compared with 3-D model predicted O_3 and NO_y and NO_z patterns, respectively, for locations with mixed or with near-zero sensitive conditions. Simulation data obtained from data file available from Sillman (2003).

This contradiction might be explained by analyzing the pattern of O_3 versus NO_z*. The narrow range of NO_z* concentrations shown in Figure 4.17 suggests that the air masses that passed over the site most likely suffered the prior removal of species such as HNO_3 and NO_3^- aerosols. Otherwise the NO_z* values should match the mixed-sensitive conditions but not those of the NO_x-sensitive region.

It is also possible that the complete opposite occurred. That is, the heated Mo converter could have a lower conversion efficiency to HNO_3 and PAN species present in the sample, leading to the measurement of relatively smaller NO_y concentrations and, therefore, to smaller differences in the subtraction of NO_y - NO_x*. Singh (1987) suggested that, like ozone, PAN is continually synthesized during the transport of air masses and that PAN acts as both carrier and reservoir of NO_2 due to the thermal instability of its molecule [$CH_3C(O)–O–O + NO_2 \leftrightarrow CH_3(O)–O–O\text{-}NO_2$].

As a result, it is possible that the analyzer had measured levels of both PAN and NO_2 in the "NO_y mode" very similar to those detected in the NO_x mode. Due to this uncertainty in the NO_y measurements and, thus, in the estimated NO_z* levels, no preliminary conclusions were drawn from the experimental results at this site.

4.2.4 Weekend/Weekday Effect Analysis

Although the monitoring period for NO_y at SUMS extended from April 14-25, the weekend/weekday (WE/WD) analysis was performed on the entire data set of hourly averages of O_3 and NO concentrations registered from April 1-30. Figure 4.18 shows the average hourly diurnal WE/WD variations of O_3 and NO for April 2004 at SUMS. Table 4.11 presents the results of the tests for statistical significance in WE and WD for 1-hr and 8-hr average O_3 maximum and 6:00-9:00 hr NO average concentrations for the same sampling period.

According to Figure 4.18, the hourly average O_3 WE and WD daily patterns were very similar. The lowest average ozone concentrations occurred in the morning hours and the peaks around 14:00 hr. The 6:00-9:00 average WD O_3 concentration was slightly lower during morning rush hours than on the WE, probably as a result of O_3 titration by NO emitted from heavy weekday traffic.

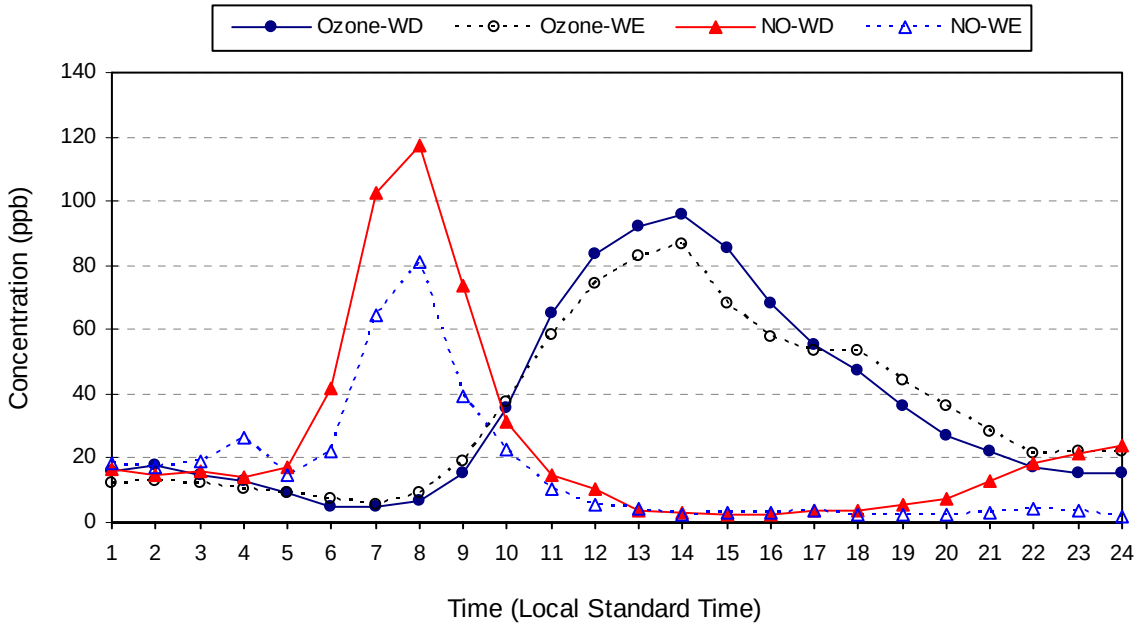

Figure 4.18. Average weekend and weekday hourly diurnal variations of O_3 and NO concentrations measured at the Santa Ursula monitoring station, Mexico City from April 1-30, 2004.

However, the average of maximum WD O_3 concentrations was around 10 ppb higher than that on the WE. Immediately after the occurrence of the peak, a relatively constant decrease in O_3 levels was observed in both cases.

In general, the O_3 WE and WD daily patterns in Santa Ursula showed a correspondence with the typical amount of emissions of ozone precursors during these days. Reduced diesel truck and gasoline vehicle traffic in WE could be associated with the reduction in NO_x emissions leading to a relatively short supply of NO for morning titration. However, the average NO-O_3 crossover time in WE was only about 30-min earlier than that in WD. The duration of the build-up and accumulation of O_3 was also slightly higher in WE (~ 4.3 hr) than in WD (~ 4 hr). The average WE/WD rate of accumulation of O_3 was also different. It was somewhat faster in WD (15.3 ppb/hr) than in WE (13 ppb/hr). This apparent inverse correspondence could be related to a proportional reduction in both anthropogenic VOC emissions and NO_x in WE.

Table 4.11. Results of the tests for statistical significance for WE/WD differences of maxima 1-hr and 8-hr average O_3 concentrations and 6:00-9:00 hr. NO average levels for data registered between April 1 through 30, 2004, at the Santa Ursula monitoring station, Mexico City.

Parameter	Mean (S.D.) ppb	No. of samples	Results of tests of significance	Interpretation
WE max 1-hr O_3	86.6 (40.5)	8	$p = 0.559$	H_0[b]: $\mu_{1\text{-hr O3WE}} = \mu_{1\text{-hr O3WD}}$ Accepted
WD max 1-hr O_3	96.1 (37.8)	21		H_1[c]: $\mu_{1\text{-hr O3WE}} < \mu_{1\text{-hr O3WD}}$ Rejected
WE max 8-hr O_3	74.0 (22.8)	8	$p = 0.505$	H_0[b]: $\mu_{8\text{-hr O3WE}} = \mu_{8\text{-hr O3WD}}$ Accepted
WD max 8-hr O_3	66.8(29.8)	17		H_1[c]: $\mu_{8\text{-hr O3WE}} < \mu_{8\text{-hr O3WD}}$ Rejected
WE 6-9 a.m. NO	61.5 (59.7)	56	$p = 0.0094$	H_0[d]: $\mu_{6\text{-9am NO WE}} = \mu_{6\text{-9am NO WD}}$ Rejected
WD 6-9 a.m. NO	97.5 (43.7)	24		H_1[e]: $\mu_{6\text{-9am NO WE}} > \mu_{6\text{-9am NO WD}}$ Accepted

[a] If $p \leq 0.05$, the difference is significant; if $0.05 \leq p \leq 0.10$ the difference between the means is marginally significant, if p>0.10, the difference is insignificant.

[b] H_0: The change in WE maximum O_3 is insignificant, likely to be caused by a VOC-sensitive condition provided that the reduction in morning WE-NO_x emissions is significant.

[c] H_1: The decrease in maximum WE maximum O_3 is significant, likely due to a NO_x-sensitive condition on condition that morning WE-NO_x emissions is significant.

[d] H_0: The reduction in morning WE-NO_x emissions is insignificant probably due to mere chance.

[e] H_1: The reduction in morning WE-NO_x is significant likely due to the reduction in WE activities.

The decreased availability of NO in WE could allow O_3 increased time for accumulation, but the relatively small supply of reactive VOCs in WE could not support a faster rate of O_3 build-up. The combination of both effects could lead to the lower O_3 peak in WE. However, the statistical differences between these peaks (see Table 4.11) show that the difference was not statistically significant at a 95% confidence level. In addition, a stricter two-tail *t-test* with unequal variances for the WE/WD average max 1-hr O_3 as well as the testing of the differences in the average max 1-hr O_3 WE and WD means from a matrix of combinations of WE/WD 2 days (equal variances) were performed. In all cases the results of the

tests were the same as those shown in Table 4.4. Appendix D shows the summary of the results for the statistical analysis for the set of two WE/WD combinations.

On the other hand, Figure 4.18 shows that NO WE/WD hourly average profiles were different in the morning and evening hours. Although morning WE and WD NO peaks occurred at the same hour (~ 8:00 hr), the WD NO peak was almost 1.4 times higher than the morning WE NO peak. The suggested association between the reduction of NO_x emissions and reduction of traffic during WE seems to be confirmed by this difference. Furthermore, the test of significance of the difference in means of the 6:00-9:00 hr WE NO average (see Table 4.11) showed that this reduction was statistically significant at a 95% confidence level.

After the occurrence of the NO morning peaks, the diurnal WE and WD NO average profiles decreased to reach almost the same level (~ 2-5 ppb) between 13:00 and 18:00 hr. This pattern changed around 19:00 hr in WD and was probably associated with evening traffic, which is the most important source of fresh NO_x emissions.

WD evening and night rush hours led to a significant increase in the average NO levels compared with the WE NO average concentrations for the same hours, in accordance with decreased WE nighttime traffic in Mexico City. After midnight, the reconstruction of the shallow mixing layer had an effect on the accumulation of NO in both WE and WD. Based on the results of Table 4.11, on the non-significant difference in WE/WD maximum 1-hr O_3 average concentrations, and on the positive significant difference between WE/WD 6:00-9:00 hr NO average levels, it is possible to suggest that a VOC-sensitive conditions dominated.

The O_3 8-hr average diurnal WE/WD patterns (see Figure 4.19) for the Santa Ursula site followed the same shape as those for the O_3 1-hr average patterns. In both, somewhat higher levels in WD are seen for almost the middle of the day. The largest difference (~ 6 ppb) occurred at 11:00 hr. The WD O_3 8-hr average peak occurred at 18:00 hr with a difference of ~ 7 ppb. Test results for the WE/WD O_3 8-hr average peaks showed that there was not a statistically significant difference between the peaks.

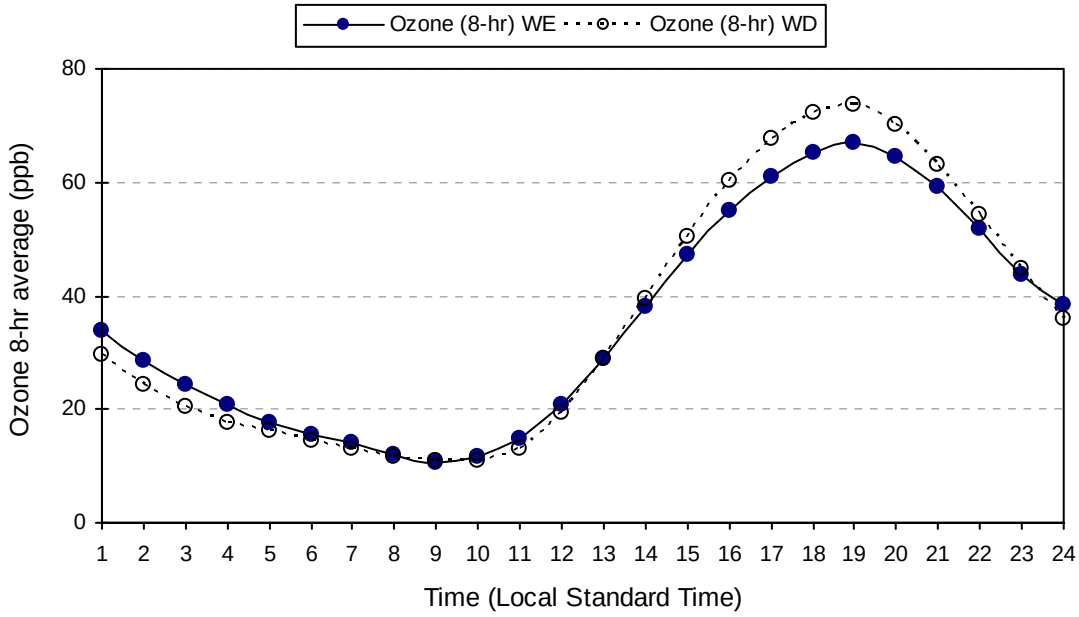

Figure 4.19. Average 8-hr O_3 weekend and weekday diurnal profile from April 1-30, 2004, at the Santa Ursula monitoring station, Mexico City.

4.2.5 Modeling Experiment

The Multiscale Climatic and Chemistry Model (MCCM) was applied for three nested domains. The first domain, with a horizontal resolution of 27 km (60 x 60 cell mesh), practically covered the whole of Mexico. The second domain, with a 9 km resolution, (34 x 34 cell mesh) covered the central part of Mexico. The third domain had a resolution of 3 km (40 x 52 cell mesh) and included the Mexico City Metropolitan Area (MCMA), the surrounding mountains, and parts of the neighboring states of Mexico, Morelos, and Puebla (see Figure 4.20).

Meteorological simulations were performed only for Domain 1 and 2, due to lack of emissions data for these areas. For Domain 3, both meteorology and chemistry were simulated. The simulation's vertical domain included several layers, varying from 20 m near the ground to about 15 km above the surface (100 mb). To initialize and to provide boundary values for MCCM, data from the National Center for Environmental Protection's historical archives were used with a time resolution of 6 hr.

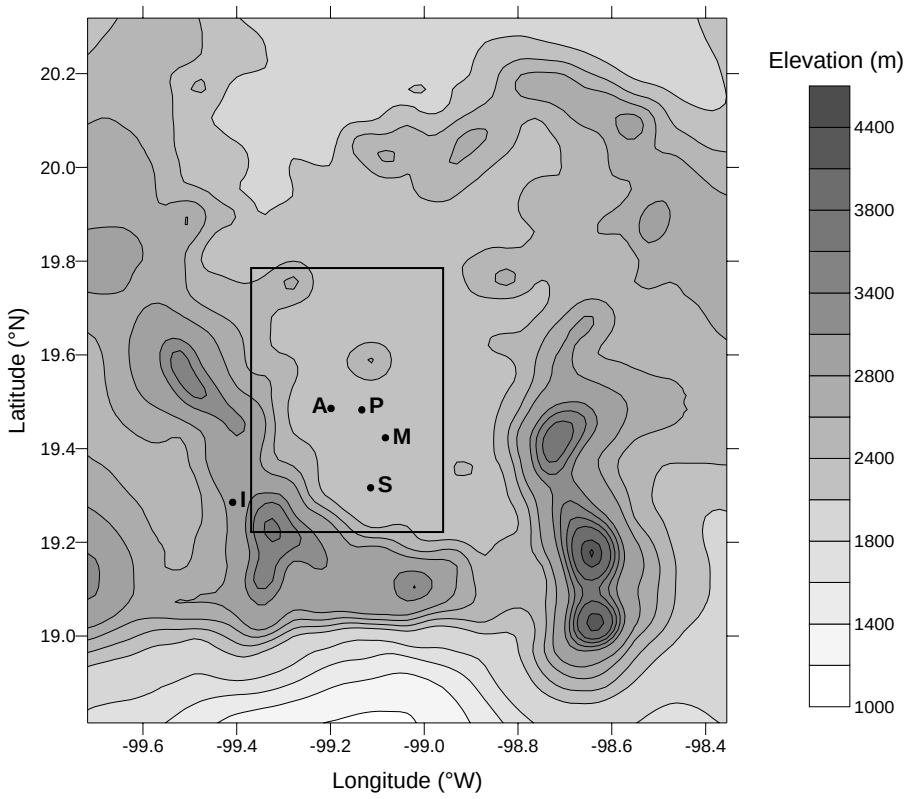

Figure 4.20. Topography of the innermost model domain (Domain 3) and position of five reference sites in MCMA. The reference sites are located in the downtown (Merced [**M**]), in the northwest (Azcapotzalco [**A**], in the north (IMP [**P**]), in the south (Santa Ursula [**S**]), and in the southwest (ININ [**I**]) of Mexico City. The extent of the Domain 3 is around 80 km in East-West direction and around 75 km in the North-South direction. The rectangle in the center shows the approximately extent of the MCMA.

The first 24 hours of modeling were used for initialization only. Boundary concentration values for this domain were obtained from Domain 2, whose boundaries were set to background concentrations. The time period selected for the computational experiments was March 2-5, 1997. This period corresponded to the entrance of a high-pressure anti-cyclonic system over the central region of Mexico, which provided favorable conditions for a typical high pollution scenario (Doran et al., 1998; García, 2002). The simulations were performed at surface level.

The event chosen for simulation with the MCCM was 14:00-15:00 hr on March 3, 1997. The species considered for the analysis were: O_3, NO_y (as the sum of the simulated NO, NO_2, PAN, HNO_3, and NO_3^- species), NO_z (as the subtraction of NO_y - NO - NO_2), HNO_3, and H_2O_2. The performance of the

MCCM has been evaluated qualitatively and quantitatively for the Mexico City case (García, 2002; Jazcilevich et al., 2003). Simulated meteorological parameters have resulted in a satisfactory statistical index in agreement with measured data. Figure 4.21 shows the vertical profile of measured and modeled temperature and wind intensity at 18:00 hr on March 4, 1997, as an example of the MCCM's ability to reproduce vertical meteorological conditions.

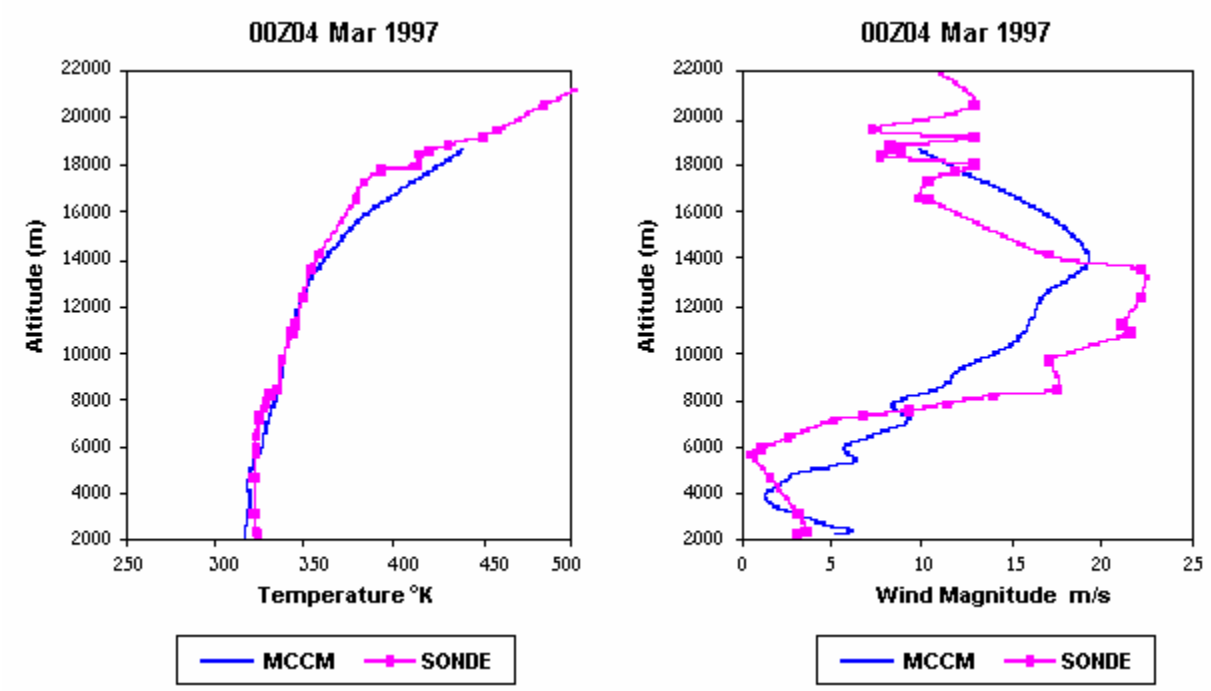

Figure 4.21. Vertical profiles comparing measured and modeled temperatures and wind velocity at the International Mexico City Airport at 18 LST March 3, 1997. (From García, 2002).

The accuracy of ozone predictions with the MCCM has been evaluated previously. Jazcilevich et al. (2003) found that the statistical index agreement between modeled and measured ozone values was above 0.7 with an overall average value of 0.78. The index has an optimum value of 1.0 for perfect agreement between model and measurements. Figure 4.22 shows the time series comparing measured and modeled O_3 concentrations for the Merced (downtown) and the Pedregal (southwest) monitoring stations. The Pedregal station is located ~ 5 km to the east of the Santa Ursula site.

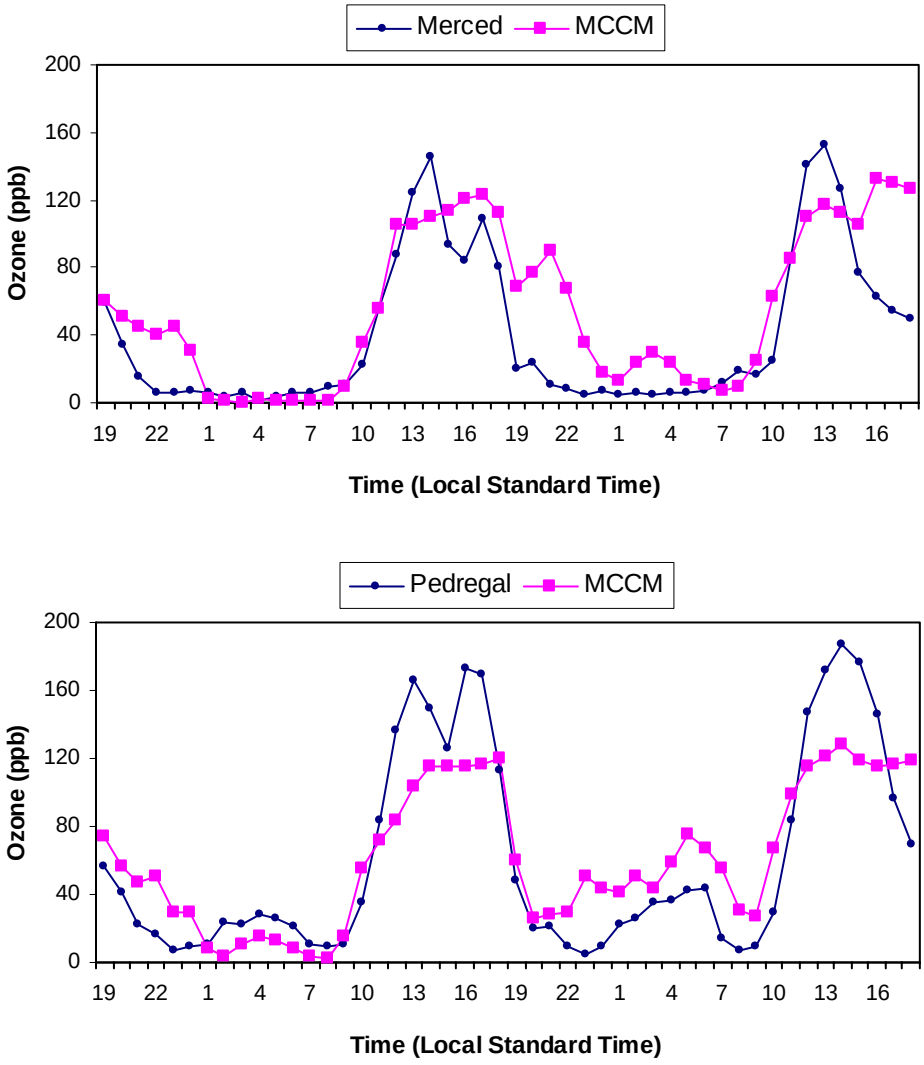

Figure 4.22. Time series of 1-hr average O_3 concentrations for 60 hours (March 2-4, 1997) using MCCM and two reference monitoring stations in ppb.

Figure 4.23 shows the spatial distribution of the simulated concentrations of O_3 over Domain 3. According to this figure, simulated O_3 concentrations were distributed across the whole Mexico City air basin and were in good agreement with observed afternoon ozone concentrations registered that day. High O_3 concentrations were found in the southwest and in the mountain range.

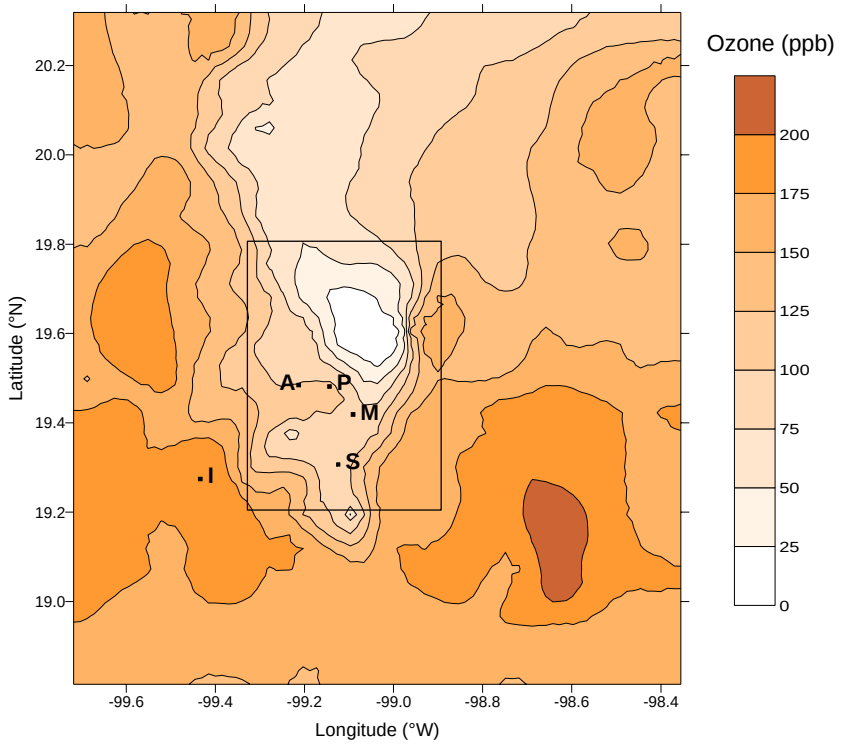

Figure 4.23. Simulated ozone concentrations distribution in ppb for MCMA air basin at the level surface at 15:00 hr Local Standard Time, March 3, 1997. The rectangle in the center shows the approximately extent of the urban area.

The simulated high O_3 levels over the elevations of the basin could be associated with photochemical reactions between reactive biogenic hydrocarbons from the forests of this region and small amounts of NO_x transported from the city. The excess of OH radicals available for photochemical reactions could easily accelerate the formation and accumulation of O_3.

The lowest O_3 concentrations were found northeast of the urban area downwind from a power plant there located. Fresh NO_x emissions from power plants can create a dominant NO_x-titration environment along the direction of their plumes. Within these plumes any available O_3 can be easily titrated. However, the nearly stagnant synoptic meteorological conditions of this event-period were able to support the transport and accumulation of relatively high ozone levels over the northeast and west areas of the MCMA. Figure 4.24 shows the spatial distribution of the simulated concentrations of NO_y and NO_z.

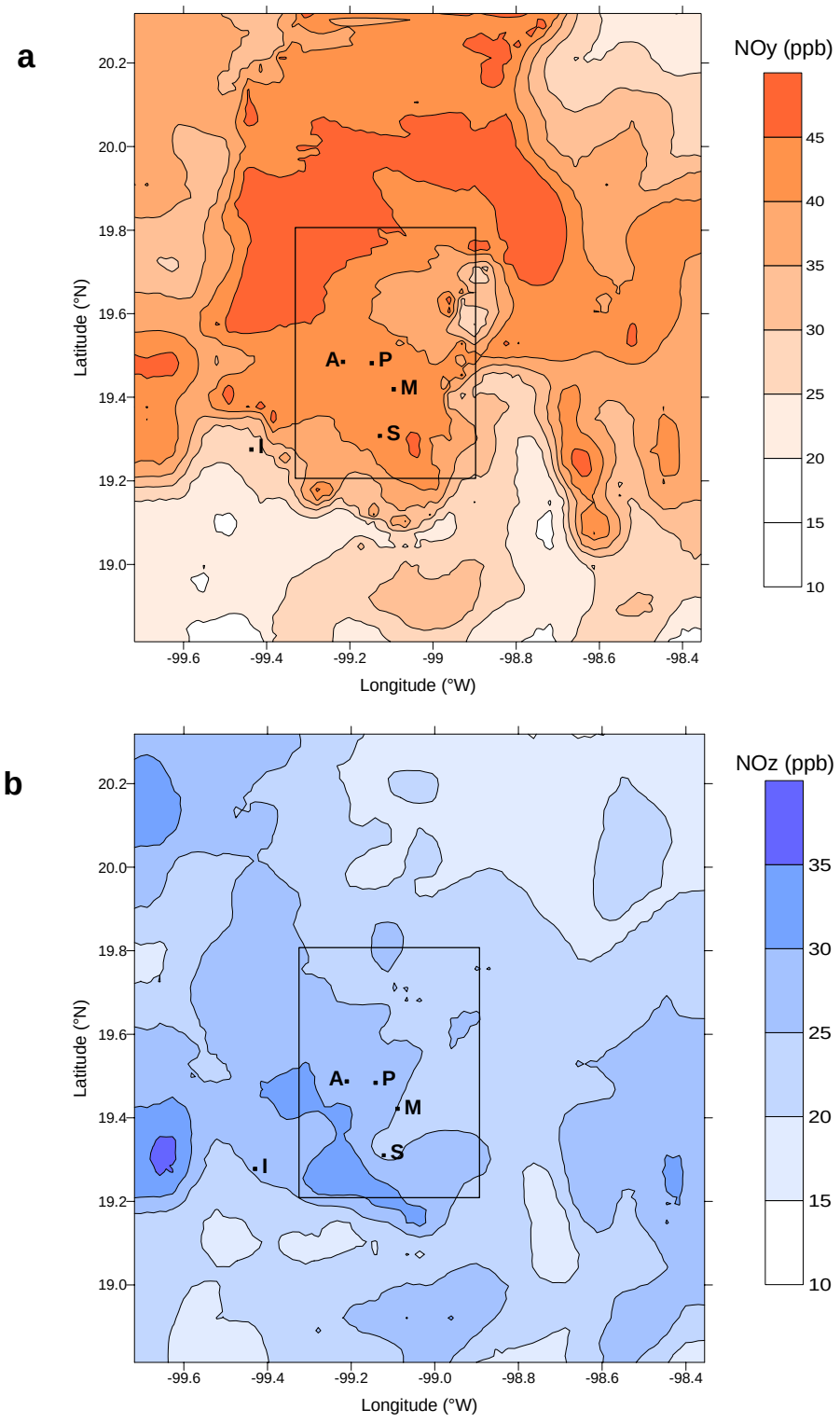

Figure 4.24. Simulated (**a**) NO_y, and (**b**) NO_z concentrations distributions in ppb, for the MCMA air basin at the level surface at 15:00 hr Local Standard Time, March 3, 1997. The rectangle in the center shows the approximately extent of the urban area.

Figure 4.24(a) shows that the plume of NO_y species over the city followed a decreasing gradient towards the southwest, following the typical afternoon wind pattern. NO_y concentrations higher to 20 ppb were simulated for practically all the MCMA indicating that higher precursors concentrations were associated to this event (Milford et al., 1994; Sillman, 1995). Figure 4.24(b) shows that NO_z species increased slightly towards the elevations of the southwest as expected. NO_z species are secondary products of the oxidation of NO_x emissions. The relatively low NO_z concentrations over the northeast of the simulation domain reinforce the above hypothesis that NO_x species were more abundant in these areas.

Figures 4.25(a) and (b) show the spatial distribution of the simulated O_3/NO_y and O_3/NO_z ratios, respectively. The contour of the band, in Figure 4.25(a), associated with the transition range between the VOC- and NO_x-sensitive conditions (6-8) suggests that most of the O_3 formed over MCMA did so under VOC-sensitive conditions ($O_3/NO_y \leq 6$). The NO_x-sensitive areas were located mainly over the southern sector of the simulation domain in agreement with what is typically observed in urban and rural regions of the U.S.A. (Sillman, 1999). The O_3/NO_y ratios within the urban area resulted in an increasing gradient towards the southwest of the city. However, this gradient rapidly changed to NO_x-sensitive ratios as the plume left the outskirts of the MCMA. Theoretically, one explanation for this is that, as the polluted air mass ages, its chemistry tends to shift to a NO_x-sensitive chemistry.

The contour of the band depicting the transition range for the O_3/NO_y ratio (8-10), shown in Figure 4.25(b), suggests also that practically all of the MCMA region was in the VOC-sensitive region ($O_3/NO_z \leq 8$). The lowest O_3/NO_z ratios were found towards the northeast of the urban area.

Figure 4.26 shows the simulated distribution of the ratio H_2O_2/HNO_3. The range of the transition value that separates VOC- and NO_x-sensitive conditions (0.25-0.35) confirms the finding of the previous indicator ratios as to the dominance of VOC-sensitive conditions ($H_2O_2/HNO_3 \leq 0.25$). The H_2O_2/HNO_3 ratio, in terms of theory and simulation results, is the most consistent of the indicator ratios for separating VOC- and NO_x-sensitive regions (Sillman, 1995; Hammer et al., 2002; Sillman and He, 2002; Thielman et al., 2002).

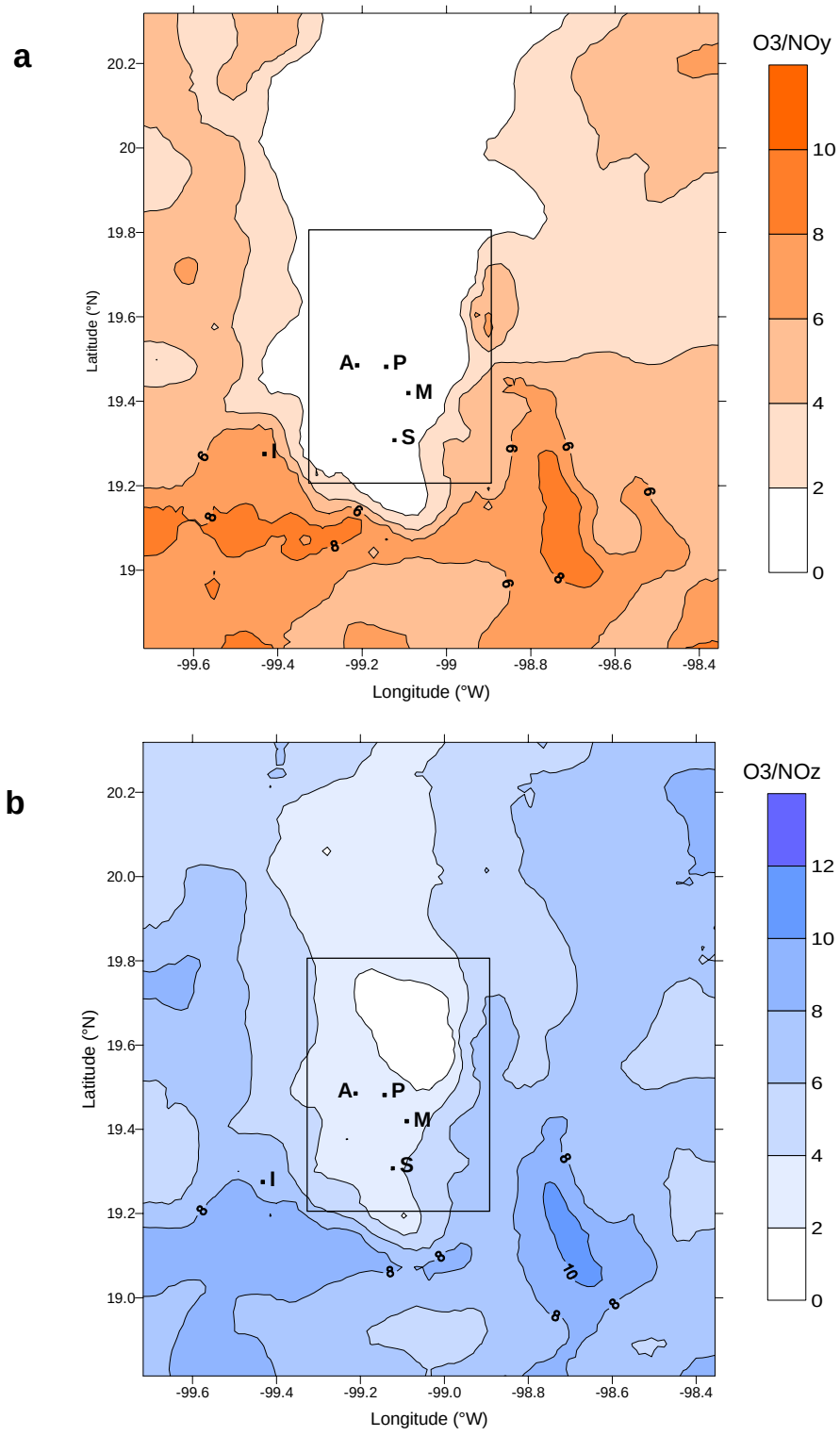

Figure 4.25. Simulated (**a**) O_3/NO_y and **(b**) O_3/NO_z indicator ratios distribution for the MCMA air basin at the level surface at 15:00 hr Local Standard Time, March 3, 1997. The rectangle in the center shows the approximately extent of the urban area.

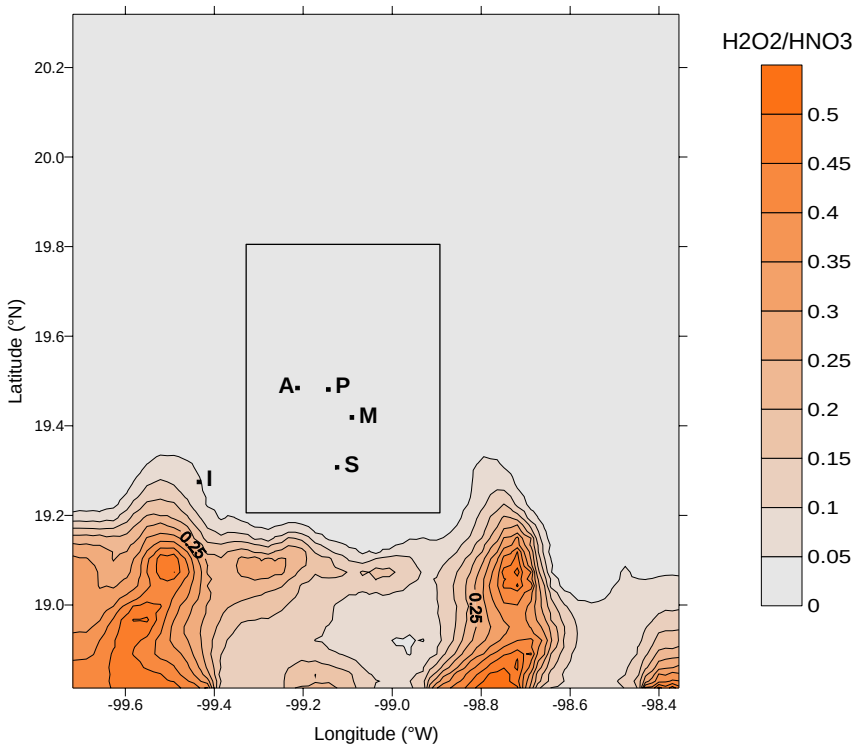

Figure 4.26. Simulated H_2O_2/HNO_3 indicator ratio distribution for the MCMA air basin at the level surface at 15:00 hr Local Standard Time, March 3, 1997. The rectangle in the center shows the approximately extent of the urban area.

Hammer et al. (2000) reviewed the theoretical basis for the calculation of the transition value of the H_2O_2/HNO_3 indicator ratio in a number of studies from Europe and U.S. They found that even with different theoretical approximations, the transition values ranged between ~ 0.18 (Berlin, Germany) and ~ 0.59 (Po Valley, Italy), although the average transition value was around 0.2.

According to Thielman et al. (2002), the H_2O_2/HNO_3 ratio is close to zero under VOC-sensitive conditions where nitric acid is the dominant sink (i.e., the production of HNO_3 >> the production of H_2O_2). As the air mass ages, NO_x is consumed faster than hydrocarbons (i.e., VOCs in general), resulting in a ratio that approaches zero. The VOC oxidation pathway shifts the ratio to higher values, when the production of H_2O_2 becomes important as a sink of radicals. In addition, the ratio H_2O_2/HNO_3 is particularly appropriate because the lifetimes of H_2O_2, HNO_3, and O_3 (controlled mainly by their deposition rates) are relatively similar.

4.2.6 Intercomparison Tests

4.2.6.1 Measured Data

As previously mentioned, Sosa et al. (2000) explored the identification of local O_3-NO_x-VOC sensitivity by applying the photochemical indicators method (PIM) to data collected at different sites of Mexico City (Merced, Azcapotzalco, and IMP) between February and March 1997 (Gaffney et al., 1999; Edgerton, et al., 1999). Table 4.12 presents a comparison between the averages of measured and estimated concentrations of indicator species and photochemical ratios for the Santa Ursula site (this study) and the Merced and Azcapotzalco sites (Sosa et al., 2000).

The results shown in Table 4.12 indicate that, in general, both the O_3/NO_y and the O_3/NO_z ratios from Sosa et al. (2000) coincided with the results from SUMS. These ratios indicate VOC-sensitive conditions in Mexico City, which contradicts their finding of NO_x-sensitive conditions from the $O_3/(HNO_3 + NO_3^-)$ ratio.

This contradiction can explained by reviewing the data that Sosa et al. (2000) used for their O_3-NO_x-VOC sensitivity analysis. In sum, these authors assumed that the concentrations of some species measured at different sites were equal to the expected concentrations of the same species in the other locations. Moreover, they did not take into account the potential interferences and the problems typical of their method during the original measurement campaigns. For example, they did not correct the original NO_x data for the well-known interferences of PAN and HNO_3 in chemiluminescence NO_x analyzers. Nor did they review in-depth the potential of NH_3 emissions to influence reported HNO_3 concentrations at the Merced site. They obtained the total NO_y concentration at the Azcapotzalco and Merced sites as: NO_x (measured at both sites) + PAN (measured at IMP) + HNO_3^- (measured only at Merced and as the sum of HNO_3 + volatilized NO_3^-).

In addition to these sources of uncertainty in the measurements, the locations selected for the indicators evaluation were not appropriate. The three sites (Merced, Azcapotzalco, and IMP) are located close to the downtown of Mexico City but upwind and far away from the south-southwestern smog

receptor sites of MCMA. Use of these sites and of data inappropriate for the application of the photochemical indicators approach account for Sosa et al.'s inconsistent conclusions.

Table 4.12. Comparison of average measured and estimated indicator ratios and photochemical indicator ratios for data collected at Santa Ursula (April, 2004) with results for Merced and Azcapotzalco sites in Mexico City (March, 1997).

Species	Santa Ursula April 14-25, 2004 13:00-17:00 hr	Merced[a] March 2-19, 1997 12:00-17:00 hr	Azcapotzalco[a] March 2-19, 1997 12:00-17:00 hr
O_3	94	92	48
NO_y	37.3	76.5[g]	51.2[g]
NO_x	16.3[c] (22.3)[d]	62.7[d]	37.5[d]
NO	2.6[d]	26.6[d]	5.2[d]
PAN	-	10.4[h]	10.4[h]
PPN	-	-	-
PBN	-	-	-
HNO_3	-	1.25[i]	1.25[i]
NO_3^-	-	0.70[i]	0.70[i]
NO_z	21[e] (15)[f]	12.3[j]	12.3[j]
O_3/NO_y	2.5	1.2	0.9
O_3/NO_z	4.47[e] (5.8)[f]	7.4	3.8
O_3/HNO_3	-	73.6	38.4
$O_3/(HNO_3 + NO_3^-)$	-	47.1[k]	24.6[k]

[a] From Sosa et al. (2000).
[b] From box model applied to measurements performed at the IMP site Gaffney et al., (1999).
[c] $NO_x^* = NO + NO_2^s$, where NO_2^s was obtained with the BUWAL equation (BUWAL, 1997).
[d] Measured by the NO_x analyzer at the site.
[e] $NO_z^* = NO_y - NO_x^*$.
[f] $NO_z = NO_y - NO_x$, where NO_x are the measurements reported by the analyzer.
[g] $NO_y = NO_x + PAN + HNO_3 +$ volatilized NO_3^-.
[h] Measured at the IMP site (Gaffney et al., 1999).
[i] Measured at the Merced site from 12:00 to 18:00 hr. NO_3^- from the volatilization of nitrate aerosols collected on the filter (Chow et al., 2002).
[j] $NO_z = PAN + HNO_3 + NO_3^-$
[k] The sum $(HNO_3 + NO_3^-)$ is taken as a surrogate of the total HNO_3.

4.2.6.2 Modeling Data

A direct comparison between the measurements carried out in Santa Ursula and the predictions from the MCCM and other models could not be performed due to differences in their date and time periods. However, several indirect comparisons could be done based on the closeness and relative

contributions of the indicator values to the final indicator ratios and based on the models' overall performance.

The criterion for the selection of the day for the intercomparison between Santa Ursula and the MCCM was that the measured O_3 concentration should be as similar as possible to the predicted concentration. In order to evaluate the consistency of the MCCM results, the predicted values, from this model, were compared with measured values registered at two reference sites and with results from the CIT and box-model simulations. The reference sites were the monitoring stations of Pedregal and Merced. The Pedregal monitoring site was chosen because the Santa Ursula monitoring station was not in operation in 1997 and because it was the closest station to Santa Ursula (~ 5 km west). The CIT modeling results for March 2, 1997 and the general box-model results for March 1997 were used for the overall intercomparison.

Table 4.13 shows the comparison of measured indicator species and indicator ratios for Santa Ursula (March 1997 and April 2004) and Merced (March 1997) with the simulated indicator species and indicator ratios from the modeling predictions of the MCCM, the CIT model (Sosa et la., 2000), and a box model approximation (Gaffney, et al., 1999).

The average 14:00-15:00 hr measured O_3 concentration on April 15, 2004 at Santa Ursula was 93 ppb, while the MCCM simulated concentration for March 3, 1997 at this site was 90 ppb. The measured O_3 concentration on March 3, 1997 at the Pedregal station was 126 ppb, while the predicted concentration at this position was 130 ppb (see Figure 4.23). Similarly, the O_3 predicted concentration at the Merced position was 94 ppb, while the average measured level was 96 ppb. Although the measured and MCCM predicted NO_y values for Santa Ursula (35 and 42.5 ppb, respectively) resulted in relatively high values, they had a difference of ~ 21%. The predicted MCCM NO_y concentration for the Merced site was also high, but it was 30% less than the reported 6-hr average measured value. The tendency towards high NO_y values was also observed with the other measured and predicted results (range of predicted NO_y concentrations: 42.5-53.4 ppb).

Table 4.13. Comparison of measured indicator species and indicator ratios for Santa Ursula (March 3, 1997 and April 15, 2004) and Merced (March 2 and 3, 1997), with the simulated indicator species and indicator ratios predictions from the MCCM (March 3, 1997), the CIT model (March 2, 1997), and a simple box model (March, 1997). All concentrations are in ppb.

Species	Santa Ursula April 15, 2004 measured 14:00-15:00 hr averages	Santa Ursula[a,b] March 3, 1997 simulated (and measured) 14:00-15:00 hr averages	Merced[a,b,c] March 3, 1997 simulated 14:00-15:00 hr (and measured 12:00-18:00 hr) averages	Merced[c] March 2, 1997 simulated (and measured) 12:00-18:00 hr averages	MCMA[d] March, 1997 Afternoon hours averages
		MCCM	MCCM	CIT	Box-model
O_3	93	90 (126)[h]	96 (107)	120[n] (154)	200
NO_y	35	42.5	42.4 (57)[i]	46[n,o] (76.8)[i]	53.4[f,j,r]
NO_x	12.3[e]	16.5 (48)[f,h]	17.3 (39)[f]	25[n] (46)[f]	20[s]
NO	2[f]	2.7 (8)[f,h]	2.7	4[n]	3.4 [f,j]
PAN	-	1.9	2 (15.5)[j]	13[n,p] (26)[j]	20[j]
HNO_3	-	21.9	22 (1.9)[k]	8[n] (4)[k]	10[t]
NO_3^-	-	1.3	1.1 (0.5)[k]	(0.5)[k]	-
NO_z	22.7[g]	25.1	25.1 (17.9)[l]	21[q] (30.8)[l]	30[q]
O_3/NO_y	2.6	2.1	2.2 (1.88)	2.6 (2.0)	4
O_3/NO_z	4.1	3.5	5.5 (5.9)	5.7 (5.0)	6.6
O_3/HNO_3	-	4.1	4.3 (44.5)[m]	15 (32.0)	20

[a] Interpolated from the results of the simulation of the spatial distribution.
[b] From historical RAMA data files (http://sma.df.gob.ma/simat/).
[c] From Sosa et al. (2000).
[d] From box model applied to measurements performed at the IMP site Gaffney et al., (1999) and additional empirical estimations.
[e] $NO_x^* = NO + NO_2^s$, where NO_2^s was obtained with the BUWAL equation.
[f] Measured by the NO_x analyzer at the site.
[g] $NO_z^* = NO_y - NO_x^*$.
[h] Measured at the Pedregal monitoring station, ~ 5 km west from the Santa Ursula site. No data were available for Santa Ursula by 1997.
[i] $NO_y = NO_x + PAN + HNO_3 +$ volatilized NO_3^-.
[j] Measured at the IMP site (Gaffney et al., 1999).
[k] Measured at the Merced site from 12:00 to 18:00 hr. NO_3^- from the volatilization of nitrate aerosols collected on the filter (Chow et al., 2002).
[l] $NO_z = PAN + HNO_3 + NO_3^-$
[m] Total HNO_3 as the sum ($HNO_3 + NO_3^-$).
[n] From modeling results with the hydrocarbon emissions inventory multiplied by a factor of three.
[o] $NO_y = NO_x + PAN + HNO_3$.
[p] Modeled at the IMP site position.
[q] $NO_z = PAN + HNO_3$.
[r] Estimated as the sum: NO_y box-model = "NO_y" + NO; where reported measured "NO_y" was NO_y – NO (Gaffney et al., 1999).
[s] NO_x = "NO_y" box model - NO_z
[t] Assuming that HNO_3 was equivalent to the 50% of the PAN concentration, based on comments of Gaffney et al., (1999).

The relative contributions of NO_x and NO_z to the total NO_y in the measured and the MCCM values were somewhat similar. In the case of the measured concentrations at Santa Ursula, 35% were from NO_x and 65% from NO_z*, while the MCCM predicted contributions for this site were 40% from NO_x and 60% from NO_z. Very similar relative contributions were found in the simulated values for Santa Ursula and those for the Merced site. However, the relative contributions from the MCCM and those measured at Merced were different. While the simulated contributions were 41% from NO_x and 59% from NO_z, the measurements were 61% from NO_x and 39% from NO_z.

The intercomparison of the relative NO_x and NO_z contributions to the predicted NO_y at the Merced site from the MCCM for March 3, 1997 and from the CIT model for March 2, 1997 resulted in similar predictions: 41% from NO_x and 51% from NO_z for the MCCM and 55% from NO_x and 45% from NO_z for the CIT model. The relative contributions predicted by the box model were also similar: 56% from NO_x and 44% from NO_z.

The measured NO_z* and MCCM simulated NO_z values for the Santa Ursula site were very similar (22.7 ppb and 25.1 ppb, respectively), while the measured and MCCM predicted NO_z values at Merced were different (12.3 ppb and 25.1 ppb, respectively). The NO_z concentrations from the CIT and the box model, as well as from the measurements for March 2, 1997, had values very close to those of the MCCM.

Despite the differences in the relative contributions of NO_x and NO_z among the measurements and models, the modeled O_3/NO_y and O_3/NO_z ratios for March 1997 were very similar to the measured conditions at Santa Ursula in April 2004. All of the models indicated VOC-sensitive conditions. However, several inconsistencies emerged from the intercomparison of the predicted and measured values for PAN and HNO_3. While the MCCM predicted a PAN contribution to the NO_z of 8%, the CIT model predicted a contribution of 61%. The MCCM predicted that HNO_3 concentrations accounted for 87% to the total NO_z, while the CIT model predicted a nitric acid contribution of 38%. Furthermore, the 12:00-18:00 hr average PAN measurements reported for both reference days, March 2 and 3, 1997, at the IMP site were ~ 15.5 and 10.5 ppb, respectively, while the measured HNO_3 concentrations were ~ 4.2 and 2 ppb respectively.

Sosa et al. (2000) suggested that the PAN and HNO_3 overestimations observed in the CIT simulations could be explained by the model's failure to reproduce both the chemical processes of these compounds and the vertical mixing processes. On the other hand, García (2004) suggested that the overestimation of HNO_3 and underestimation of PAN in the MCCM predictions could be related to deficiencies in the official VOC emission inventory used in the simulation. In the opinion of this researcher, the underestimation of ammonia emissions and the poor balance contributions of aldehydes in the official VOC inventory affected the correct prediction of these compounds.

The lack of NH_3 emissions in a photochemical model may cause errors in both the simulation of HNO_3 because of the particular chemistry of these two compounds in the air. The equilibrium reaction among ammonia and nitric acid ($HNO_{3(g)} + NH_{3(g)} \leftrightarrow NH_4NO_{3(s,\ aq)}$) implies that the concentration of these gases in the air depends on the initial proportions of each of them (Finlayson and Finlayson-Pitts, 2000). While the lack of NH_3 emissions in modeling simulations results in an obvious overestimation of HNO_3 (i.e., there is no possibility of conversion of nitric acid to ammonium nitrate), in the sampling and measurement of nitric acid, the presence of high NH_3 levels may interfere strongly with the real ambient HNO_3 concentration. Chow et al. (2002) report that measured NH_3 concentrations at the Merced site were, on average, ~ 3.7 times greater (in ppb) than the HNO_3 concentrations there. Therefore, it is possible that reported measurements of HNO_3 were strongly affected by NH_3 resulting in a "strong" underestimation of the real values. It is not clear if both models overestimated the real HNO_3 concentrations simply because their simulated values were compatible with the range of nitric acid values reported by Limón-Sánchez (2002).

On the other hand, because aldehydes can react with OH radicals to produce peroxyacetyl radicals that rapidly react with NO_2, thereby producing PAN (Singh, 1987), a poor balance of aldehydes in the VOC emissions inventory used in the models could result an underestimation of PAN concentrations.

Although not stated explicitly, Sosa et al. (2000) artificially increased PAN and HNO_3 concentrations to validate the performance of the CIT model. They used a combination of the measured PAN concentrations from IMP and the CIT predicted HNO_3 concentrations to obtain an adjusted O_3/NO_y

ratio. The resulting adjusted ratio was very similar to the O_3/NO_y ratio estimated from the measurements for the same day. In this way, they indirectly validated the performance of the CIT to study the effect of varying NO_x and VOC emissions on the spatial distribution of O_3 in the MCMA.

The impact of the overestimation of HNO_3 and underestimation of PAN in the final balance of the NO_z species predicted by the MCCM cannot be clarified with the available information. However, a readjustment of the emission inventories used by the model probably would not change, to a large extent, the final result because there would be a redistribution of the oxidized nitrogen among these species. In addition, Sillman (1999), Sillman et al. (2003), and Tonessen and Dennis (2000) have suggested that the correlation between NO_x-VOC sensitivity and O_3/NO_y and O_3/NO_z ratios is driven specifically by HNO_3 rather than by PAN and other organic nitrates.

It should be noted, however, that the MCCM predictions were within the range of acceptability given by Sillman (1995). According with this author, in modeling experiments with predicted high O_3 concentrations, the ratio $O_3/(2H_2O_2 + NO_z)$ should have a near-constant value between 5 and 8, regardless of VOC- or NO_x-sensitivity. Taking the predicted distribution of the individual concentrations for each of the species in this ratio, the resulting $O_3/(2H_2O_2 + NO_z)$ ratio was 6.7 (s.d. = 0.71) for 165 data points representative of the MCMA.

The general tendency of the MCCM and the CIT model to predict VOC-sensitive conditions in the Mexico City Metropolitan Area suggests that the results of the indicator measurements in Santa Ursula were consistent with the PIM approach.

4.3 Comparative Assessment of the Ozone Formation in Cincinnati and Mexico City

This section presents a comparative assessment of the main characteristics of the Cincinnati and Mexico City metropolitan areas associated with the formation of ozone and with O_3-NO_x-VOC sensitivity in the two airsheds. The results of this assessment are combined with several conceptual definitions to evaluate the consistence of the NO_x-VOC sensitivity dictated by the PIM and the VOC/NO_x ratio under

severe air pollution conditions. Table 4.14 contains a comparison of selected statistics between the two urban areas for the year 2000.

Table 4.14. Comparison of selected statistics between Greater Cincinnati and the Mexico City Metropolitan Area (year 2000).

Statistic parameter	Greater Cincinnati[a]	Mexico City Metropolitan Area[b]
Population	1'817,571 (331,285)[c]	18'171,318 (8'605,239)[d,e]
Total Area (km^2)	16,583 (206)[c]	5,300 (1,602)[d,e]
Population density (inhabitants/km^2)	109 (1,608)[c]	12,000 (central area)[e] 2,700 (periphery)[e]
GDP per capita in US dollars	34,646[f]	7,750[e]
Vehicle fleet	1.6 million[g]	3.2 million[e]
Average vehicle age	~ 6 years (projected)[h]	~ 10 years[e]
VKT (kilometers per day)	134 million (total)[g]	153 million (total)[e]
Industries (major & small)	~ 1000[g]	~ 35,000[e]
NO_x emissions (tons/yr)	239,277[g] 63,861 (27% vehicles) 119,115 (49% power plants) 17,832 (7.4% fuel combustion industrial)	193,451[i] 156,695 (81% vehicles) 11,626 (6% power plants) 6,155 (3.2 % fuel combustion industrial)
VOC emissions (tons/yr)	161,072[g] 41,510 (25% vehicles) 39,151 (24% biogenic) 308 (0.2% fuel combustion industrial)	429,755[i] 194,517 (45% vehicles) 15,425 (3.6% biogenic) 7,876 (1.8% fuel combustion industrial)
NO_x emissions density (tons/day-km^2)	0.039	0.100
VOC emissions density (tons/day-km^2)	0.026	0.222
VOC/NO_x ratio (ton/ton)	0.67	2.2
VOC/NO_x ratio (ppmC/ppm)	1.9	15.1
O_3 1-hr maximum 2003 (ppb)	140[j]	243[k]
PM_{10} 24-hr maximum 2003 ($\mu g/m^3$)	80[j]	744[k]
PM_{10} arithmetic mean maximum 2003 ($\mu g/m^3$)	23[j]	59[k]

[a] Includes 5 counties of Ohio, 6 counties of Kentucky, and 2 counties of Indiana.
[b] Includes 16 delegations from Mexico City and 17 municipalities of the State of Mexico.
[c] City of Cincinnati.
[d] Mexico City.
[e] Molina and Molina (2002).
[f] Demographia/Wendell Cox Consultancy. Belleville, IL 62222, USA, 2003. www.demographia.com.
[g] US EPA (2004).
[h] Ohio Department of Transportation. 1998 State of the Transportation System. www.dot.state.oh.us/sos98/sosPT.htm.
i SMA (2003).
j HCDOES (2004).
k SMA (2004).

There are a number of differences between Greater Cincinnati (GC) and the Mexico City Metropolitan Area (MCMA) directly related to the air quality in both regions. By the year 2000, the population in the MCMA was almost 10 times greater than in GC, but its total area was nearly three times smaller than that of GC. This situation is clearly reflected in estimates of population density. The number of inhabitants per square kilometer was almost 12 times greater in the MCMA than that in GC. Strongly related to population density, the use of cars for transportation represents an additional factor in the higher estimations of vehicle emissions in the MCMA. While the vehicle fleet in GC was ~ 1.6 million with an estimated vehicle age of 6 years, the number of vehicles in the MCMA was almost two times that and with an estimated age of 10 years. However, the VKT (vehicle kilometers traveled) per day in both urban areas was very similar. The combination of the vehicle fleet age (around 30% of cars without a catalytic converter) and very severe traffic problems in the MCMA (average speed ~ 11 km/hr) generated much higher vehicle emissions than expected according to the local VKT. The number of industrial facilities in the MCMA was ~ 35 times than in GC. However, the NO_x and VOC contributions from industrial activity, in both regions, were not significant compared with other sources.

Power plant NO_x emissions were 10 times greater in GC than in the MCMA. While in GC the contribution of NO_x emissions from power plants to the total balance was almost 50%, in the MCMA this contribution was only 6%. This apparent inconsistency between population density and power generation is due to the fact that most of the electricity consumed in the MCMA comes from sources located in other parts of the country. Almost 25% of all electricity produced in Mexico is consumed in the MCMA. However, the higher NO_x emissions from cars in the MCMA, make this region to have its total NO_x emissions balance very close to that for GC.

On the other hand, the estimated total VOC emissions in MCMA were ~ 2.7 times higher than the same balance for GC. VOC emissions from cars in MCMA were almost 5 times greater than the same emissions contributions in GC, while biogenic VOC emissions in GC were estimated to be nearly 2.6 times greater in this region than in MCMA.

The estimated combined ratio of VOC/NO_x emissions (as ton VOC/ton NO_x) seemed to be dominated by NO_x emissions in GC (VOC/NO_x = 0.67) and by VOC emissions in MCMA (VOC/NO_x = 2.2). Sillman (1999) has suggested that in general, NO_x emissions within an urban area determine the total amount of O_3 that is formed after air moves downwind and chemical processes have run to completion, while VOC emissions control the rate of initial buildup of O_3. Therefore, it might be expected that O_3 levels were higher in GC. Moreover, the estimated emissions of biogenic VOC precursors in GC were almost twice that of the MCMA. Biogenic VOC species are extremely reactive with most anthropogenic VOC (Chameides et al., 1992). Consequently, the impact of biogenic VOC can be large relative to their ambient concentrations. Even very small concentrations of reactive biogenic VOC may have a very strong impact on the total VOC reactivity. However, the higher reactivity of VOC from car emissions in MCMA and the relatively limited use of catalytic converters give this region a potential higher VOC reactivity than that for GC.

The combined effect of the reactivity-weighted VOC (the sum of each VOC species mass emission weighed by its reaction rate with OH radicals) and the particular physical conditions (total area, emissions density, meteorology, orography, altitude, latitude, etc.) seems to be the difference in the magnitude of the O_3 peak in each region.

4.3.1 Ozone Formation Scenarios

Topographically, the GC region is a plateau bisected by the Ohio River, composed of a mix of rugged slopes and gently rolling hills. In general, the hills and valleys in the region have only a minimal effect on air movement, although the region's location in the Ohio River Valley makes it prone to morning thermal inversions (OKI, 1979). Large scale movement of air masses in North America, the lack of high elevations across the region, and the relatively fast heating of the ground during the warm months favors the vertical and horizontal dispersion of air pollutants. Because of its latitude (39.8°N) and its relatively high afternoon summer temperatures (average ~ 27.7°C), GC is susceptible to higher ozone concentrations

in the summer and early fall. Ozone is a strongly seasonal secondary pollutant in mid-latitude regions, with the warm months exhibiting higher concentrations than the cool months.

In contrast, the MCMA lies in an elevated basin of the Mexican Plateau. The basin is confined on three sides (east, south, and west) by mountain ridges but has a broad opening to the north and a narrower gap to the south-southwest. The surrounding ridges vary in elevation with several peaks rising to nearly 2000 m above the mean urban floor. Quite the opposite of mid-latitude regions, the subtropical latitude (19°N) and high altitude of the MCMA makes this the area vulnerable to ozone production during winter as well as summer. During the dry winter months, the basin is normally under the influence of high-pressure systems with light winds above the basin and nearly cloudless skies. This favors the formation of strong surface-based inversions at night that persist for several hours following sunrise, trapping morning emissions within a shallow thermal inversion layer that is closed off by the surrounding elevation (Bravo and Torres, 2002). The solar heating of the ground generates sufficient turbulent mixing to erode these inversions by mid-morning, producing deep boundary layers by the afternoon. However, there is sufficient time in the morning hours for photochemical ozone formation.

These differences result in very dissimilar photochemical scenarios for GC and the MCMA. Table 4.15 presents a comparison of ozone formation and related parameters obtained during late summer in Cincinnati (Taft site) and late winter in Mexico City (Santa Ursula site). Although the O_3 concentrations were always higher in Mexico City, there were several similarities between some of the parameters leading to O_3 formation. The average 24-hr NO concentrations were very similar in both cities (~ 14.5 ppb). The afternoon average was similar as well (~ 2.7 ppb).

However, there was a strong difference between the 6:00-9:00 hr NO and NO_x concentrations in Cincinnati and Mexico City: 25.9 and 73.9 ppb for NO and 47 and 116 ppb for NO_x, respectively. The apparent resemblance in the 24-hr and afternoon averages suggests that there could be a similarity between NO_x emissions. The difference in morning NO and NO_x concentrations seems to be due to the difference in emission density and in the strength of the morning inversion layer. The inversion layer is likely stronger in the MCMA as a result of the barrier effect of the surrounding mountains.

Table 4.15. Comparison of ozone formation and related parameters measured at the Taft monitoring station, Cincinnati (September 3-30, 2003) and the Santa Ursula monitoring station, Mexico City (April 14-25, 2004).

Statistic parameter	Taft monitoring station	Santa Ursula monitoring station
O_3 (24-hr average), ppb	24.8	44.7
O_3 max, ppb	73	172
O_3 afternoon average, ppb	59	94
NO (24-hr average), ppb	14.3	14.8
NO (afternoon average), ppb	2.9	2.6
NO (6-9 a.m. average), ppb	25.9	73.9
NO_y (24-hr average), ppb	41.2	54.7
NO_y (maximum morning peak), ppb	213	228
NO_y (afternoon average), ppb	21.6	37.3
NO_x[a] (6-9 a.m. average), ppb	47.0	116
NO_z* (afternoon average), ppb	7.9	21
O_3/NO_y	2.7 (VOC-sensitive)	2.5 (VOC-sensitive)
O_3/NO_z*	5.9 (VOC-sensitive)	4.4 (VOC-sensitive)
NO_x*/NO_y (average air masses age)	0.62	0.44
Average rate of O_3 accumulation (ppb/hr)	5.3	21.4
Average time of effective O_3 build up (hr)	5.2	3.3
Average rate of NO depletion (ppb/hr)	3.3	17
WE-O_3 max (ppb)	48.6	86.6
WD-O_3 max (ppb)	46.4	96.1
WE-NO 6-9 a.m. (ppb)	16.1	61.1
WD-NO 6-9 a.m. (ppb)	31.7	97.5
Ambient temperature (average), °C	18.1	19.7
Wind speed (average), m/s	1.8	1.5
Afternoon mixing layer height (average)[a] m	1416	1917

[a] As measured by the NO_x instrument.

[b] Average of mixing layer estimations from READY model interpolations to FNL datasets. Real-Time Environmental Applications and Display System. National Climatic and Atmospheric Administration. Office of Oceanic and Atmospheric Research. Air Resources Laboratory. www.arl.noaa.gov/ready.html.

The average NO_y morning peak was a little higher in Mexico City (229 ppb) as compared to that in Cincinnati (213 ppb). Nevertheless, the difference increased notably for the average afternoon NO_y concentrations: 37.3 ppb in Mexico City and 21.6 ppb in Cincinnati. The balance of the NO_y was likely

associated with the difference in NO_z* afternoon species. While in Mexico City the NO_z* afternoon level had an average of 21 ppm, in Cincinnati the same species had an average of 7.9 ppb.

As previously discussed, measured and simulated PAN and HNO_3 concentrations strongly suggest that these species are present in the ambient air of the MCMA at relatively high levels compared to other parts of the world. On the other hand, the measured HNO_3 concentrations in Cincinnati, which are within the range typical of the midwestern U.S., suggest that nitric acid is the most important and abundant oxidized nitrogen species in this region.

The O_3/NO_y ratios were similar for both cities (2.7 in Cincinnati and 2.5 in Mexico City). However, the scatterplot correlations of these two species were different although both indicate VOC-sensitive conditions (see Figure 4.27 (a)). The relatively wide scattering of the data points for Mexico City could imply that the chemistry character of the air parcels in the MCMA airshed were strongly variable, while remaining within the VOC-sensitivity regime. According Sillman (2003), the O_3/NO_y ratio reflects two separate processes, both of which are related to O_3-NO_x-VOC sensitivity. On the one hand, the ratio reflects the process of photochemical ozone production. On the other, it reflects the process of NO_x titration and the immediate removal of O_3 by reaction with directly emitted NO. The other secondary species are unaffected by NO_x titration. The fact that there was relatively little variation in the O_3 versus NO_y correlation in Cincinnati could be interpreted to mean that the NO_x titration processes were preventing the accumulation of ozone. Thus, it could be assumed that O_3 production efficiency in Cincinnati was strongly limited by the relatively high NO_x emissions in the region. The large variation observed in the O_3 versus NO_y correlation in Mexico City could indicate that both O_3 production and NO_x were acting simultaneously. However, because NO_y by itself may be considered an indicator of the impact of stagnant meteorology on the photochemical processes (Sillman, 1995), the observed variation in the O_3-NO_y correlation in Mexico City could be taken as an indication of the variations of the meteorological conditions during the monitoring campaign. According Sillman, Stagnant meteorology and associated high NOx, VOC, and NOy cause an increase in the photochemical lifetimes of NOx and VOC.

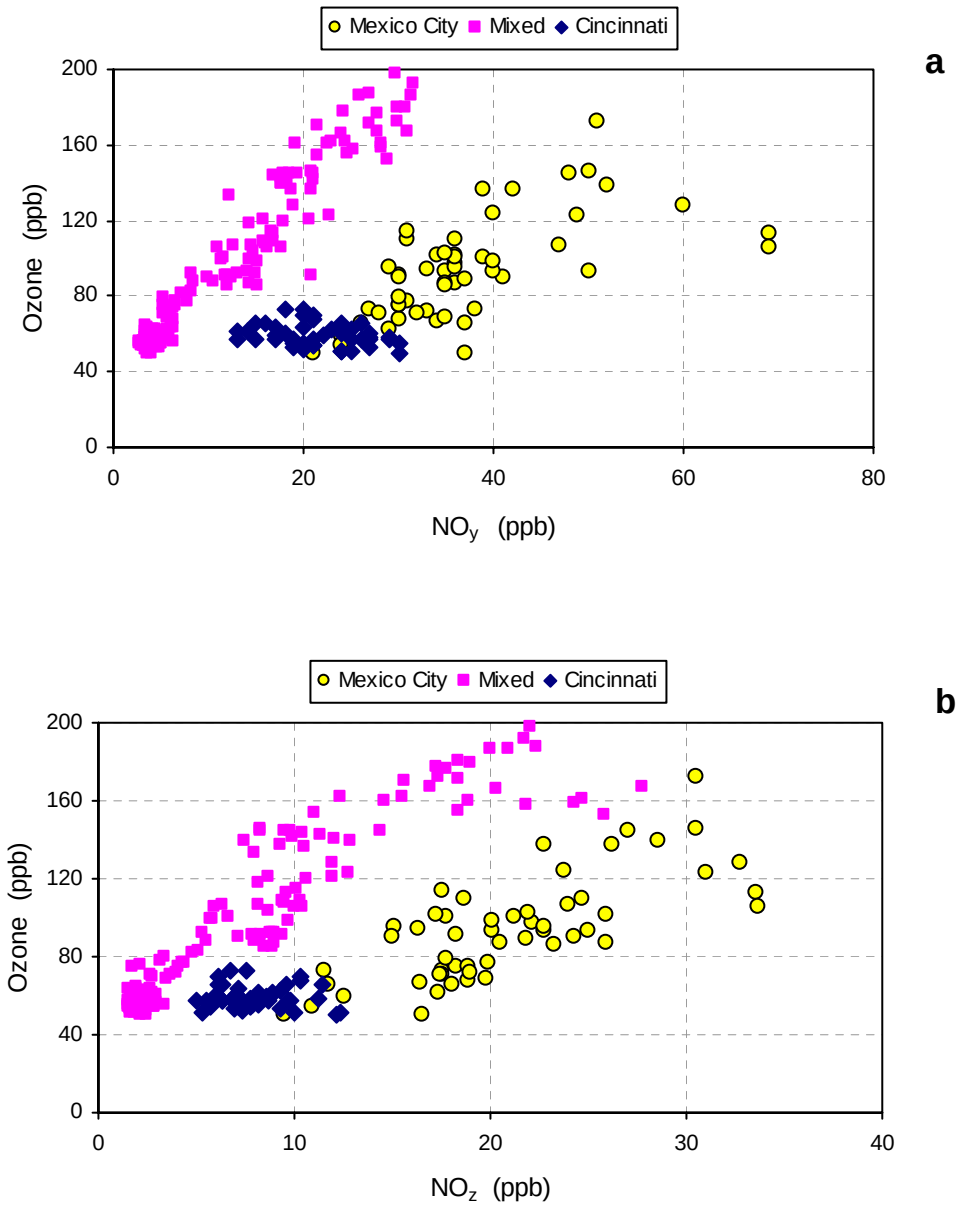

Figure 4.27. Scatterplot patterns comparison of (**a**) measured afternoon O_3 and NO_y concentrations and, (**b**) measured afternoon O_3 and estimated NO_z* concentrations in Cincinnati (Taft monitoring station) and Mexico City (Santa Ursula monitoring station), and 3-D model predicted scatterplot patterns for O_3 and NO_y, and O_3 and NO_z for locations with mixed or with near-zero sensitive conditions. Simulation data obtained from data file available from Sillman (2003).

The O_3/NO_z* ratios were somewhat different (5.9 in Cincinnati and 4.4 in Mexico City), suggesting that ozone production was more efficient in Cincinnati. However, Figure 4.27 (b) shows that the correlation of O_3 versus NO_z* for Cincinnati lacked the covariance seen in Mexico City. This confirms that the apparent excess of NO_x in Cincinnati was controlling the O_3 accumulation, while in Mexico City the photochemical processes were dominating the NO titration process. In both cases, the PIM method showed that VOC-sensitive conditions were dominant as was confirmed by the statistical analysis of the differences in the WE/WD peak O_3.

The effect of the VOC emissions on the strength of the O_3 initial buildup in each region can be explained by analyzing conceptual factors associated with ozone formation process. Figure 4.28 presents the estimated averages of: time of O_3 inhibition, time of net O_3 accumulation, and rate of O_3 accumulation for each of the sites and monitoring periods.

Although the predawn NO available to start the morning ozone production was in general lower in Cincinnati compared to those in Mexico City, the morning NO peak in the latter city surpassed by far the respective NO peak observed in Cincinnati, resembling a clear effect of the extent of morning precursors emissions and stagnant morning meteorology in Mexico City. It is generally accepted that in the morning O_3 formation is inhibited by high concentrations of NO, which restrain radical formation by titrating O_3. During this period, formaldehyde (and to a lesser extent, nitrous acid), are the main source of OH radicals. Because the length of the O_3 inhibition is essentially determined by the concentration of NO, it is expected that this period be shorter in areas of high amounts of fresh NO_x emissions. However, the average O_3 inhibition period in both cities had approximately the same length (~ 2.7 hr). The possible explanation to this inconsistency is that the production of OH radicals from relatively high morning levels of formaldehyde in Mexico City was of such extent that could rapidly dim the NO titration effect of the photostationary state.

Back in the early 1990s, Bravo et al. (1991) found that the introduction of methyl-t-butyl ether (MTBE) as an additive in Mexican gasoline showed an association with an increase in the morning atmospheric formaldehyde levels and on the O_3 production in MCMA.

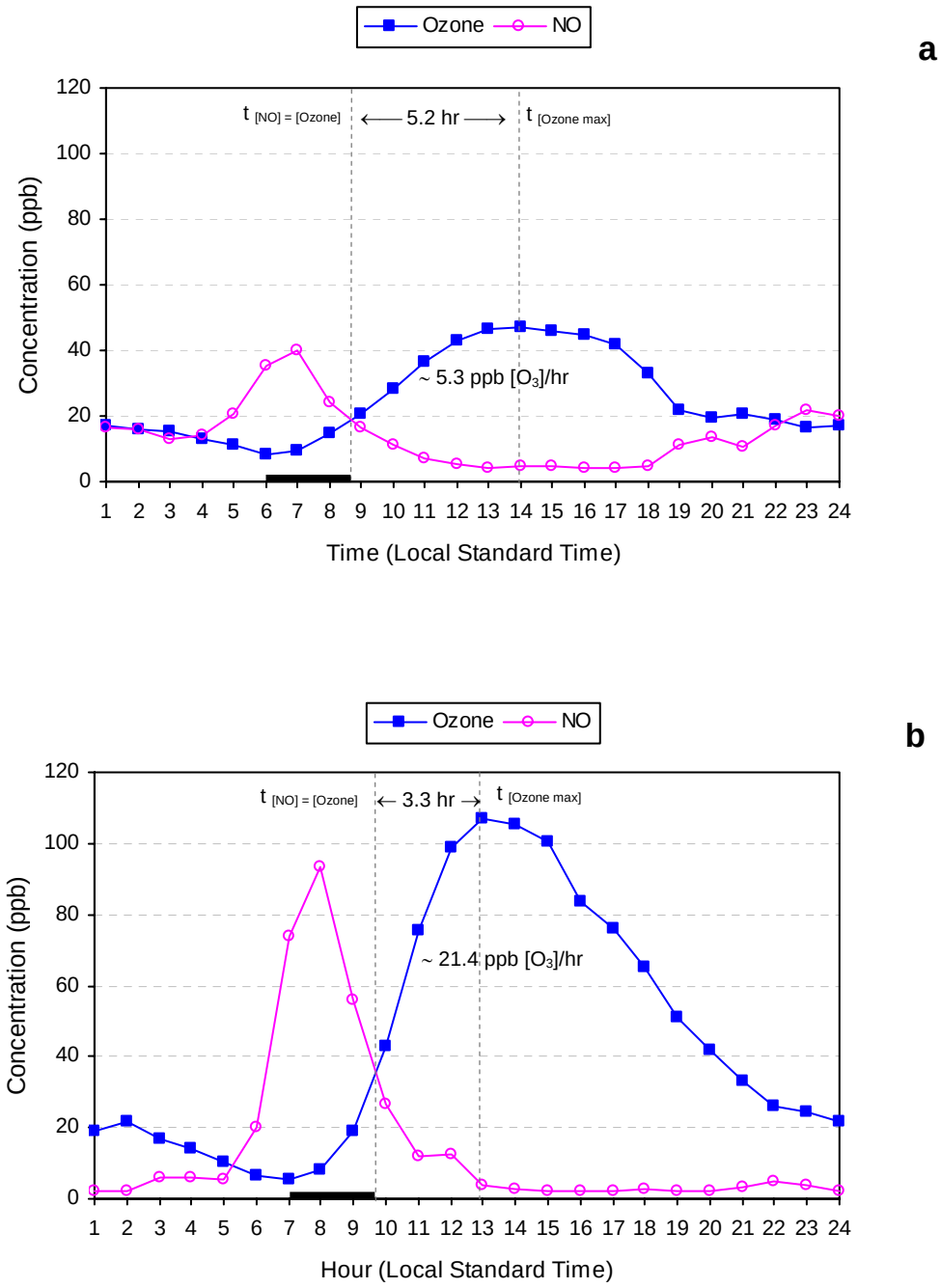

Figure 4.28. Average hourly diurnal variations of O_3 and NO concentrations and average rate of O_3 accumulation and of time of effective O_3 buildup at the: (**a**) Cincinnati (Taft Monitoring Station, September 3-30, 2003), and (**b**) Mexico City (Santa Ursula Monitoring Station, April 14-25, 2004). The horizontal solid bars represent the approximately length of the O_3 inhibition periods.

Grosjean (2003) has suggested that use of MTBE in nonleaded gasoline is an important source of isobutene and formaldehyde emissions from vehicles. Baez et al. (2000) have reported that they measured formaldehyde and acetaldehyde concentrations in the range of 20 ppb from 1993 to 1996 in a smog receptor site of Mexico City. Therefore, it is feasible to assume that VOC emissions from cars in Mexico City could be one additional important source of aldehydes compounds.

As a result of the strong differences in the initial morning emissions and production of OH radicals in both cities, the average NO-O_3 crossover concentration in Mexico City (~ 35 ppb) was almost 1.5 times higher than that for Cincinnati (~ 20 ppb). The average rate of O_3 accumulation and NO depletion was almost four times greater in Mexico City than in Cincinnati. This suggests that, despite the high emission of NO_x in both regions, the production of NO_2 available for O_3 formation and the removal of NO by organic radicals was strongly enhanced in Mexico City by its higher availability of VOCs.

Fujita et al. (2002) have suggested that timing of maximum O_3 generally coincides with distance of pollutant transport. The ozone peak in Cincinnati and Mexico City occurred in the early afternoon hours suggesting that both airsheds were within the influence of local regional emissions. While the average duration of the net O_3 accumulation was around 1.5 times longer in Cincinnati (~ 5.2 hr) than in Mexico City (~ 3.3 hr) however, the average rate of O_3 build up was almost four times faster in Mexico City (~ 21.4 ppb/hr) than in Cincinnati (~ 5.3 ppb/hr). In addition, the estimated rate of NO depletion was significantly higher in Mexico City (~ 17 ppb/hr) than in Cincinnati (~ 3.3 ppb/hr). The average afternoon mixing layer was relatively higher in the MCMA region than in GC, although the average wind speed was somewhat lower in Mexico City than in Cincinnati.

The above results confirm that despite of GC and MCMA have almost the same load of NO_x emissions into their air basins, the O_3 formation scenarios are different and strongly influenced by the severity of the local stagnant morning meteorological conditions and by the load and reactivity potential of VOC emissions.

4.3.2 Implications of the Results

According with the fundamentals of O_3 photochemistry, under a VOC-sensitive system (VOC/NO_x ratios << 8), the short supply of sources of OH radicals and the fact that OH radicals react predominantly with NO_2 lead to enhance the production of HNO_3 and to retard the O_3 formation. On the opposite, under a NO_x-sensitive system (VOC/NO_x ratios >> 8) the ample abundance of sources of OH radicals is sufficient to react with the relatively short abundance of NO_2 and with other VOCs to generate more radicals. As a result, the production of O_3 is accelerated and the formation of H_2O_2 is increased.

Following the fundamentals above, O_3 formation in Cincinnati (VOC/NO_x ~ 1.9 ppmC/ppm) should have a VOC-sensitive condition while Mexico City (VOC/NO_x ~ 15.1 ppbC/ppm) a NO_x-sensitive limitation. Although the above definition for VOC-sensitivity seems to be in agreement with the results of the previous observation driven analyses (PIM and WE/WD effect) for the Cincinnati data, the theoretical NO_x-sensitivity definition that could be applied to Mexico City looks to be in contradiction with the experimental finding that O_3 formation in Mexico City is likely VOC-sensitive.

The response to this apparent contradiction could be related to the limitation of the VOC/NO_x ratio to reflect the "real" NO_x-VOC sensitivity under certain conditions, particularly the true impact of VOC in terms of reactivity-weighted concentrations and severity of the air pollution event (Sillman, 1999). Usually, estimations of VOC to calculate VOC/NO_x ratios are influenced by uncertainties in the emission inventories calculations and the practical limitation to measure all the VOC species present in ambient air samples. As a result, the final estimated VOC are generally dominated by relatively less reactive but very abundant alkanes. This situation seems to be an important factor in the misleading of the true load of VOC with direct impact on O_3 formation in Mexico (Molina and Molina, 2002). However, after adjustments in the MCMA VOC reactivity, the VOC/NO_x ratio still indicates a NO_x-sensitive condition (VOC/NO_x > 8).

Milford et al. (1994) and Sillman (1999) have used a combination of theoretical analysis and results from photochemical models to demonstrate the existence of stronger correlations between events of

higher overall concentrations of O_3 precursors and VOC-sensitive chemistry systems, and between events with lower concentrations of ozone precursors and NO_x-sensitive conditions, even with identical initial VOC/NO_x emissions ratios. They have suggested that environmental conditions prone to have higher ozone precursors can be associated with either higher emission densities (i.e., larger urban areas) or with more restricted meteorological conditions (i.e., light winds and low daytime vertical mixing) or with a combination of both. Sillman has proposed an explanation for the severity of event effect by doing an analogy with the theoretical concept of Kleinman (1991, 1994) that states that, the split between the NO_x-sensitive and *NO_x-saturated* (or VOC-sensitive) regimes is related to the relative supply of NO_x (from emissions) in comparison with supply of radicals generated by sunlight. Freshly emitted plumes of polluted air have an initial NO_x supply that greatly exceeds the supply of radicals. As the plume ages, the total amount of radicals created during the process of photochemical evolution becomes equal with and eventually surpasses the initial NO_x-source, causing a switch from *NO_x-saturated* to NO_x-sensitive conditions. Therefore, if the source of NO_x source per unit volume in an airbasin is high (after considering the effect of dilution through daytime vertical mixing), it will take more time for the accumulated source of radicals (from the VOCs) to become equal with and surpass the NO_x source. As a result, a *NO_x-saturated* (VOC-sensitive) condition will persist for a longer time. But, if the NO_x source is low, the accumulated radical source will exceed the NO_x source after a short period of photochemical aging and the system will shift to NO_x-sensitive conditions.

Because MCMA has both a high precursors emission density and prevalent stagnant meteorology conditions, it is possible that the combination of these two factors is favoring the persistence of a *NO_x-saturated* (VOC-sensitive) condition, situation that is not seen by the initial VOC/NO_x ratio. Furthermore, the very high PAN concentrations observed in Mexico City may allows one to hypothesize that this is an additional factor influencing the limitation of the radical sources to surpass the NO_x source in the MCMA airbasin. PAN is produced by reaction of acetaldehyde, CH_3CHO, with OH and O_2 to form CH_3CO_3, which combines with NO_2 to form PAN (net reaction R12). Using steady-state approximations on the chemistry of PAN formation, Sillman et al. (1990) have shown that PAN concentration increases as

O_3 increases sequestrating temporarily OH radicals and carbonyl molecules ([PAN] $\propto$ k*[OH][CH_3CHO][O_3]; where k* represents a composite of all of the reaction constants involved in the reactions sequence). Gaffney et al. (1999) have reported the occurrence of a very strong diurnal variation of PANs (PAN, peroxyacetyl nitrate; PPN, peroxypropionyl nitrate; and PPB, peroxybutiryl nitrate) with PAN levels as high as 30 ppb. Therefore, it is reasonably to assume that PAN formation is acting as an important temporal reservoir of radicals from the accumulated burden of radicals necessary to switch the VOC-sensitive system to NO_x-system.

All of the mentioned above factors seem to be well represented by the evaluation of the NO_y and the O_3/NO_y indicators for MCMA and justify the experimental finding of the prevalence of VOC-sensitive conditions in the Mexico City air basin. The observed high afternoon O_3 concentrations suggests that there were large radical sources, while the high NO_y values suggests that there were a higher number of radical sinks, such as the OH + NO_2 and CH_3CHO + OH reactions.

The resulting VOC-sensitivity in Mexico City would seem to be in contradiction with prior studies. There are two reasons that could explain this contradiction. The first one that has been thoroughly discussed by Molina and Molina (2002), points out that the MCMA emission inventories, particularly the VOC inventory, are highly uncertain. As a consequence, photochemical simulations and other studies that used these inventories have given confusing O_3-sensitivity results. The second is that the use of morning VOC/NO_x ratios is not appropriate as a direct justification for the MCMA NO_x-VOC sensitivity because this ratio is not able to detect the effect of the severity of the event and the “true” reactivity of the VOCs.

Another implication of the PIM experimental results is that present model-based O_3 control strategies for Cincinnati and Mexico City should be carefully reviewed. This research has shown that the current strategy of reducing NO_x emissions in both airshed regions might, in fact, result in an increase in O_3 concentrations.

4.4 References

Baez, A.P., Padilla, H., Torres, M.C., Belmont, R. (2000) Ambient levels of carbonyls in Mexico City. Atmósfera, **13**, 121-131.

Bravo, H.A., Camacho, R.C., Roy, G.A., Sosa, R.E., Torres, R.J. (1991) Analysis of the change in atmospheric urban formaldehyde and photochemistry as a result of using methyl-*ter*-butyl ether (MTBE) as an additive in gasolines of the metropolitan area of Mexico City. Atmos. Environ. **25B**, 285-288.

Bravo, H. A., Torres, R.J. (2002) Air Pollution Levels and Trends in the México City Air Basin. Chapter 6. **In:** Urban Air Pollution and Forests. Resources at Risk in the Mexico City Air Basin. Fenn, M.E., de Bauer, L.I., Hernandez-Tejeda, T., Eds. Springer-Verlay, New York. Pp. 121-159.

BUWAL (1997) NO_2 Immissione in der Scweiz 1990-2010. Schriftreihe Umwelt nr. 289, Bundesamt für Umwelt, Wald und Landschaft, Bem, Switzerland.

Chameides, W.L., Fehsenfeld, F., Rodgers, M.O., et al. (1992) Ozone precursor relationships in the ambient atmosphere. J. Gephys. Res. **97**, 6037-6055.

Chow, J.C., Watson, J.G., Edgerton, S.A., Vega, E. (2002) Chemical composition of $PM_{2.5}$ and PM_{10} in Mexico City during winter 1997. Sci. Total. Environ. **287**, 177-201.

Daum, P.H. (1990) Observations of H_2O_2 and S(IV) in air, cloudwater and precipitation and their implications for the reactive scavenging of SO_2. Atmos. Res. **25**, 89-102.

de Leeuw, F., Moussiopoulos, N., Bartonva, A., Sahm, P., Pulles, P., Visschedijk, A. (2001) Air Quality in Larger Cities in the European Union. Topic Report 3/2001. Prepared to European Environmental Agency. Copenhagen, Denmark. February.

Doran, S.C., Abbott, J.L., Archuleta, J., et al., (1998) The IMADA-AVER boundary layer experiment in the México City area. Bull. Am. Meteor. Soc. **79**, 2497-2508.

Edgerton, S.A., Bian, X., Doran, J.C., et al., (1999) Particulate air pollution in Mexico City: a collaborative research project. J. Air & Waste Manage. Assoc. **49**, 1221-1229.

Finlayson-Pitts, B.J., Pitts, Jr., J.N. (2000) Chemistry of the Upper and Lower Atmosphere. Academic Press. San Diego, CA.

Fujita, E.M., Campbell, D.E., Stockwell, W., Keislar, W., Zrelinska, R.E., Sagebiel, J.C., Goliff, W., Keith, M., Bowen, J.L. (2002) Weekend/Weekday Ozone Observations in the South Coast Air Basin: Volume II – Analysis of the Air Quality Data. Final Report. Contract No. ACI-0-29086-01. Coordinating Research Council. Alpharetta, GA. April.

Gaffney, J.S., Marley, N.A., Cunningham, M.M., Doskey, P.V. (1999) Measurements of peroxyacyl nitrates (PANS) in Mexico City: implications for megacity air quality impacts on regional scales. Atmos. Environ. **33**, 5003-5012.

García, J.A.R. (2002) Evaluación de Escenarios Utilizando el Modelo Regional de Calidad del Aire *Multiscale Climate Chemistry Model*. Tesis Doctorado. Universidad Nacional Autónoma de México. Mexico City, Mexico. May.

García, J.A.R. (2004) Private communication. Center for Atmospheric Sciences, National Autonomous University of Mexico. Mexico City, Mexico.

Gerboles, M., Lagler, F., Rembges, D., Brum, C. (2003) Assessment of uncertainty of NO_2 measurements by the chemiluminescence meted and discussion of the quality objective of the NO_2 European Directive. J. Environ. Monit. **5**, 529-540.

Grosjean, D. (2003) Ambient PAN and PPN in southern California from 1960 to the SCOS97-NARSTO. Atmos. Environ. **37**, Supplement No. 2, S221-S238.

Hammer, M. -U., Vogel, B., Vogel, H. (2002) Findings on H_2O_2/HNO_3 as an indicator of ozone sensitivity in Baden-Württemberg, Berlin-Brandenburg, and the Po Valley based on numerical simulations. J. Geophys. Res. **107**, D18, doi:10.1029/2000JD000211.

HCDOES (2004) Air Quality Data and Progress Report. Hamilton County Department of Environmental Services. Cincinnati, OH.

Hering, S.V., Lawson, D.R., Allegrini, I., et al., (1988) The nitric acid shootout: field comparison of measurement methods. Atmos. Environ. **22**, 1519-1539.

Jazcilevich, A.D., Garcia, A.R., Ruiz-Suárez, L.G. (2003) A study of air flow patterns affecting pollutant concentrations in the Central Region of Mexico. Atmos. Environ. **37**, 183-193.

Kleinman, L.I. (1991) Seasonal dependence of boundary layer peroxide concentration: the low and high NO_x regimes. J. Geophys. Res. **96**, 20721-20734.

Kleinman, L.I. (1994) Low and high-NO_x tropospheric photochemistry. Geophys. Res. **99**, 16831-16838.

Kok, G.L., Darnall, K.R., Winer, A.M., Pitts, Jr., J.N., Gay, B.W. (1978) Ambient measurements of hydrogen peroxide in the California South Coast Air Basin. Environ. Sci. Technol. **12**, 1077-1080.

Limón-Sánchez, M.A.T. (2003) Implementación de un método de muestreo y de análisis de ácidos carboxílicos en aire ambiente: materia particulada y fase gaseosa. Tesis Doctorado. Universidad Nacional Autónoma de México. Mexico City, Mexico. March.

Milford, J.B., Gao, D., Sillman, S., Blossey, P., and Russell, A.G. (1994) Total Reactive Nitrogen (NO_y) as an Indicator of the Sensitivity of Ozone to Reductions in Hydrocarbon and NO_x Emissions. J. Geophys. Res. **99**, 3533-3542.

Molina, L.T., Molina, M.J. Eds. (2002) Air Quality in the Mexico Megacity: An Integrated Assessment. Alliance for Global Sustainability Bookseries. Volume 2. Kluwer Academic Publishers. Dordrecht, The Netherlands.

NCDC (2003) National Climatic Data Center. Local Climatological Data. Available at: http://www.ncndc.noaa.gov/ncdc.html.

OKI (1979) Regional Air Quality Management Plan. Ohio-Kentucky-Indiana Regional Council of Governements. Cincinnati, OH. February.

Possanzini, M., DiPalo, V., Liberti, A. (1988) Annular denuder meted for determination of H2O2 in the ambient atmosphere. Sci. Total Environ. **77**, 203-214.

Singh, H.B. (1987) Reactive nitrogen in the troposphere. Environ. Sci. Technol. **21**, 320-327.

Sillman, S. (1995) The use of NO_y, H_2O_2, and HNO_3 as indicators for O_3-NO_x-VOC sensitivity in urban locations. J. Geophys. Res. **100**, 11497-11508.

Sillman, S. (1999) The relation between ozone, NO_x, and hydrocarbons in urban and polluted rural environments. Atmos. Environ. **33**, 1821-1845.

Sillman, S. (2002) Evaluation of Observation-Based Methods For Analyzing Ozone Production and Ozone-NO_x-VOC Sensitivity. Report to: National Exposure Research Laboratory. National Exposure Research Laboratory. Office of Research and Development. U.S. Environmental Protection Agency. Research Triangle Park, NC 27711.

Sillman, S. (2003) Observation-Based Methods (OBMs) For Analyzing Urban/Regional Ozone Production and Ozone-NO_x-VOC Sensitivity. University of Michigan. Available at: http://www-personal.engin.umich.edu/~sillman.

Sillman, S., He, D., Cardelino, C., Imhoff, R.E. (1997) The use of photochemical indicators to evaluate ozone-NO_x-hydrocarbon sensitivity: case studies from Atlanta, New York and Los Angeles. J. Air & Waste Manage. Assoc. **47**, 1030-1040.

Sillman, S., He, D. (2002) Some theoretical results concerning O_3-NO_x-VOC chemistry and NO_x-VOC indicators. J. Geophys. Res. **107**, D22, 4659, doi:10.1029/2001JD001123.

Sillman, S., Vaudatard, R., Menut, L., Kley, D. (2003) O_3-NO_x-VOC sensitivity and NOx-VOC indicators in Paris: results from models and Atmospheric Pollution Over the Paris Area (ESQUIF) measurements. J. Geophys. Res. **108**, D17, 8563, doi:10.1029/20002JD001561.

SMA (2003) Inventario de Emisiones a la Atmósfera del Valle de México, 2000. Secretaría del Medio Ambiente. Gobierno del Distrito Federal. Ciudad de México, D.F. México.

SMA (2004) Indicadores de la Calidad del Aire. Sistema de Monitoreo Atmosférico de la Ciudad de México. SIMAT. Gobierno del Distrito Federal. Secretaría del Medio Ambiente. Ciudad de México. D.F. México. Available at: http://www.sma.df.gob.mx/simat/pnindicadores.htm.

Sosa, G., West, J., San Martini, F., Molina, L.T., Molina, M.J. (2000) Air Quality Modeling and Data Analysis for Ozone and Particulates in Mexico City. Rep. No. 15. MIT Integrated Program on Urban, Regional and Global Air Pollution. Cambridge, MS. October.

Thielmann, A., Prévôt, A.S., Staehelin, J. (2002) Sensitivity of ozone production derived from field measurements in the Italian Po basin. J. Geophys. Res. **107**, D22, 8194, doi:10.1029/2000JD000119.

Tonnesen, G.S., Dennis, R.L. (2000) Analysis of radical propagation efficiency to assess ozone sensitivity to hydrocarbons and NO_x, 2, long-lived species as indicators for ozone concentration sensitivity. J. Geophys. Res. **105**, 9227-9241.

US EPA (1999) Determination of Reactive Acidic and Basic Gases and Strong Acidity of Atmospheric Fine Particles (<2.5 μm). Compendium Method IO-4.2; EPA-625/R-96/010a; Center for Environmental Information. Office of Research and Development. U.S. Environmental Protection Agency, Cincinnati, OH.

US EPA (2004) Cincinnati-Hamilton, OH-KY-IN MSA. Technology Transfer Network Ozone Implementation.Envirofacts. U.S. Environmental Protection Agency. Available at: http://www.epa.gov/ttn/naaqs/ozone/areas/msaindex/htm.

Williams, E.J., Baumann, K., Roberts, J.M., et al., (1998) Intercomparison of ground based NO_y measurement techniques. J. Geophys. Res. **103**, 22261-22280.

Chapter 5
Conclusions and Recommendations

Understanding the sensitivity of ozone concentrations to changes in emissions of NO_x and VOC has been an important task for formulating effective policies to reduce O_3 formation in urban areas. The use of 3-D photochemical models has been the traditional scientific tool used to predict and design O_3 air quality strategies. However, a number of uncertainties associated with the required input data, such as the NO_x and VOC emission inventories, have called into question the resulting predictions and, therefore, the proposed control strategies. Observation-based methods (OBMs), along with advances in the instrumentation for measuring O_3 precursors, have been suggested as supplementary means for deriving the O_3-NO_x-VOC sensitivity and for testing the reliability of model predictions. However, OBMs have not been universally accepted within the regulatory and scientific communities because of a lack of research on the effectiveness of their methods.

In this study, the combination of an OBM with additional conceptual and data analysis was used to investigate the O_3-NO_x-VOC sensitivity of two dissimilar urban areas. This approach was selected with the hope that it would provide an improved diagnosis for the O_3-air-quality management process.

Measurements of O_3, NO_y, and NO in one representative site of Cincinnati, Ohio (U.S.A.) and Mexico City, Federal District (Mexico) were used as the basis to evaluate these cities' O_3-NO_x-VOC sensitivity through the photochemical indicator method (PIM). Photochemical indicators are species ratios of the O_3 concentration, which has built-up in the time since the precursor emissions occurred, to the total reactive nitrogen species or another secondary species. Individual species such as NO_y are also reliable indicators of the history of photochemically aged air parcels. The evaluation of the indicator species and indicator ratios was complemented with additional measurements of HNO_3 and H_2O_2 in Cincinnati and with 3-D simulation results of NO_y, NO_z, PAN, HNO_3, and H_2O_2 in Mexico City. In addition, a semi-empirical estimate of the NO_z* concentration was applied in both cases. The estimated NO_2* afternoon concentrations were within the operational uncertainty range suggested for NO_x chemiluminescent

analyzers. The consistency of the measured and the estimated indicator ratios was evaluated through the comparison of their correlation patterns with 3-D predicted correlation scatterplots for reference locations.

Assuming as "universal" the Sillman transition values for the different indicators between NO_x and VOC sensitivity conditions it was found that in both cities the chemistry of O_3 formation was likely VOC-sensitive.

In both cases, the above finding was corroborated with a statistical analysis of the differences in the weekend/weekday (WE/WD) effect of morning NO emissions (with NO as a surrogate of the total NO_x emissions) on the respective maximum O_3 concentrations. The statistical test was formulated based on the chemistry of NO_x-VOC sensitivity. The analysis showed that, although there was a statistically significant difference in the reduction of NO emissions on WE with respect to the WD emissions, the difference on the maximum ozone concentrations was not statistically significant in either city. In a NO_x-sensitive environment, a reduction of NO_x emissions would bring down the maximum O_3 concentration. The statistical analysis showed that this was not the case. Therefore, the results of these "natural" experiments indirectly pointed to the existence of VOC-sensitive conditions in both regions.

The consistency of the PIM diagnosis in Mexico City was exercised in an intercomparison of the indicator results with previous preliminary measurements and modeling experiments done in this urban area. The results of the intercomparison showed that, independent of the methods and approaches used to arrive at the indicator ratios, all of them tended to diagnose VOC-sensitive conditions. Furthermore, an indirect comparison of the photochemical indicators results with the predictions from the 3-D photochemical model (i.e., the MCCM) led to the conclusion that the performance of the model could be improved if the actual contribution of aldehydes and ammonia emissions was included in the emissions inventory input data files.

The conceptual analysis of the descriptive parameters related to O_3 formation helped to assess the behavioral differences of the photochemical process for both cities. The rate of accumulation and the peak levels of O_3, as well as the rate of depletion of NO, were higher in Mexico City than in Cincinnati. This phenomenon was seen as the result of the combination of stronger morning stagnant meteorological

conditions and larger contribution of reactive VOCs to the photochemical process in Mexico City, even though NO_x emissions for both areas seemed to be similar.

The experimental finding of VOC-sensitive conditions in both regions was interpreted as the result of the predominance of the reaction for formation of HNO_3 in an environment with low free radical sources ("low" VOC emissions) but higher radical sinks ("high" NO_x emissions) in Cincinnati, and of the predominance of *NO_x-saturated conditions* (continuous "high" NO_x supply exceeding the supply of radical sources) combined with formation reactions of PAN and HNO_3 in an environment with large free radical sources ("high" reactive VOC emissions) and high radical sinks ("high" NO_x emissions) in Mexico City. The combination of these results led to confirm the inconsistency of the initial emissions VOC/NOx ratio as a tool for diagnosis of the O_3-NO_x-VOC sensitivity in regions with high precursors emissions densities and restrictive natural ventilation conditions.

The findings of this applied research suggest that present model-based O_3 control strategies for Cincinnati and Mexico City should be carefully reviewed. This research has shown that the current strategy of reducing NO_x emissions in both airshed regions could, in fact, result in an increase in O_3 concentrations.

As demonstrated by this study, the combination of the PIM with the WE/WD statistical analysis and the conceptual analysis of empirical O_3-formation related parameters has the potential to be a more comprehensive complementary tool for the identification of the O_3-NO_x-VOC sensitivity of even dissimilar geographic and urban regions.

Although the results of this applied research have suggested the dominance of VOC-sensitive conditions in both regions, more research is needed to further investigate the ozone sensitivity in the entire Greater Cincinnati and the Mexico City Metropolitan Area regions. This implies the simultaneous collection of O_3 and NO_y data in at least three sites of both airshed regions (one upwind and two downwind of the urban area), including at least one site with HNO_3 and H_2O_2 measurements. If possible, these measurements should include the determination of PAN and NO_3^-concentrations.

One effort to measure photochemical indicators simultaneously in Cincinnati and Mexico City during one period in which the conditions were relatively similar is recommended. Although summer is the season more conducive to ozone formation in southwest Ohio, this is not the case in Mexico City because this period corresponds to the rain season. The most favorable month could be May; the end of the smog season in Mexico City and the beginning of the smog season in Cincinnati.

In addition, the implementation of a 3-D photochemical modeling effort for the southwestern Ohio region (including parts of Ohio, Kentucky, and Indiana), calibrated against the results of the indicators measurements, is also recommended. The sampling and analysis of 6:00-9:00 hr VOC species concentrations in Cincinnati is mandatory for the appropriate setting of the photochemical model. In the case of Mexico City, it is recommended to calibrate the MCCM photochemical model considering scenarios with different aldehydes and ammonia contributions and also to calibrate the results against the indicator measurements. Once the model is calibrated, it would be desirable to investigate if the transition values suggested by Sillman should be adjusted for the particular geographic situation of Mexico City.

It is hoped that the present applied research will contribute to the development of better O_3 air quality management policies as recommended by the NARSTO for North America.

APPENDIX A

CLASSIFICATIONS OF O_3- SENSITIVIVITY CHEMISTRY IN 3-D MODELING SIMULATIONS

The classifications for predicted NO_x-VOC sensitivity with 3-D chemistry models are based on the relative impact of reduced NO_x versus reduced VOC. These simulations predict distinct patterns of the correlation between simulated afternoon O_3 and NO_y and between O_3 and NO_z among other combinations. The patterns have been classified according to the differences found between simulated O_3 in a model base case and equivalent scenarios with 25% or 35% reductions in NO_x and in anthropogenic VOC in several locations of the U.S. Locations have been classified according to the following definitions:

NO_x-sensitive: A given reduction in NO_x emissions causes a significant (>5 ppb) reduction in simulated O_3, in both the base case and in the scenario with the same equivalent reduction in anthropogenic VOC.

VOC-sensitive: A given reduction in VOC results in an O_3 concentration at least 5 ppb lower than in both the base case and in the scenario with the same equivalent reduction in NO_x.

Mixed or near-zero sensitive: Reduced NO_x and reduced VOC emissions result in a simulated O_3 within 5 ppb of each other, and both scenarios result in a simulated O_3 lower than in the base case by at least 5 ppb.

dominated by NO_x-titration: A given reduction in NO_x causes a significant increase in the simulated O_3 in the base case by at least 5 ppb. At the same time, a given reduction in VOC results in a simulated O_3 not lower than 5 ppb or more relative to the base case.

Reference

Sillman, S., He, D. (2002) Some theoretical results concerning O_3-NO_x-VOC chemistry and NO_x-VOC indicators. J. Geophys. Res. **107**, D22, 4659, doi:10.1029/2001JD001123.

APPENDIX B

SUMMARY OF THE MAIN CHARACTERISTICS OF THE MCCM

The air quality model: Multiscale Climate Chemistry Model (MCCM) is a coupled complex meteorology/chemistry model, which is based on the fifth generation Penn State/NCAR nonhydrostatic mesoscale model (MM5) and the Regional Air Deposition Model version 2 (RADM2). MCCM does include modules for meteorology, photolysis, biogenic emissions, radiation, and deposition among others. MM5 is non hydrostatic with terrain following coordinates, has a multiscale option, is capable of four-dimensional data-assimilation interface with actual weather forecast models (general circulation model and observations), contains explicit cloud schemes and multilevel soil/vegetation parameterization.

An advantage of MCCM is that MM5 is directly coupled with a chemistry-transport-model and photolysis module. Several parameterizations schemes are used for the calculation of turbulent transport variables. The parameterization scheme includes a soil/vegetation scheme that calculates the soil temperature and moisture stratification, and determines the heat and moisture fluxes at the interface between atmosphere and soil. The photolysis module uses a radiative transfer model that calculates photolysis frequencies for the 21 photochemical reactions of the gas-chemistry model at each grid point. This module considers changes in the radiation with height and changes in air composition such as ozone, aerosols and water vapor. The biogenic module calculates organic emissions of isoprene, monoterpenes, other biogenic VOCs, and nitrogen emissions by the soil. This module takes into account the effects of temperature, radiation and type of vegetation because they affect directly the emissions of biogenic VOCs. The dry deposition module calculates the elimination of trace compounds from the atmosphere depending on deposition velocity, which is calculated using aerodynamic, sub-layer and surface resistance. Because of the simultaneous on-line coupling between the meteorology and the chemistry, the MCCM gives consistent results without the necessity of interpolation as with the models that use non-coupled schemes.

The gas-phase chemistry is based on the RADM2 mechanism. This mechanism considers for inorganic species, 14 stable species, 4 reactive intermediates and 3 abundant (oxygen, nitrogen and water). The organic part is represented by 26 stable species and 16 peroxy radicals. The RADM2 mechanism represents organic chemistry through a reactivity aggregated molecular approach. Similar organic compounds are grouped together into a limited number of model groups through the use of reactivity weighting with respect to the OH radical. For the numerical solution, MCCM uses a Quasi-Steady-State Approximation (QSSA) method with 22 diagnosed, 3 constant and 38 predicted species. MM5 contains a four-dimensional data assimilation technique. This technique insures that the model solution does not diverge strongly from observations.

The input data to the MCCM consists of meteorological information, anthropogenic emissions, use of land, and topography files, which must be preprocessed in order to prepare the data for running the model. A scheme of the structure of the main preprocessors used to run the MCCM is shown in Figure B.1.

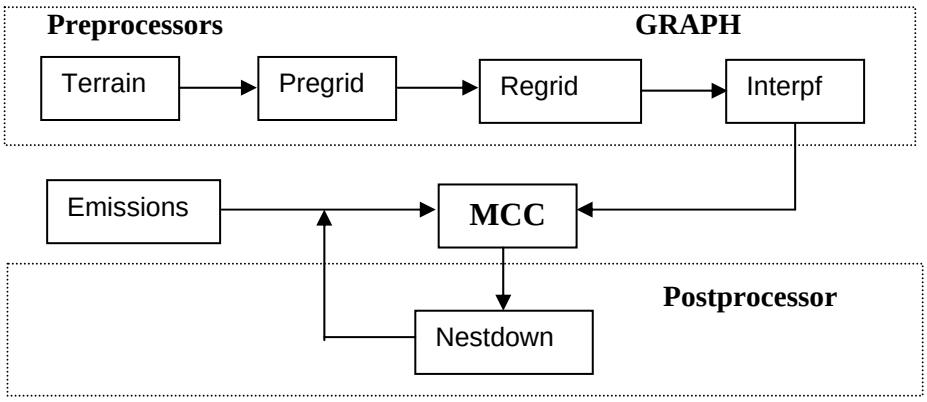

Figure B.1. Schematic flow diagram of the different processors used to run the MCCM.

In the *Terrain* preprocessor, the physical domains and geographical locations, as well as the nested strategy are specified. This module prepares the topography and the use of land information through an interpolation process. The purpose of the *Regrid* preprocessor is to read synoptic scale meteorological files or predicted output data and to interpolate the information to the topographical mesh previously specified in *Terrain*. The *Pregrid* preprocessor reads the files and prepare the output data in the format required by *Regrid*. Within the *Regrid* preprocessor it is included a preprocessor called *Rawins* which improves the quality of the predicted results from the first approximation through an intercomparison with observed rawinsondes. The *Interpf* program generates the initial meterological field, and the upper and lower boundary conditions through an interpolation scheme. *GRAPH* is part of MM5 and allows one to visualize the preliminary output information. *Nestdown* is a post-processor that generates the input data for a "new" nested domain from the results of a mother-domain generated from a previous run. The *Emissions* preprocessor prepares the anthropogenic emissions from area and lineal sources in the format required by MCCM. The input VOC data must be in terms of the several reactivity family groups defined by RADM2.

The general resolution of the different meteorological domains is shown in Table B.1. The temporal resolution of the output data is generally of 1-hr.

Table B.1. Details of the extent of domain and scale of the modeling time of MCCM.

Domain	Cell Size Resolution (km)	Number of Cells		Modeling time (hr)
		x	***y***	
1	27	60	60	96
2	9	34	34	72
3	3	52	40	72

The limitations of the MCCM are all related with the quality of information, particularly, the meteorological information for the larger domain. As well as other photochemical models, the quality of the emission inventory is reflected in the modeling results. Other important operational limitation of the

MCCM is the preparation of the input data. This process requires the conversion of a number of different input data formats into specific formats required by the model.

References

García, J.A.R. (2002) Evaluación de Escenarios Utilizando el Modelo Regional de Calidad del Aire *Multiscale Climate Chemistry Model*. Tesis Doctorado. Universidad Nacional Autónoma de México. Mexico City, México. May.

Garcia, J.A.R., (2003) Manual: Multiscale Climate Chemistry Model (MCCM). Prepared for: Instituto Nacional de Ecología, México. Mexico City, Ocotber.

Grell, G.A., Emeio, S., Stockwell, W.R., Schenemeyer, T., Forkel, R., Michalakes, J., Knoche, R., Seidl, W. (2000) Application of a multiscale, coupled MM5/chemistry model to the complex terrain of the VOTALP valley campaign. Atmos. Environ. **34**, 1435-1453.

APPENDIX C

SUMMARY OF THE STATISTICAL ANALYSIS OF DIFFERENCES OF 1-hr MAX O_3 MEANS FROM A MATRIX COMBINATION OF WEEKDAYS AND WEEKEND DAYS IN CINCINNATI

Table C.1. Results of the tests of statistical analysis on differences (two-tail *t*-test; equal variances; *p* at a 95% confidence level), in average 1-hr max O_3 concentrations from a matrix combination of two WD and two WE days for data observed at the Taft Monitoring Station (Cincinnati), September 3-30, 2003.

Pair of days	Mean (S.D.) ppb	No. of Samples	Result of test of significance[a]	Interpretation[b]
Mon-Tue	49.2 (15.3)	5	**p = 0.947**	***H₀*: Accepted**
Sat-Sun	48.6 (14.4)	8		*H₁*: Rejected
Mon-Wed	47.3 (20.6)	7	**p = 0.885**	***H₀*: Accepted**
Sat-Sun	48.6 (14.4)	8		*H₁*: Rejected
Mon-Thur	47.4 (12.5)	7	**p = 0.867**	***H₀*: Accepted**
Sat-Sun	48.6 (14.4)	8		*H₁*: Rejected
Mon-Fri	41.4 (13.2)	7	**p = 0.335**	***H₀*: Accepted**
Sat-Sun	48.6 (14.4)	8		*H₁*: Rejected
Tue-Wed	50.5 (19.8)	6	**p = 0.840**	***H₀*: Accepted**
Sat-Sun	48.6 (14.4)	8		*H₁*: Rejected
Tue-Thur	50.7 (8.4)	6	**p = 0.763**	***H₀*: Accepted**
Sat-Sun	48.6 (14.4)	8		*H₁*: Rejected
Tue-Fri	43.7 (11.7)	6	**p = 0.505**	***H₀*: Accepted**
Sat-Sun	48.6 (14.4)	8		*H₁*: Rejected
Wed-Thur	48.6 (16.)	8	**p = 0.999**	***H₀*: Accepted**
Sat-Sun	48.6 (14.4)	8		*H₁*: Rejected
Wed-Fri	39.3 (21.4)	8	**p = 0.322**	***H₀*: Accepted**
Sat-Sun	48.6 (14.4)	8		*H₁*: Rejected
Thur-Fri	43.5 (9.6)	8	**p = 0.416**	***H₀*: Accepted**
Sat-Sun	48.6 (14.4)	8		*H₁*: Rejected

a. If $p \leq 0.05$, the difference in means is significant; if $0.05 \leq p \leq 0.10$, the difference in means is marginally significant; if $p \geq 0.10$, the difference in means is insignificant.

b. H_O: $\mu_{O3WE} = \mu_{O3WD}$; the change in WE average maximum O_3 is insignificant; likely to be caused by a VOC-sensitive condition provided that the reduction in morning WE-NO_x emissions is insignificant.
H_1: $\mu_{O3WE} < \mu_{O3WD}$; the change in WE average maximum O_3 is significant; likely to a NO_x-sensitive condition prov that the reduction in morning WE-NOx emissions is insignificant.

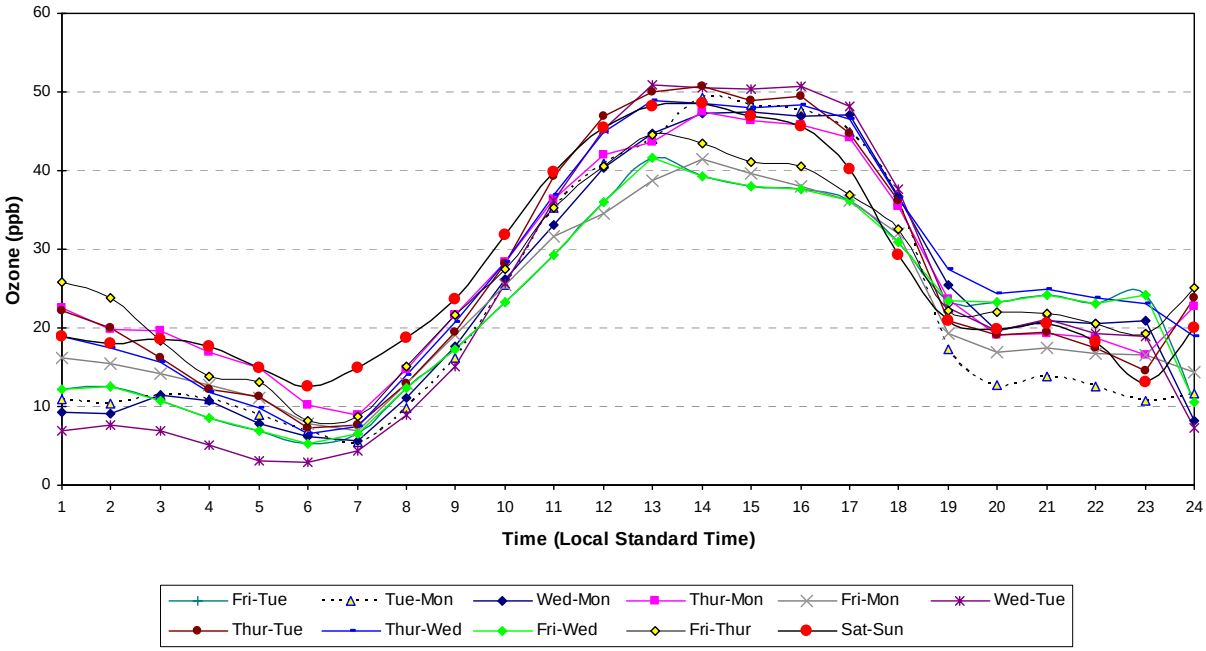

Figure C.1. Diurnal 1-hr average O_3 concentrations from a matrix combination of two weekdays and two weekend days registered at the Taft Monitoring Station (Cincinnati), September 3-30, 2003.

APPENDIX D

SUMMARY OF THE STATISTICAL ANALYSIS OF DIFFERENCES OF 1-hr MAX O_3 MEANS FROM A MATRIX COMBINATION OF WEEKDAYS AND WEEKEND DAYS IN MEXICO CITY

Table D.1. Results of the tests of statistical analysis on differences (two-tail *t*-test; equal variances; *p* at a 95% confidence level), in average 1-hr max O_3 concentrations from a matrix combination of two WD and two WE days for data observed at the Santa Ursula Monitoring Station (Mexico City), April 1-30, 2004.

Pair of days	Mean (S.D.) ppb	No. of Samples	Result of test of significance[a]	Interpretation[b]
Mon-Tue	87.1 (39.2)	7	**p = 0.98**	***H₀*: Accepted**
Sat-Sun	86.6 (40.5)	7		*H₁*: Rejected
Mon-Wed	109.8 (47.6)	7	**p = 0.33**	***H₀*: Accepted**
Sat-Sun	86.6 (40.5)	7		*H₁*: Rejected
Mon-Thur	93.5 (33.7)	8	**p = 0.72**	***H₀*: Accepted**
Sat-Sun	86.6 (40.5)	7		*H₁*: Rejected
Mon-Fri	87.6 (38.3)	8	**p = 0.96**	***H₀*: Accepted**
Sat-Sun	86.6 (40.5)	7		*H₁*: Rejected
Tue-Wed	104.8 (44.9)	8	**p = 0.41**	***H₀*: Accepted**
Sat-Sun	86.6 (40.5)	7		*H₁*: Rejected
Tue-Thur	90.9 (30.8)	9	**p = 0.81**	***H₀*: Accepted**
Sat-Sun	86.6 (40.5)	7		*H₁*: Rejected
Tue-Fri	85.7 (34.8)	8	**p = 0.43**	***H₀*: Accepted**
Sat-Sun	86.6 (40.5)	7		*H₁*: Rejected
Wed-Thur	108.56 (37.9)	9	**p = 0.27**	***H₀*: Accepted**
Sat-Sun	86.6 (40.5)	7		*H₁*: Rejected
Wed-Fri	103.3 (43.7)	9	**p = 0.43**	***H₀*: Accepted**
Sat-Sun	86.6 (40.5)	7		*H₁*: Rejected
Thur-Fri	90.9 (30.9)	10	**p = 0.80**	***H₀*: Accepted**
Sat-Sun	86.6 (40.5)	7		*H₁*: Rejected

[a] If $p \leq 0.05$, the difference in means is significant; if $0.05 \leq p \leq 0.10$, the difference in means is marginally significant; if $p \geq 0.10$, the difference in means is insignificant.

[b]. H_O: $\mu_{O3WE} = \mu_{O3WD}$; the change in WE average maximum O_3 is insignificant; likely to be caused by a VOC-sensitive condition provided that the reduction in morning WE-NO_x emissions is insignificant.

H_1: $\mu_{O3WE} < \mu_{O3WD}$; the change in WE average maximum O_3 is significant; likely to a NO_x-sensitive condition provided that the reduction in morning WE-NOx emissions is insignificant.

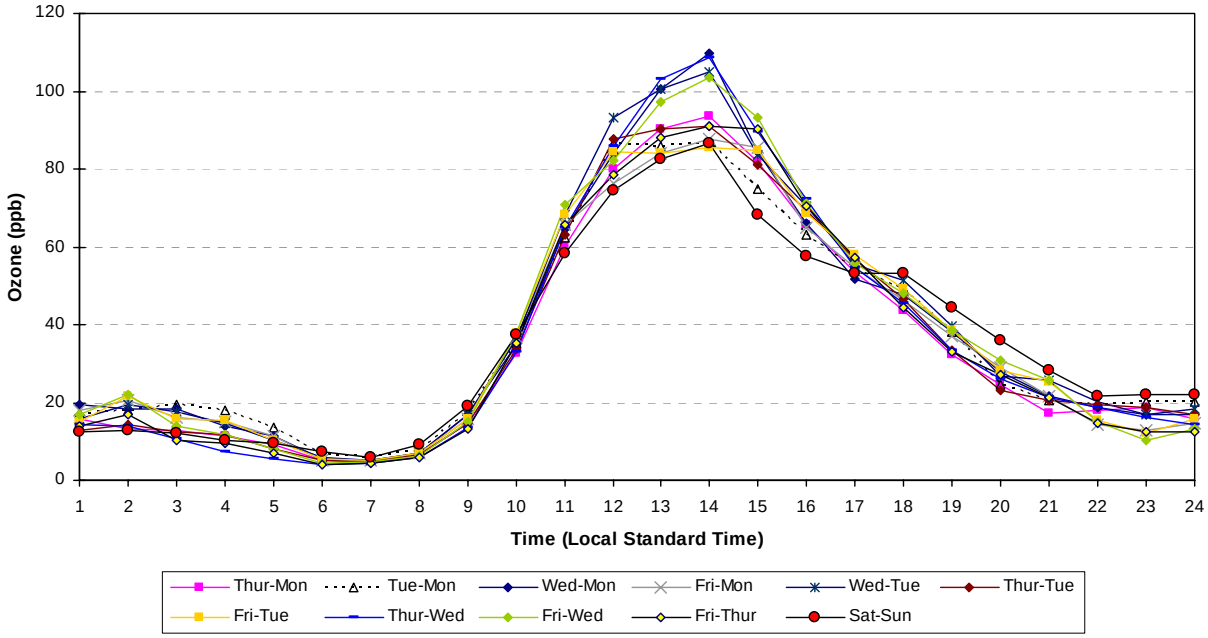

Figure D.1. Diurnal 1-hr average O_3 concentrations from a matrix combination of two weekdays and two weekend days registered at the Santa Ursula Monitoring Station (Mexico City), April 1-30, 2004.